Synthesis and characterization of onion-like carbons for adsorption of tartrazine dye in water

By

Herbert Qaqambile Cwayi

Person Number: 1438739

Supervisors:

Dr Manoko S. Maubane-Nkadimeng

Prof Neil J. Coville

Dr Winny K. Maboya

A dissertation submitted to the Faculty of Science,

University of the Witwatersrand, Johannesburg,

in fulfilment for the degree of

Master of Science in Chemistry

March, 2024

DECLARATION

I declare that this dissertation, which is hereby submitted for a degree of Master of Science in the Faculty of Science, School of Chemistry, University of the Witwatersrand, Johannesburg is my own unaided work and has not been submitted for examination at any institution.

UNIVERSITY OF THE
WITWATERSRAND,
JOHANNESBURG

(*Signed*) Herbert Qaqambile Cwayi

On this 5th day of August 2024

DEDICATION

This work is dedicated to my family:

My mother (Qaqamba Cwayi), My grandfather (Mzoliswa R. Cwayi), and my late loving grandmother (Ncediswa Cwayi)

ACKNOWLEDGEMENTS

I would like to thank **God Almighty** for giving me the strength to persevere when things were difficult. The journey was not easy, but it was worth it.

There are numerous individuals whom I would like to thank for contributing to this work but most importantly I would like to thank; **Dr Manoko S. Maubane-Nkadimeng,** for the helpful guidance, motivation, patience, kindness, understanding spirit and for taking this journey with me. I am extremely thankful to my co-supervisors, **Prof Neil J. Coville** and **Dr Winny K. Maboya,** for their valuable guidance and support throughout completing this project. Lastly, **Dr Themba "The Beast" Ntuli** for giving me huge assistance in designing the research project and equipping me with problem solving skills. Thank you for your endless support, thank you for your assistance, thank you for your patience, and thank you for believing in me.

I extend my gratitude to my Lab mates namely, **Dr Bokome Shaku, Lindokuhle Magagula**, and **Dr Ludwe Sikeyi** for assisting me in the Lab. To the School of Chemistry and also CATMAT, C-dots research groups at the University of the Witwatersrand - thanks for the enthusiasm, support and for making the lab the greatest place to be.

I am thankful to the microscopy and microanalysis unit (MMU) headed by **Prof. Alexander Ziegler** and the staff, i.e., **Dr MS Maubane-Nkadimeng**, **Dr E Linganiso**, and **Dr Z Tetana** for the training of instruments such as XRD and TEM. Many thanks to **Prof Rudolph Erasmus** for his kind assistance with the Raman spectroscopy analysis. Special thanks to **Rhandzu Rikhotso** for allowing me to do high resolution transmission electron microscopy (HRTEM) analysis through the Council for Scientific and Industrial Research (CSIR) characterization facility. Special thanks to **Petra Dinham** for assisting with scanning electron microscopy (SEM).

Special gratitude to the National Research Foundation **(NRF)** of South Africa. Thanks a lot for settling all my academic fees, stipends, chemicals and conference expenses.

PRESENTATIONS

- Wits Cross Faculty 2022 Symposium: Poster presentation "*Synthesis and functionalization of onion-like carbons for the adsorption of tartrazine dye from wastewater*" University of the Witwatersrand, South Africa.
- CATSA conference 2022: Poster presentation "*Synthesis and functionalization of onion-like carbons for the adsorption of tartrazine dye from wastewater*" Champagne Sports Resorts, KwaZulu-Natal, South Africa.

ABSTRACT

Industrial effluent often can contain a significant amount of synthetic dyes. The discharge of wastewater containing dyes into water streams without proper treatment consequently enters the soil and disturbs the aquatic and terrestrial life. Several wastewater treatment technologies have been proposed that can efficiently reduce the amount of synthetic dyes from the environment, in particular azo dyes. Among all the existing technologies for wastewater treatment, physical adsorption is a popular technology because it is inexpensive, simple, and efficient. The aim of this study is to synthesize, modify, and characterize onion-like carbons (OLCs) derived from four different waste oils for the adsorption of tartrazine dye in water. The OLCs derived from different carbon precursors (waste household oil, restaurant waste oil, engine waste oil, and paraffin oil bath waste) were synthesized using a flame pyrolysis method. The synthesized materials were doped with nitrogen using a chemical vapor deposition technique using 10% ammonia gas as a source of nitrogen. The N-doped OLCs were attached with hydroxyl groups through oxidation reactions to improve their solubility and adsorption efficacy. According to the high-resolution transmission electron microscopy and scanning electron microscopy images, the OLCs from all four-carbon precursor were quasi-spherical, agglomerated, and presented a chain-like structures of multi-layers. The distance between the graphitic layers was found to be 0.32 nm. The average particle size of OLCs was calculated to be 40.2 ± 2.5 nm. Adsorption studies revealed that the initial dye concentration, contact time, and pH of the dye solutions influenced the adsorption capacity of the tetrazine. Nitrogen doping of OLCs increased its capacity to adsorb the tartrazine dye. The nitrogen doped OLCs from household waste oil (H-N-OLCs) and engine waste oil (E-N-OLCs) were used in equilibrium adsorption studies in this work. For a concentration of 20 mg/L of tartrazine dye, an adsorption capacity of 28.9 mg/g was achieved using the N-doped OLCs from household waste oil. The adsorption process follows the pseudo second-order kinetic model. The adsorption isotherm is best fitted to the Freundlich mathematical model. The results obtained show that, the source of oil did not have major effect on the physicochemical properties of OLCs and that incorporation of nitrogen onto carbon matrix enhanced the adsorption of the anionic tartrazine dye in aqueous solution.

TABLE OF CONTENTS

LIST OF FIGURES

Chapter 2

Chapter 3

Appendix

LIST OF TABLES

Chapter 2

Chapter 3

Chapter 4

Chapter 5

LIST OF SYMBOLS AND ABBREVIATIONS

BCP	Brass Collecting Plate
BET	Brunauer-Emmett-Teller
BODIPY	Boron dipyrromethene
BPA	Bisphenol A
CNOs	Carbon Nano-Onions
CNTs	Carbon Nanotubes
CVD	Chemical Vapour Deposition
DTG	Derivative Thermal Gravimetric
EFSA	European Food Safety Authority
E-N-OLCs	Engine Nitrogen doped Onion-like carbons.
E-ox-OLCs	Engine Oxidised Onion-like carbons.
FAO	Food and Agriculture Organization
GAC	Granular Activated Carbon
HRTEM	High Resolution Transmission Electron Microscopy
H-N-OLCs	Household Nitrogen Doped carbons.
H-ox-OLCs	Household Oxidised Onion-like carbons.
IUPAC	International Union of Pure and Applied Chemistry
JECFA	Joint Expert Committee on Food Additive
MCNOs	Magnetic Carbon Nano-Onions
NCO	Nano Carbon Onion
N-OLCs	Nitrogen Doped Onion-Like Carbons
OLCs	Onion-Like Carbons
ox-OLCs	Oxidised Onion-like carbons

ORR	Oxygen Reduction Reaction
PAHs	Polycyclic Aromatic Hydrocarbons
PNCs	Porous Nano-Carbons
pOLCs	Pristine Onion-like carbons.
SEM	Scanning Electron Microscopy
TGA	Thermogravimetric Analysis
USEPA	United States Environmental Protection Agency
WO	Waste Oil
WRI	World Resource Institute
XRD	X-ray Diffraction
FP	Flame pyrolysis
FWHM	Full Width at Half Maximum
NOR	Norfloxacin
PFO	Pseudo-First Order
PNCs	Porous Nano-Carbons
pOLCs	pristine OLCs
PSO	Pseudo-Second Order
PZC	Point of Zero Charge
SWCNTs	Single-Walled Carbon Nanotubes

CHAPTER 1

1. Introduction

1.1 Background and Motivation

Dyes are used to colour the final product in the paper, textile, leather, printing, food, cosmetics, plastics, and rubber industries [1] . Dye pollution from industrial effluents jeopardizes human health and the ecological balance. Azo dyes account for approximately half of the 800,000 tons of synthetic dye products produced each year [2] . Azo dyes are organic compounds bearing the functional group R−N=N−R′, in which R and R′ are usually aryl and substituted aryl groups [3]. Tartrazine is an azo dye found in pharmaceuticals, cosmetics [4] , and food additives [5] . This substance is highly toxic to humans because it causes hyperactivity and causes asthma, migraines, urticaria, angioedema, thyroid cancer, lupus, eczema, and other behavioural issues [6].

Azo dyes are generally resistant to light, biodegradation, temperature, ozonation, and oxidation as they contain aromatic compounds. Dyes accumulate in living organisms, causing severe diseases and function disorders [7] . The presence of colour in effluent has received significant critical attention from dyestuff manufacturers and textile companies [8] . Nowadays, there is a foremost focus about decolorization and wastewater treatment because several industries, such as those used in textiles, leather, and food processing, rely on dyes to colour their products [9].

For the treatment of dye wastewater, various techniques have been used in the past, including oxidation, filtration, irradiation, ion-exchange, membrane separation, and so forth [10]. Many researchers have thoroughly investigated the benefits, drawbacks, and limitations of each technique [9, 11,12] . Today, dyestuff manufacturers and paper industries rarely use the above-mentioned techniques to treat their wastewater effluents due to numerous drawbacks such as process complexity, low removal efficiencies, and extremely high cost. In terms of initial operational costs [13] , ease of operation, and equipment design simplicity, many researchers prefer the adsorption technique owing to its simplicity, effectiveness, and low cost [13].

Many materials, such as porous carbon, perovskite-type oxides, microcrystalline cellulose, chitosan, and zeolite, are employed as adsorbents. Importantly, carbon has been widely used

as the traditional adsorbent. Activated carbon, graphene, carbon nanotubes, and carbon quantum dots are among the common porous carbon materials used to study dye adsorption [14]. They pose a high specific surface area, a large porosity, a well-developed pore structure composed of micropores, mesoporous, and macropores, and a large number of oxygen-containing functional groups, all of which provide favourable adsorption sites [15].

Among a family of nano-structured carbons, onion-like carbons (OLCs) have emerged as a promising adsorbent material due to their hydrophobicity, porosity, and they have surface curvature and strain energy, which leads to their higher chemical reactivity [16], [17]. OLCs consist of multiple enclosed incomplete (or complete) fullerene layers and they have shown excellent adsorption capacity and cyclic compression performance [18].

Interestingly, studies have shown that in various OLCs applications, different oils can be used as precursors for the OLC synthesis. In a recent study, Shaikh *et al*. have used natural castor oil derived OLCs for electrochemical determination of nitrite [19] . Tripathi *et al*. used flaxseed oil based OLCs for visible light induced photocatalytic applications and label free detection of Al (III) ions [20]. Frying oil was also used by Jung *et al*. as a precursor of OLCs as the electrode material to fabricate high performance and durable supercapacitors [21] . While the above studies demonstrated the successful synthesis of OLCs from oil, pure oil was used, which could hinder the synthesis of OLCs in bulk due to its related cost. As such, this study is based on the use of waste oil for the synthesis of OLCs using a wick-oil flame pyrolysis method.

In this study, we have explored the conversion of environmental degrading waste materials such as waste oils (from engines, households, fast food restaurants, and laboratory paraffin oil) into useful adsorbing materials. These waste oils are used as precursors for the synthesis of OLCs, which are then used as adsorbents for the removal of tartrazine (a model azo dye) in water.

1.2 Purpose of the study

1.2.1 Aim of the study

The adsorption by carbon materials has been widely used by researchers for the removal of dyes in wastewater over the years [22]. However, the materials performance can be optimized by increasing their surface area and porosity. This increase can be achieved by incorporating

heteroatoms such as nitrogen and boron into the carbon matrix, and by introducing functional groups into the surface of the carbon matrix. This hypothesis leads to the following aim:

To synthesize, improve by modification, and characterize, OLCs derived from four different waste oils for the removal of tartrazine dye in wastewater by adsorption.

1.2.2 Objectives

- To synthesize pristine OLCs using precursors such as waste oils from a local restaurant, car engine, household frying oil, and laboratory bath oil by flame pyrolysis.
- To N-dope the pristine materials with ammonia gas as a source of nitrogen using the chemical vapour deposition (CVD) method and to functionalize the N-OLCs with nitric acid using the reflux-oxidation method.
- To apply and compare all the materials (pristine, N-doped, and functionalized) for the removal of tartrazine dye in wastewater.
- All the synthesized materials to be characterized using techniques such as: high resolution transmission electron microscopy (HRTEM), scanning electron microscopy (SEM), thermogravimetric analysis (TGA), Raman spectroscopy, Brunauer-Emmett-Teller surface area analysis, and X-ray powder diffraction (BET).

1.3 Justification

The demand for pure drinking water is increasing at an alarming rate, with estimates indicating that agriculture, industry, and households use 70%, 19%, and 11% of available water, respectively [23]. By 2030, approximately 47% of the world's population will face the challenge of clean water scarcity [24]. Currently, water contamination caused by the inability of the textile industries to properly dispose of their waste water is one of the major challenges that affects the whole world. Textile industries are major contributors to the global economy but also environmental pollution in many countries, including China and South Africa [25]. Azo dyes, which contain one or more azo groups , are the largest class (above 60%) among the various groups of textile dyes and one of the most widely used dyes in the textile industry [23]. Inefficient textile dyeing processes cause 15–50% of azo dyes that are not bound to fibres and fabrics to be released into the wastewater [26]. Some azo dyes can be carcinogenic without being cleaved into aromatic amines. However, the carcinogenicity of many azo dyes is due to their cleaved product such as benzidine. Benzidine induces various human and animal tumors [27]. Many azo dyes and their reductively cleaved products as well

as chemically related aromatic amines are reported to affect human health, causing allergies and other human maladies [28]. This study is based on remediation of azo-dye polluted water, and it is necessary to acknowledge the fact that it also plays a role in controlling oil spills. Oil spills are one of the biggest challenges faced by the wastewater treatment industry worldwide.

Based on wastewater properties, wastewater can be treated physically, chemically, biologically, or by utilizing a combination of these methods [29]. It has been reported that physical approaches such as adsorption are used to treat dye-containing wastewater with a very high removal efficiency ranging from 85% to 99% [30]. However, this method varies with the type of adsorbent. Thus, it is necessary for researchers to focus on developing high quality and eco-friendly adsorbents to add value on water treatment technology.

1.4 Outline of the dissertation

The layout of the dissertation followed an order of:

Chapter 1

This chapter gives background information of the study as well as motivation, justification, and research objectives are briefly stated.

Chapter 2

It presents a review of literature to put the study into perspective and provide background information on water scarcity, an overview on azo dyes, dye remediation strategies, and in particular, gives details of the adsorption technique. The chapter also entails the synthesis method, structural architecture, modifications, and applications of OLCs as nanomaterial adsorbents.

Chapter 3

This chapter presents the synthesis of pristine OLCs from different carbon precursors using an oil-wick pyrolysis method. The physicochemical properties of the synthesized materials using various analysis such as XRD, SEM, HRTEM, Raman spectroscopy, and BET are reported.

Chapter 4

This chapter presents the methods used to modify the pristine OLCs. It briefly gives background information on the significance of modifying the carbon nanomaterials through

N-doping and functionalisation. It discusses the changes in physicochemical properties of OLCs post modification and compares modified OLCs with pristine.

Chapter 5

This chapter discusses and compares the adsorption findings from carbons derived from four different waste oils. The superior adsorbents amongst the four pristine OLCs were found to be those that were N-doped and functionalised. Their adsorption capabilities are explored, including kinetics and isotherms.

Chapter 6

This final chapter of the dissertation gives the concluding remarks showing the importance of the study and covers the way forward with possible future work.

REFERENCES

[1] S. Sahnoun, M. Boutahala, C. Tiar, and A. Kahoul, "Adsorption of tartrazine from an aqueous solution by octadecyltrimethylammonium bromide-modified bentonite: Kinetics and isotherm modeling," *Comptes Rendus Chimie*, vol. 21, no. 3–4, pp. 391–398, Mar. 2018, doi: 10.1016/J.CRCI.2018.01.008.

[2] M. Greluk and Z. Hubicki, "Efficient removal of Acid Orange 7 dye from water using the strongly basic anion exchange resin Amberlite IRA-958," *Desalination*, vol. 278, no. 1–3, pp. 219–226, Sep. 2011, doi: 10.1016/J.DESAL.2011.05.024.

[3] "azo compounds," *The IUPAC Compendium of Chemical Terminology*, Sep. 2008, doi: 10.1351/GOLDBOOK.A00560.

[4] A. Mittal, J. Mittal, and L. Kurup, "Adsorption isotherms, kinetics and column operations for the removal of hazardous dye, Tartrazine from aqueous solutions using waste materials—Bottom Ash and De-Oiled Soya, as adsorbents," *J Hazard Mater*, vol. 136, no. 3, pp. 567–578, Aug. 2006, doi: 10.1016/J.JHAZMAT.2005.12.037.

[5] M. Mincea *et al.*, "Adsorption of Three Commercial Dyes onto Chitosan Beads Using Spectrophotometric Determination and a Multivariate Calibration Method," *J Water Resour Prot*, vol. 5, no. 4, pp. 446–457, Apr. 2013, doi: 10.4236/JWARP.2013.54044.

[6] M. Wawrzkiewicz and Z. Hubicki, "Removal of tartrazine from aqueous solutions by strongly basic polystyrene anion exchange resins," *J Hazard Mater*, vol. 164, no. 2–3, pp. 502–509, May 2009, doi: 10.1016/J.JHAZMAT.2008.08.021.

[7] R. K. Gautam *et al.*, "Synthesis of bimetallic Fe–Zn nanoparticles and its application towards adsorptive removal of carcinogenic dye malachite green and Congo red in water," *J Mol Liq*, vol. 212, pp. 227–236, Dec. 2015, doi: 10.1016/J.MOLLIQ.2015.09.006.

[8] G. Annadurai, R. S. Juang, and D. J. Lee, "Use of cellulose-based wastes for adsorption of dyes from aqueous solutions," *J Hazard Mater*, vol. 92, no. 3, pp. 263–274, Jun. 2002, doi: 10.1016/S0304-3894(02)00017-1.

[9] T. Robinson, G. McMullan, R. Marchant, and P. Nigam, "Remediation of dyes in textile effluent: a critical review on current treatment technologies with a proposed alternative," *Bioresour Technol*, vol. 77, no. 3, pp. 247–255, May 2001, doi: 10.1016/S0960-8524(00)00080-8.

[10] W. Xiao *et al.*, "Adsorption of organic dyes from wastewater by metal-doped porous carbon materials," *J Clean Prod*, vol. 284, p. 124773, Feb. 2021, doi: 10.1016/J.JCLEPRO.2020.124773.

[11] P. Klán and M. Vavrik, "Non-catalytic remediation of aqueous solutions by microwave-assisted photolysis in the presence of H2O2," *J Photochem Photobiol A Chem*, vol. 177, no. 1, pp. 24–33, Jan. 2006, doi: 10.1016/J.JPHOTOCHEM.2005.05.008.

[12] S. Sahnoun, M. Boutahala, C. Tiar, and A. Kahoul, “Adsorption of tartrazine from an aqueous solution by octadecyltrimethylammonium bromide-modified bentonite: Kinetics and isotherm modeling,” *Comptes Rendus Chimie*, vol. 21, no. 3–4, pp. 391–398, Mar. 2018, doi: 10.1016/J.CRCI.2018.01.008.

[13] A. Gürses, S. Karaca, Ç. Doğar, R. Bayrak, M. Açikyildiz, and M. Yalçin, “Determination of adsorptive properties of clay/water system: methylene blue sorption,” *J Colloid Interface Sci*, vol. 269, no. 2, pp. 310–314, Jan. 2004, doi: 10.1016/J.JCIS.2003.09.004.

[14] W. Xiao *et al.*, “Adsorption of organic dyes from wastewater by metal-doped porous carbon materials,” *J Clean Prod*, vol. 284, p. 124773, Feb. 2021, doi: 10.1016/J.JCLEPRO.2020.124773.

[15] W. Xiao *et al.*, “Adsorption of organic dyes from wastewater by metal-doped porous carbon materials,” *J Clean Prod*, vol. 284, p. 124773, Feb. 2021, doi: 10.1016/J.JCLEPRO.2020.124773.

[16] O. Mykhailiv, H. Zubyk, and M. E. Plonska-Brzezinska, “Carbon nano-onions: Unique carbon nanostructures with fascinating properties and their potential applications,” *Inorganica Chim Acta*, vol. 468, pp. 49–66, Nov. 2017, doi: 10.1016/J.ICA.2017.07.021.

[17] O. Mykhailiv *et al.*, “Improvement of the Structural and Chemical Properties of Carbon Nano-onions for Electrocatalysis,” *ChemNanoMat*, vol. 3, no. 8, pp. 583–590, Aug. 2017, doi: 10.1002/CNMA.201700161.

[18] A. Shaikh, B. K. Singh, and S. Parida, “Natural oil derived carbon nano-onions as a sensitive electrocatalyst for nitrite determination,” *Mater Chem Phys*, vol. 235, p. 121744, Sep. 2019, doi: 10.1016/J.MATCHEMPHYS.2019.121744.

[19] K. Malika Tripathi, T. Sang Tran, Y. Jin Kim, and T. Kim, “Green Fluorescent Onion-Like Carbon Nanoparticles from Flaxseed Oil for Visible Light Induced Photocatalytic Applications and Label-Free Detection of Al(III) Ions,” *ACS Sustainable Chemistry & Engineering*, vol. 5, no. 5, pp. 3982–3992, Apr. 2017, doi: 10.1021/acssuschemeng.6b03182.

[20] S. Jung *et al.*, “Carbon nano-onions from waste oil for application in energy storage devices,” *New Journal of Chemistry*, vol. 44, no. 18, pp. 7369–7375, May 2020, doi: 10.1039/d0nj00699h.

[21] J. Ahlawat, S. Masoudi Asil, G. Guillama Barroso, M. Nurunnabi, and M. Narayan, “Application of carbon nano onions in the biomedical field: Recent advances and challenges,” Feb. 07, 2021, *Royal Society of Chemistry*. doi: 10.1039/d0bm01476a.

[22] S. Ho and S. Ho, “Removal of Dyes from Wastewater by Adsorption onto Activated Carbon: Mini Review,” *Journal of Geoscience and Environment Protection*, vol. 8, no. 5, pp. 120–131, May 2020, doi: 10.4236/GEP.2020.85008.

[23] S. Thangaraj, P. O. Bankole, and S. K. Sadasivam, “Microbial degradation of azo dyes by textile effluent adapted, Enterobacter hormaechei under microaerophilic condition,” *Microbiol Res*, vol. 250, p. 126805, Sep. 2021, doi: 10.1016/J.MICRES.2021.126805.

[24] A. Islam *et al.*, “Step towards the sustainable toxic dyes removal and recycling from aqueous solution- A comprehensive review,” *Resour Conserv Recycl*, vol. 175, p. 105849, Dec. 2021, doi: 10.1016/J.RESCONREC.2021.105849.

[25] C. Olisah, J. B. Adams, and G. Rubidge, “The state of persistent organic pollutants in South African estuaries: A review of environmental exposure and sources,” *Ecotoxicol Environ Saf*, vol. 219, p. 112316, Aug. 2021, doi: 10.1016/J.ECOENV.2021.112316.

[26] K. Singha, P. Pandit, S. Maity, and S. R. Sharma, “Harmful environmental effects for textile chemical dyeing practice,” *Green Chemistry for Sustainable Textiles: Modern Design and Approaches*, pp. 153–164, Jan. 2021, doi: 10.1016/B978-0-323-85204-3.00005-1.

[27] K. T. Chung, “Azo dyes and human health: A review,” *J Environ Sci Health C Environ Carcinog Ecotoxicol Rev*, vol. 34, no. 4, pp. 233–261, Oct. 2016, doi: 10.1080/10590501.2016.1236602.

[28] W. G. Levine, “Metabolism of AZO dyes: Implication for detoxication and activation,” *Drug Metab Rev*, vol. 23, no. 3–4, pp. 253–309, 1991, doi: 10.3109/03602539109029761/ASSET//CMS/ASSET/2079F919-2DCF-4ED4-90C8-FDB1CFA6D650/03602539109029761.FP.PNG.

[29] R. Al-Tohamy *et al.*, “A critical review on the treatment of dye-containing wastewater: Ecotoxicological and health concerns of textile dyes and possible remediation approaches for environmental safety,” *Ecotoxicol Environ Saf*, vol. 231, p. 113160, Feb. 2022, doi: 10.1016/J.ECOENV.2021.113160.

[30] S. Samsami, M. Mohamadi, M. H. Sarrafzadeh, E. R. Rene, and M. Firoozbahr, “Recent advances in the treatment of dye-containing wastewater from textile industries: Overview and perspectives,” *Process Safety and Environmental Protection*, vol. 143, pp. 138–163, Nov. 2020, doi: 10.1016/J.PSEP.2020.05.034.

CHAPTER 2

Literature review

2. Introduction

This chapter gives a review of literature to put the study into perspective and provide background information on CNOs, referred to in this dissertation as OLCs, as well as their synthesis and their application as adsorbents. An overview on azo dyes, and in particular, tartrazine is also provided in the chapter. The chapter also gives a brief overview of reaction kinetics as applied to studied system.

2.1 Clean water scarcity and pollution in South Africa

South Africa is a water-scarce country and based on current usage and trends, it is estimated that by 2025, the water demand will exceed its availability [1] . Urbanization and industrialization are expected to further place continuous pressure on the country's water supply unless appropriate corrective action is taken. Inadequate water supply from municipalities has caused many people to resort to the use of renewable water resources such as springs and self-supply (surface and groundwater sources) as an alternative source, especially in the developing world [2] . Hence, the protection of water treatment systems against possible biological and chemical contaminants is becoming a critical issue in the water sector as is the impact of an increase in the rate at which freshwater is being converted into domestic, industrial, hospitals, and agricultural wastewater [3].

The World Resources Institute (WRI) scored and ranked future water stress—a measure of competition and depletion of surface water—in 167 countries by 2020, 2030, and 2040 and revealed that about 33 countries will face extremely high-water stress in 2040 (see **Figure 2.1**). South Africa is amongst the countries that could face significant increase in water stress by 2040. This means that businesses, farms, and communities in these countries may be more vulnerable to scarcity than they are today [4] . South Africa's Metropolitan areas such as Nelson Mandela Bay, Gauteng, eThekwini, and many other small municipalities are water-stressed, and this will eventually affect everyone in South Africa. This has resulted in the metropolitan areas and municipalities to occasionally introduce water restrictions [5] . The areas that had limited water problems before the projections are at their worst and their water problems are no less than that of Cape Town. Thus, the Cape Town drought that intensified in 2017/2018 and then subsided later in 2019, not forgetting the countdown to "day zero",

received much attention, as the city is known worldwide as a tourist destination and one of South Africa's economic hub [6].

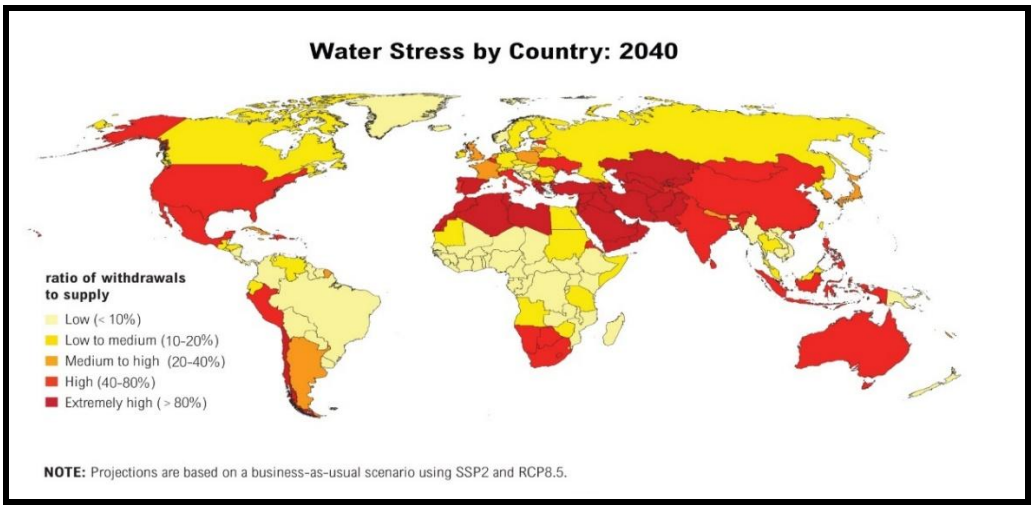

Figure 2.1: Future Projection Water Scarcity, adapted without modification from Maddocks *et al.* [7].

Water pollution can be seen as any undesirable change in the state of water, when contaminated with harmful substances. Human activity such as mining, agriculture, industrialisation, and domestic waste (**see Figure 2.2**) are the major factors contributing to water-pollution [8]. There are, however, other various micro-biological agents that include bacteria, viruses and protozoa which can also cause water pollution and may cause various water-borne diseases [9]. Due to water pollution, the entire ecosystem gets disturbed. This becomes more frightening and life threatening when a large proportion of the sewage emanating from South African urban areas is not treated properly prior to discharge [10]. The reasons for this situation are twofold: the sewer systems are insufficient, or sewage treatment plants are overloaded. This is particularly true in densely populated areas and in those areas where summer storm runoff enters sewerage systems [11].

Industrial development has been identified as another aspect of human activity that has left its mark on South Africa's water resources. Many industrial processes produce waste products that contain hazardous chemicals, and these are sometimes discharged directly into sewers, rivers, or wetlands. Even those waste products that are disposed of in landfills or slag heaps, for example, may release substances that eventually seep into nearby watercourses resulting

in both wildlife and human deaths [11]. The common sources of water pollution are shown in **Figure 2.2**.

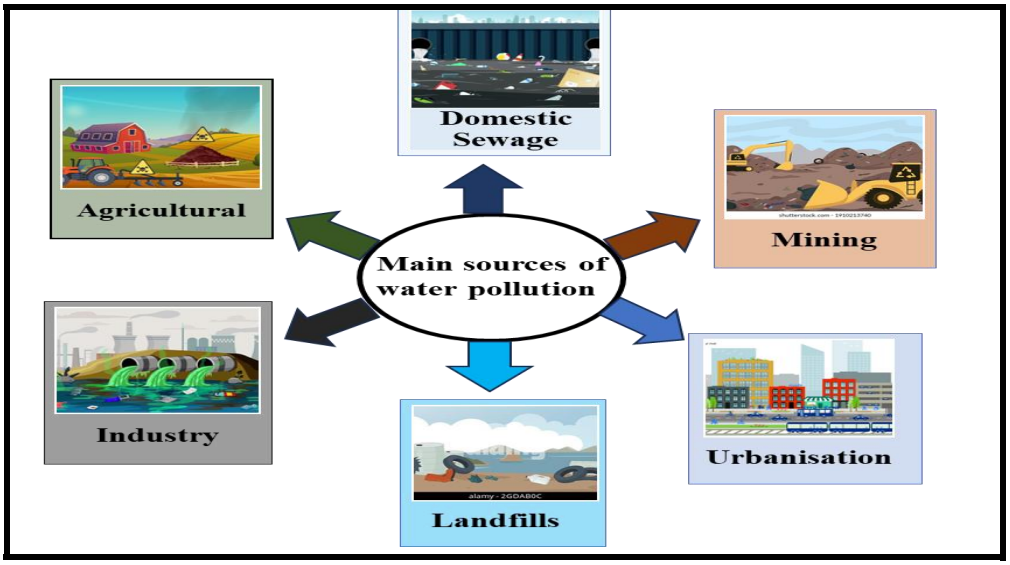

Figure 2.2: Sources of water pollution.

2.2. The synthetic azo dyes in the textile industry

Textile wastewater has been found to contain a wide range of toxic dyes, and heavy metals such as mercury, chromium, cadmium, lead, and arsenic which are required in the production of textile dye colour pigments. The large amounts of water used in fabric manufacturing results in equally large amounts of wastewater containing high levels of dissolved solids, organics, metals, salts, and dyes [12]. Azo dyes, which contain one or more azo groups , are the largest class (above 60%) among the various groups of textile dyes and the most widely used dye in the textile industry [12,13] . Inefficient textile dyeing processes cause 15–50% of azo dyes that are not bound to fibres and fabrics to be released into generated wastewater [14,15].

Azo compounds are chemically represented as R–N=N-R', where –N=N- is the azo group, and the R or R' can be either aryl or alkyl compounds. The International Union of Pure and Applied Chemistry (IUPAC) defines azo compounds as a "derivative of diazene (diimide), HN=NH, wherein both hydrogens are substituted by hydrocarbyl group, e.g., PhN=NPh azobenzene or diphenyldiazene" [16] . Azo dyes are compounds consisting of a diazotized amine coupled to an amine or a phenol and contain one or more azo linkages. The essential precursors of azo dyes are aromatic amines. Azo compounds have vivid colours and comprise about two-thirds of all synthetic dyes and are by far the most widely used and structurally

diverse class of organic dyes in commerce [17]. At least 3,000 azo dyes available have been used in the pharmaceutical and paper industries as well as in printing inks, paints, varnish, lacquer, and wood stains [18]. About 10–15% of azo dyes are discharged into water during the dyeing process [19]. Data indicates that till 1999, about 50,000 tons of azo dyes were discarded into the environment, which severely polluted the surrounding ecosystem. Recently, it has been estimated that the dye concentration drastically increased by 6.9 million tons in 2017 in wastewater [20].

Azo dyes discharged into water reduce light penetration that affects the photosynthesis of plants, impairing the performance of algae and growing aquatic plants. Furthermore, dyes ingested by fish and other living organisms can be metabolized in their bodies into toxic intermediates, which can have a negative impact on the health of both the fish and their predators [21]. Humans and other mammals can be exposed to azo dyes in industrial effluents through oral ingestion or direct skin contact as demonstrated on **Figure 2.3** [22].

According to Kadirvelu *et al.*, most dyes are carcinogenic, mutagenic, teratogenic, and can also damage the organs of human beings such as kidneys, lungs, liver, brain, reproductive system, and central nervous system [23]. Intestinal microflora in the human gut converts azo dyes into toxic amino acids, which have a negative impact on various tissues in the human body [24]. In the 1930s, some azo derivatives such as 4-dimethyl aminoazobenzene (Butter Yellow, CI Solvent Yellow 2, CI 11020) and *o*-aminoazotoluene were found to be carcinogenic to the liver and bladder after feeding [25]. As well as having carcinogenic and mutagenic activity, azo dyes can also alter biochemical markers and they can provoke allergic reactions [26]. Azo dyes often used in manufacturing of pharmaceuticals are: E 102 (Europe number) Tartrazine, E110 Sunset Yellow FCF, Ponceau 4R (Cochineal Red A), Azorubine (Carmoisine), Amaranth, E133 Brilliant Blue and E129 Allura Red [26].

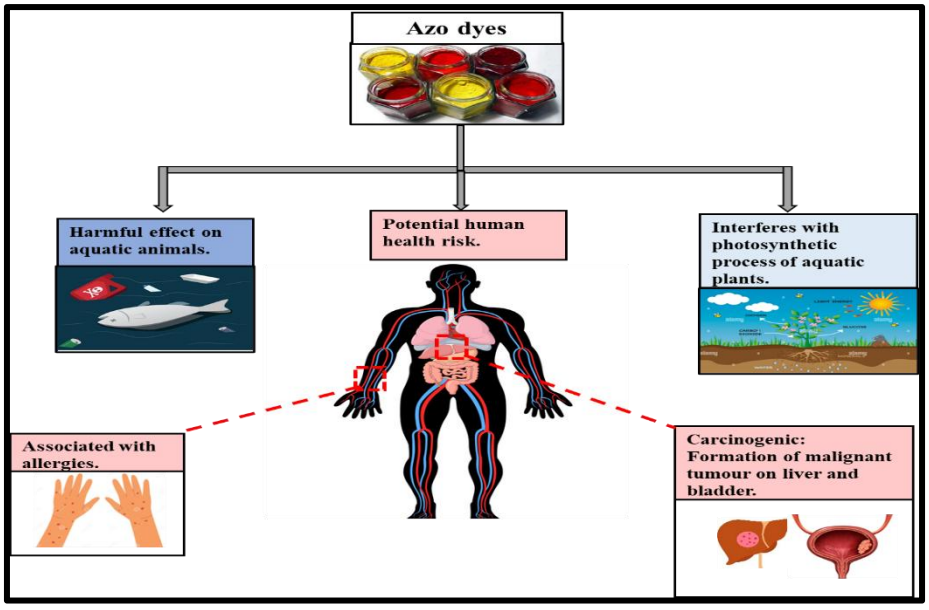

Figure 2.3: Harmful effects of azo dyes on humans and environment.

2.2.1 General overview of tartrazine dyes

Tartrazine, also known as lemon yellow, is a highly water-soluble, anionic, and polar azo dye used in many applications. It is one of the most important azoic dyes and is a widely employed synthetic yellow food colouring agent [27]; sometimes, it may be found in small amounts in gudrons of coals, or even in illicit drugs like ecstasy [28]. Tartrazine is employed under the code E102 in the food industry by the Food and Agriculture Organization (FAO) and European Food Safety Authority (EFSA). It is also used in the cosmetic and drug sectors, being biologically active when interacting with living matter [27]. Tartrazine can be prepared from 4-aminobenzenesulphonic acid (sulfonic acid diamine) by dissolving it in a diazotate compound using hydrochloric acid and sodium nitrite; then coupling the diazo compound with 4,5-dihydro-5-oxo-1-(40 -sulphophenyl)-1H-pyrazole-3-carboxylic acid (Pyrazolone T) [29] . The resulting dye obtained is then purified and isolated as the sodium salt. This is shown in **Figure 2.4**.

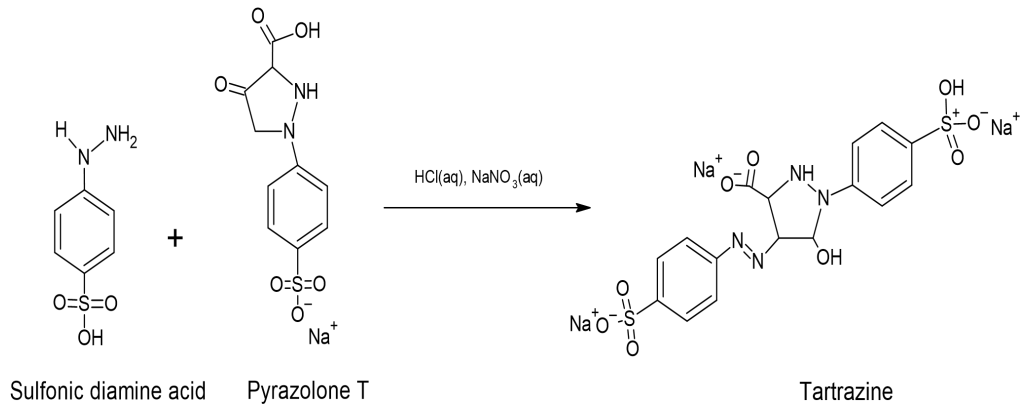

Figure 2.4: Structural representation for the synthesis of tartrazine [29].

2.2.2. Health implications of tartrazine

Studies have shown that the intake of tartrazine can cause a series of biochemical markers changes at both high doses and low doses, which are significantly harmful to asthma patients and children [30]. The acceptable daily intake for tartrazine is allocated as 7.5 mg/kg /day by JECFA (Joint Expert Committee on Food Additive) in 1964, but many countries have banned or restricted tartrazine [30]. Tartrazine is reduced inside an organism to an aromatic amine as it is a nitrous derivative (azo class). The chief metabolite recognized so far is sulfanilic acid. Tartrazine has been identified to cause allergies such as urticaria and asthma. The emphasis of studies on its carcinogenesis and mutagenesis is as a result of its metabolic conversion into an aromatic amine (sulfanilic acid) via the gut microflora and possibly by mammalian azo reductase in the hepatic or intestinal wall after consumption [31,32]. When these azo dyes are reduced totally into aromatic amines, they are oxidized to N-hydroxy derivatives by the enzymatic system of P450 [33]. This mechanism of biotransformation takes place in many species including humans, which is responsible for various disorders including anaemia, pathological lesions in the brain, liver, kidney and spleen, besides allergic reactions, tumours, and cancer [31]. However, Tanaka *et al*., did not determine any adverse role of tartrazine in the development of neurobehavior, and the harmful impact on reproductive markers was not established at tartrazine doses of 1225 and 773 mg/kg BW/day for females and males, respectively [34]. In earlier assessments, there were no suggestions of tartrazine-linked contrary effects on reproduction. However, the superoxide anion, hydroxyl radicals and H_2O_2 reactive oxygen species might be formed in the nitrosamines metabolism and raise oxidative stress [35].

2.2.3 Remediation of dye polluted water

Amine groups present in azo dyes are responsible for the toxicity of azo dyes. Water soluble reactive dyes in water also cause serious problems for the aquatic environment [36] . Therefore, dyes are a dangerous class of organic pollutants in the environment and are released into water resources in direct and indirect ways, and dye treatment from wastewater or drinking water is a great environmental concern. Many methods (shown in **Figure 2.5**) such as physical (sedimentation, filtration, floatation, coagulation, reverse osmosis, solvent extraction, and adsorption), chemical (neutralization, reduction, oxidation, catalysis, ion exchange and electrolysis), and biological (stabilization, aerated lagoons, trickling filters, activated sludge, fungal treatment, flocculation, and anaerobic digestion) are being utilized for the removal of dyes from water [37] . These methods are reliable and show results for removal of toxic dyes from water. However, they also have some limitations, like high processing charges, being less effective for low concentration and are tough to handle. Adsorption is most effective method for the removal of toxic dyes from water, in terms of its simplicity, low cost, easy handling and operation [38]. Today, the adsorption phenomenon is beneficial in implementing water purification. Dyes contain a chromogenic group which helps the dye molecules to easily adsorb onto the adsorbent surfaces [39].

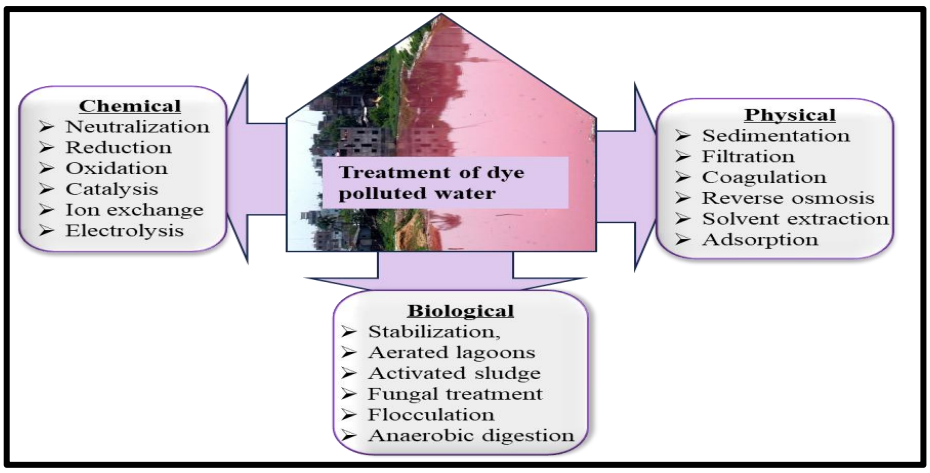

Figure 2.5: Recently reported dye polluted water remediation methods.

2.2.4 Adsorption

Adsorption is a surface phenomenon where a molecule (solute) is attached to the surface of a solid substance by chemical and physical bonds [40] . Such substances that provide the surface (space) are called adsorbents, while the molecule which is removed from the liquid

phase is known as the adsorbate [41,42]. A schematic representation of the removal of dye using an adsorbent from the wastewater is shown in **Figure 2.5.** Out of all treatment methods that have been developed, adsorption is the one of the most pertinent and promising methods for removing organic and inorganic micro pollutants [43,44]. Most often, the process is used to remove synthetic macrobiotic compounds during drinking water treatment. The process has copious advantages [45] such as:

- Simple to operate and to design.
- Handling micro level of pollutants.
- Continuous and batch processes.
- Toxicity removal.
- Low investment cost.
- Environmentally benign.
- Probability of adsorbent reuse and regeneration.

Adsorption is effective in treating the dissolved pollutants that remain even after chemical oxidation processes or biological treatment [46,47].

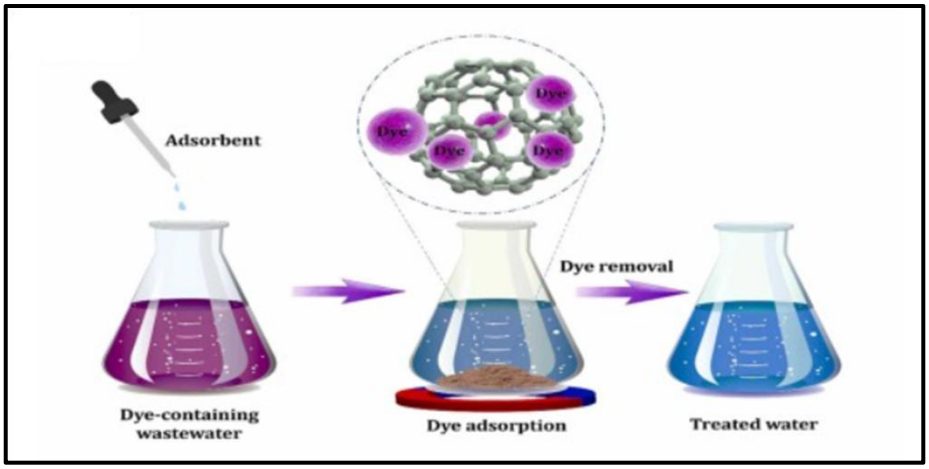

Figure 2.6: Adsorption of a dye process [48].

2.2.4.1 Main concepts and bases of adsorption

Adsorption is a mass transfer process that involves the sorption of gases or solutes by solid or liquid surfaces [49]. The adsorption on the solid surface is due to the atoms on the solid surface having residual surface energy due to unbalanced forces. When a substance collides with the solid surface, it is attracted by these unbalanced forces and stays on the solid surface. The adsorption process can be divided into two categories: physical adsorption and chemical

adsorption (**Table 2.1**). Physical adsorption is produced by the interaction of intermolecular forces (i.e., van der Waals forces), for example, the adsorption of activated carbon for a gas. Physical adsorption is generally carried out at a low temperature, and has a fast adsorption rate, low adsorption heat, and is nonselective [50] . As the effect of an intermolecular attraction is weak, the structure of the adsorbate molecules hardly changes, and the adsorption energy is small, and the adsorbed substance is easily separated again. The adsorption due to the action of chemical bonds is called chemical adsorption [51]. A chemical adsorption process includes the formation and destruction of chemical bonds. The absorption or release of adsorption heat is large, and the activation energy required is also large. Physical adsorption and chemical adsorption are not isolated and often occur together. In wastewater treatment technology, most of the adsorption is the result of these two kinds of adsorption processes [52].

Table 2.1: Differences between chemical adsorption and physical adsorption [52].

	Adsorption categories	
	Physical adsorption	**Chemical adsorption**
Adsorption force	Van der Waals force	Chemical bond force
Selectivity	Nonselective adsorption	Selective adsorption
Adsorption layer	Single or Multiple layers	Single layer
Adsorption heat	Low	High
Adsorption rate	Fast	Slow
Stability	Instable	Stable

2.2.4.2 Factors affecting adsorption process

The efficiency of liquid phase adsorption, and therefore the optimal operation of the water treatment process, depends on several parameters. The sorption performance is influenced by physico-chemical factors, the type of pollutant (in this study, the dyes) and its chemical structure, and the properties of the adsorbent used [53]. Such physicochemical parameters are adsorbate-adsorbent interaction, adsorbent surface area, adsorbent to adsorbate ratio,

adsorbent particle size, temperature, pH and contact time, which are responsible for the removal rate of pollutants (**Figure 2.7**) [42].

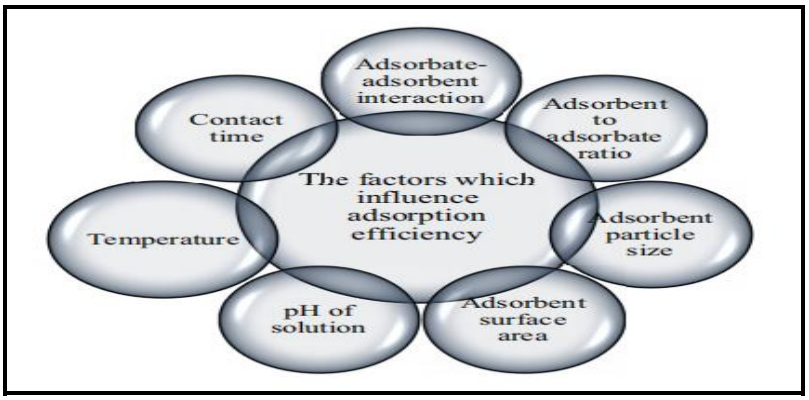

Figure 2.7: Factors affecting adsorption efficiency in adsorption process [42].

2.2.4.2.1 Effect of pH (solution)

The pH of the solution influences the adsorption of a dye on the adsorbate e.g. on a OLCs. It affects the adsorption process as OH^- and H^+ ions have an interaction with the adsorbents. At a pH (solution) higher than that of pH_{pzc} (i.e. point of zero charge), it results in electrostatic interactions due to a negative surface that is favourable in absorbing cations [54] . The decrease in pH results in the neutralization of the charge, wherein the adsorption cations decrease [54].

2.2.4.2.2 Effect of initial adsorbent (dye) concentration

The initial concentration provides an important driving force for alleviating the mass transfer resistance of dye molecules between the aqueous solution and solid phases. In most cases, at low concentration, the ratio of the initial number of dye molecules to the available surface area is low, subsequently, the fractional adsorption become independent on the initial concentration [55]. At higher concentration, the available sites for adsorption become fewer (saturation of the sorption sites) and hence, the percentage removal of dye is dependent upon the initial concentration [56] . At fixed adsorbent doses, the adsorption capacity (mg/g) increases proportional to the dye concentration, but the percentage of removal decreases, indicating a residual dye concentration is higher than the initial concentration [57].

2.2.4.2.3 Effect of contact time

Generally, adsorption capacity and dye removal efficiency increase with prolonged contact time. Initially the amount of dye adsorbed onto the carbon surface increases rapidly, and at some point, the process slows down and reaches a plateau (constant value) [58]. At this point, the amount of the dye desorbing from the adsorbent is in a state of dynamic equilibrium with the amount of the dye being adsorbed onto the activated carbon. The time required to attain this state of equilibrium is termed the equilibrium time [59]. This phenomenon is attributed to a reduction in solute adsorption due to the lack of available open sites for dye adsorption (saturation), and in turn supported film diffusion [60].

2.2.4.2.4 Temperature

Temperature has two major effects on the adsorption process. Firstly, increasing temperature is known to enhance the diffusion rate of adsorbate molecules across the external boundary layer and in the internal pores of adsorbent particle, owing to the decrease in viscosity of the solution [61]. In addition, temperature alteration will change the equilibrium capacity of the adsorbent for a particular adsorbate (increase the tendency of de-aggregation) [62] . The adsorption equilibrium usually decreases with a rise in temperature, indicating the exothermic nature of the adsorption reaction. The reduction in adsorption capacity is contributed primarily by the enhancement of the desorption step in the sorption mechanism and the weakening of sorptive forces (physical bonding) between active sites on the activated surface and the dye species, or between adjacent dye molecules on the sorbed phase [62].

2.2.4.2.5 Nature of adsorbent

Substances that provide large surface area for a give mass are effective as adsorbents [63]. Since adsorption is a surface phenomenon, the number of adsorptions increases according to the amount of surface area of the adsorbent [64]. The higher the surface area of an adsorbent, the finer the surface division or the rougher the surface texture as a result of which the adsorption will be larger. For example, silica gel and charcoal are effective adsorbents due to the high surface are and porous nature [65].

2.2.4.2.6 Adsorbent surface area

When the surface area of the adsorbent is increased there is an increase in the adsorption of the adsorbate of interest. e.g. a dye substance. This is because when an increase in the

surface area gives a greater number of adsorbing sites. Finely divided solids and some porous substances are good adsorbents [65].

2.3 Adsorption isotherms

When a system reaches equilibrium, the adsorption of the substance from the liquid phase to the solid surface in the system results in a thermodynamically defined distribution of the substance between the two phases; that is, the adsorption rate of the solute on the adsorbing surface is the same as the desorption rate from the adsorbing surface. At this point, no more net adsorption occurs [66].

Several mathematical relationships have been developed to describe the equilibrium distribution of solutes between the solid and liquid phases, at constant temperature, which helps to explain the adsorption process. The most widely used models are the Langmuir and Freundlich isotherms. They can be used to describe the adsorption capacity of a specific adsorbent [66].

2.3.1 The Langmiur isotherm

The Langmiur equation of a solid-liquid system is generally written as:

$$q_e = \frac{K_L C_e}{1 + bC_e} \tag{1}$$

In the formula, q_e is the adsorption capacity per unit weight of the adsorbent (mg/g), C_e is the concentration of the adsorbate in the equilibrium solution after the adsorption is completed (mg/L), and K_L is the amount of adsorbate adsorbed per unit mass of the adsorbent to form a complete monolayer (mg/g) on the surface, and b is a constant related to adsorption energy or net enthalpy [66]. The linear form of Langmuir expression is:

$$\frac{C_e}{q_e} = \frac{1}{K_L} + \frac{b}{K_L} C_e \tag{2}$$

A graph of the relationship between C_e/q_e and C_e gives a straight line with a slope of b/K_L, and $1/K_L$ intercepts. The basic characteristics of the Langmuir isotherm can be expressed by a

dimensionless constant, a separation factor or an equilibrium parameter r, which is defined as follows:

$$r = \frac{1}{1 + bC_0} \tag{3}$$

where C_0 is the initial concentration of the adsorbate (mg/L), and b is the Langmuir constant (L/mg) related to the adsorption energy. The value of r represents the form of the adsorption isotherm to understand whether the adsorption is unfavorable (r > 1), linear (r = 1), favorable (0 < r <1), or irreversible ((r = 0) [67].

2.3.2 The Freundlich model

The Freundlich isotherm can be applied to the non-ideal adsorption on heterogeneous surfaces, as well as multilayer adsorption, and is expressed by the following equation:

$$q_e = K_f C_e^{\frac{1}{n}} \tag{4}$$

A linear form of this expression is

$$logq_e = logK_f + \frac{1}{n} logC_e$$

where K_f is the Freundlich equilibrium constant, which represents the adsorption capacity, n is the Freundlich constant, which represents the affinity of the adsorbate for the surface of the adsorbent, q_e is the amount of adsorbate per unit weight of the adsorbent (mg/g), and C_e is the concentration after the adsorption is completed (mg/L) [67].

2.4 Adsorption kinetic models

At present, adsorption reaction models have been widely developed or employed to describe the kinetic process of adsorption, however, there still exist some problems [68]. For example, a pseudo-second-order rate equation based on chemical adsorption was employed to describe organic pollutants adsorption onto several non-polar polymeric adsorbents. This is essentially a process of physical adsorption [69]. In addition, Lagergren (1898) models were still widely applied to data modelling, though no adsorption mechanisms wase reasonably available [70].

Attention has been paid to several widely used batch kinetic models and their boundary conditions.

2.4.1 Pseudo-first-order rate equation

Lagergren et al. presented a first-order rate equation to describe the kinetic process of liquid-solid phase adsorption of oxalic acid and malonic acid onto charcoal, which is believed to be the earliest model pertaining to the adsorption rate based on an adsorption capacity. It can be presented as follows:

$$\frac{dq_t}{dt} = k_{pl}(q_e - q_t), \quad (5)$$

where q_e and q_t (mg/g) are the adsorption capacities at equilibrium and time t (min), respectively. k_{pl} (min^{-1}) is the pseudo-first-order rate constant for the kinetic model. Integrating Eq. (5) with the boundary conditions of $q_t = 0$ at $t = 0$ and $q_t = q_t$ at $t = t$, yields [56]

$$\ln\left(\frac{q_e}{q_e - q_t}\right) = k_{pl}t, \quad (6)$$

which can be rearranged to:

$$\log(q_e - q_t) = \log q_e - \frac{k_{pl}}{2.303}t. \quad (7)$$

To distinguish kinetic equations based on adsorption capacity from solution concentration, Lagergren's first order rate equation has been called pseudo-first-order [71]. In recent years, it has been widely used to describe the adsorption of pollutants from wastewater in different fields, such as the adsorption of methylene blue from aqueous solution by broad bean peels and the removal of malachite green from aqueous solutions using oil palm trunk fibre [72].

2.4.2 Pseudo-second-order rate equation

In 1995, Ho et al. described a kinetic process for the adsorption of divalent metal ions onto peat, in which the chemical bonding among divalent metal ions and polar functional groups on peat, such as aldehydes, ketones, acids, and phenolics are responsible for the cation-exchange capacity of the peat. Therefore, the peat-metal reaction may be presented as shown in Eq. (8) and (9), which can be dominant for the adsorption of Cu^{2+} ions onto peat [73].

$$2P^- + Cu^{2+} \leftrightarrow CuP_2 \quad (8)$$

and

$$2HP + Cu^{2+} \leftrightarrow CuP_2 + 2H^+ \quad (9)$$

where P^- and HP are active sites on the peat surface. The main assumptions for the above two equations were that the adsorption may be second order, and the rate limiting step may be chemical adsorption involving sharing or the exchange of electrons between the peat and divalent metal ions. In addition, the adsorption follows the Langmuir equation [73].

The rate of adsorption described by Eqs. (8) and (9) is dependent upon the amount of divalent metal ions on the surface of the peat at time t and that adsorbed at equilibrium. Therefore, the rate expression may be given as:

$$\frac{d(P)}{d_t} = k_{P^2}[(P)_0 - (P)_t]^2, \quad (10)$$

where $(P)_0$ denote the amount of equilibrium sites available on the peat, $(P)_t$ denotes the number of active sites occupied on the peat at time t, and k_{p2} (g/(mg·min)) is the pseudo-second-order rate constant of adsorption. The driving force, $(q_e - q_t)$, is proportional to the available fraction of active sites [74]. Then, it yields:

$$\frac{dq_t}{dt} = k_{p^2}(q_e - q_t)^2, \quad (11)$$

Similarly, Ho's second-order rate equation has been called a pseudo-second-order rate equation to distinguish kinetic equations based on adsorption capacity from the concentration of the solution [74]. This equation has been successfully applied to the adsorption of metal ions, dyes, herbicides, oils, and organic substances from aqueous solutions [75].

2.4.3 Second-order rate equation

The typical second-order rate equation in solution systems is [75]

$$\frac{dC_1}{dt} = -k_2 C_1^2 \quad (12)$$

Eq. (12) was integrated with the boundary conditions of $C_t = 0$ at $t = 0$ and $C_t = C_t$ at $t = t$ to yield

$$\frac{1}{C_1} = k_2 t + \frac{1}{C_0}, \quad (13)$$

where C_0 and C_t (mg/L) are the concentrations of solute at equilibrium and at time t (min), respectively, and k_2 (L/(mg·min)) is the rate constant. In earlier years, the second-order rate equations were reasonably applied to describe adsorption reactions occurring in soil and soil minerals. Recently, the equation has also been used to describe fluoride adsorption onto acid-treated spent bleaching earth and phosphamidon adsorption on an antimony(V) phosphate cation [76].

2.5 Mitigation of waste oil spills

Oil forms part of our everyday lives as it is used in many domestic and industrial processes such as cooking/frying, in machinery, for energy, in toiletries, car engines, mills etc. Once the oil is used, or it is no longer suitable for its original use, due to either impurities or loss of its original properties, it can be classified as waste oil (WO) [77]. WO is one of the biggest nuisances of modern-day civilisation and a major factor in the degradation of the environment, particularly in urban settlements. Among different forms of oils, cooking/frying oil is common in both domestic and commercial use. Large scale commercial use of cooking oil by the snacks manufacturing industry, hotels, restaurants, caterers, road-side eateries, and even street vendors result in the production of hundreds of tons of waste cooking oil with little or no planned and scientific method of disposal [77]. Discarding waste cooking oil in the open causes water pollution due to poor solubility and creates a film on the water, which hinders diffusion of oxygen and results in a toxic effect on the aquatic biota [78].

Removal techniques for oils are different and include in-situ burning, containment booms, dispersants, and biodegradation, but all show an incomplete separation of oil from the water [79]. Research has shown that waste oil can be repurposed and converted into a material known as OLCs [80]. Earlier studies refer to this material as carbon nano-onions (CNOs); however, studies by Mongwe *et al.* [10] showed that the flame pyrolysis derived material differs from the diamond-derived materials (CNOs) and thus the material is better referred to as OLCs. This is the nomenclature used in this study. Examples of the use of OLCs have been reported in our group. Shaku *et al.* used flame pyrolysis of grapeseed oil to synthesise OLCs that were applied in supercapacitors [81]. This flame pyrolysis method was also used by Sikeyi *et al.* with olive oil as a starting material for OLCs that were applied in fuel cells [82].

In studies by others, Jung *et al.* also produced OLCs from waste frying oil for application in energy storage devices using flame pyrolysis [83]. The conversion of frying oil into OLCs is

illustrated in **Figure 2.8.** Oil waste is rich in carbon and has been used in microbial fatty acids production, biohydrogen, and bioplastic production. Waste oil has been a potential feedstock for the production of biodiesel via biological or chemical processes [78]

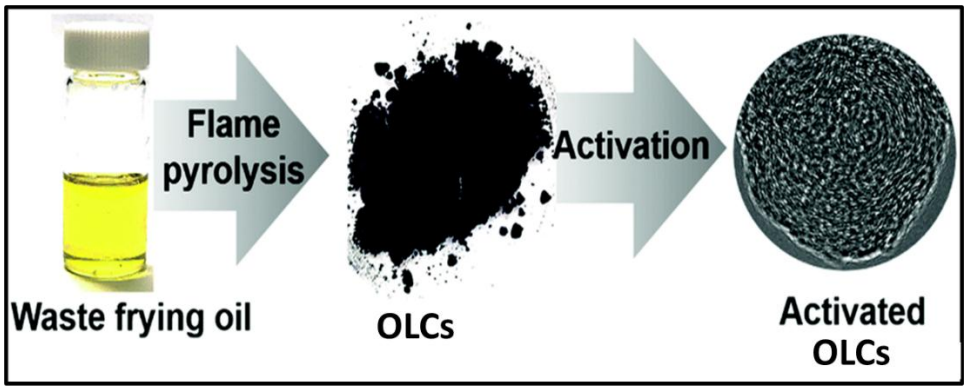

Figure 2.8: Schematic representation of the use of waste oil as a precursor for the synthesis of CNOs and activated CNOs [83].

2.6 Carbon nano-onions/onion-like carbons (ONC/OLC)

OLCs have a carbon nanostructure composed of multiple concentric layers of carbon with a fullerene type arrangement. Due to their unique chemical and physical properties, these cage-in-cage structures remain an exciting and fascinating form of carbon [84] . As shown on **Figure 2.9a and 2.9b**, OLCs can be viewed as members of the fullerene family, which consist of quasi-spherical and polyhedral graphite layers close to each other [85] . However, the layers are not continuous as found in a fullerene or nano carbon onion (NCO). The distance between the graphitic layers is 0.35 nm, and it is approximately equal to the distance between two graphitic planes (0.35 nm) (**Figure 2.9b**) [86] . Depending on the synthesis method and processing parameters, the size of carbon onions may range from around 2–50 nm [87] . The structure of OLCs contains hexagonal and pentagonal rings. The carbon atoms at the vertices form two single bonds and one double bond with the adjacent carbon atoms by the delocalized p-electrons in the molecule **(Figure 2.9c)** [88].

OLCs were first produced by irradiation of nanoparticles under an electron beam by Ugarte in 1992. The first-time onion-like structures were observed in 1980 by Iijima, in amorphous carbon films prepared by a vacuum evaporation method [89]. Precursors and synthetic routes determine the structural architecture, physical and chemical properties of OLCs [90] . OLCs are a form of nanocarbon allotropes, which have been extensively studied for applications

such as catalysis, electrochemical energy storage, biomedical applications, and water treatment [91]. In recent years, OLCs have become attractive adsorbents due to their unique chemical properties and structure [92]. The unaltered OLCs have low solubility in protic and aprotic solvents, but due to the intramolecular interaction by van der Waals forces, they easily agglomerate [93]. OLCs has a fully usable outer surface, with a large surface area and curved edges, which helps to connect multiple functional groups to its surface, thereby improving solubility. The high curvature of OLCs shells gives them certain defects, holes and pentagons. Due to the nature of its chemical bonds and higher stress, OLCs has relatively higher chemical reactivity than other nano-carbon materials [93].

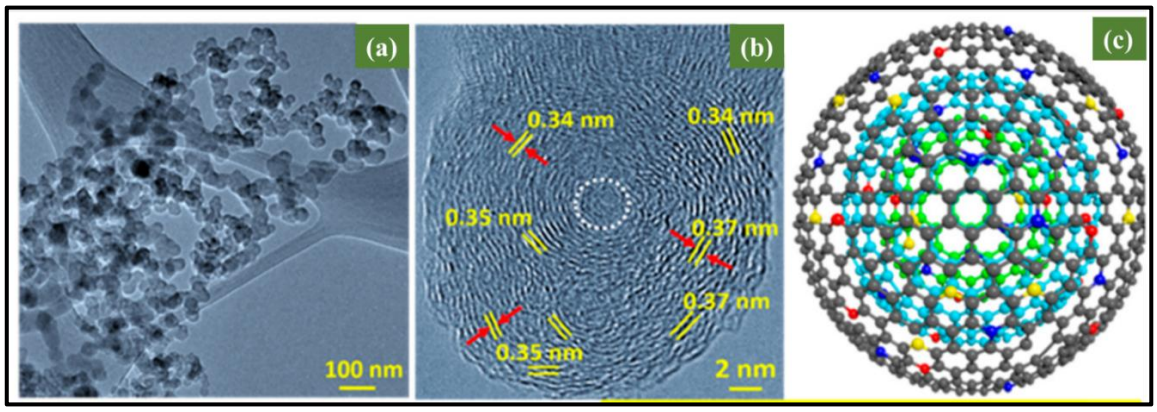

Figure 2.9: Images of OLCs. (a) HRTEM, (b) SEM image of OLCs produced by wick-oil flame pyrolysis, and (c) structural representation of OLCs [94].

Several methods have been reported to prepare CNOs/OLCs in large amounts having uniform morphology and size. For example, Mahapatra *et al.* synthesized OLCs for their application supercapacitors using flame pyrolysis [95] . Kuznetsov *et al.* showed that CNOs can be obtained by high temperature annealing of ultra-dispersed diamond (nanodiamond) under vacuum [96]. The annealing can also be performed under a slightly positive pressure of an inert gas [97]. Sano *et al.* used arc discharge between two graphite rods immersed in water to produce OLCs [98].

2.7 Flame pyrolysis method to make OLCs.

Recently, a flame pyrolysis technology has been developed to produce OLCs [10]. This method requires only simple equipment and a cheap and readily available carbon source. The

wick is immersed in oil (which serves as a carbon source) and ignited to create a flame. The deep-black powder is then produced by the flame and gathered onto a collecting plate for approximately 60 minutes [99]. Various carbon sources, such as paraffin oil, linseed oil, and naphthalene, have been reported for the synthesis of highly stable OLCs. This method can easily be extended to produce OLCs on a large scale and produce pure OLCs [81] and it is thus a preferred method for this study. A simplified set up of wick-oil flame pyrolysis for the production of OLCs has been illustrated on **Figure 2.10**.

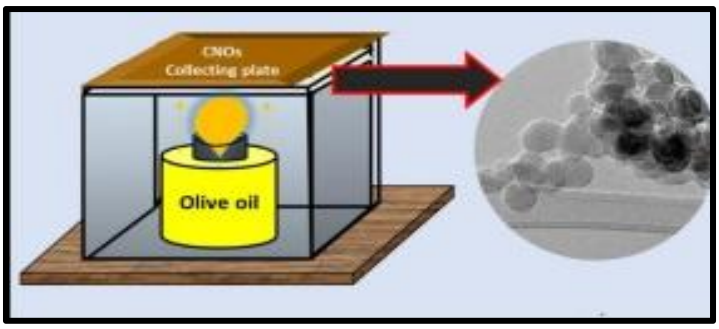

Figure 2.10: Synthesis of OLCs using flame pyrolysis [100].

2.8 Modification of OLCs: Functionalization and Doping

After the discovery of CNOs and OLCs, the chemical modification of their surface was studied [101] . It is well known that due to decreased surface curvature (and associated deformation), the reactivity of the fullerene-like structure decreases as its size increases [102]. Many OLCs are chemically resistant. Similarly, the solubility of OLCs in organic and inorganic solvents is poor due to aggregation, which is due to a very strong intermolecular interactions, such as van der Waals forces [103]. Compared to other graphite nanostructures, the edges with highly curved surfaces show relatively high chemical reactivity. The properties of OLCs can be enhanced through surface modifications. Not only does functionalization introduce the functional groups on the surface of OLCs but it is also linked to the presence of defects in the carbon lattice and the presence of sp^3-hybridized carbon atoms on the surface of nanoparticles [104]. Covalent and non-covalent reactions can occur in OLCs to connect multiple groups on their surface to improve their solubility and change their physical and chemical properties [104] . The covalent as well as the non-covalent functionalization of OLCs [105] have been widely studied in the past decades and can serve as inspiration for possible synthetic strategies to decorate OLCs with a variety of functional

groups and to increase the solubility of OLC materials [102]. Frasconi *et al.* (**Figure 2.11**) produced high surface functionalised OLCs for bright light bioimaging [106].

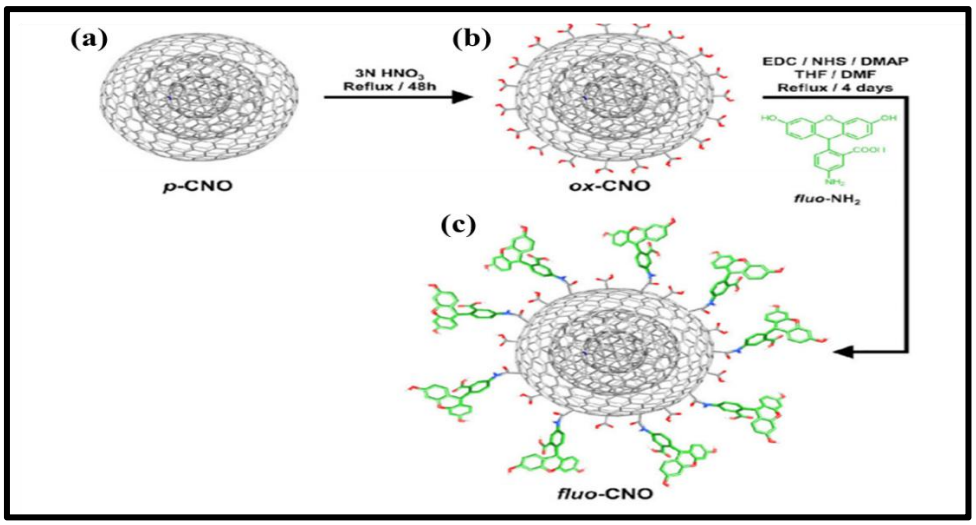

Figure 2.11: Functionalization of pristine (a) OLCs (p-OLCs) to form carboxyl functionalized (b) OLCs (ox-OLCs) through oxidation reaction and incorporation of fluorescein functionalities to ox-OLCs to (c) form fluo-OLCs [107].

Covalent and noncovalent functionalization of OLCs have been extensively used in various applications such as ion-lithium batteries, bright light bioimaging, supercapacitor, electrodes, and environmental remediation. For instance, Borgohain *et al.* oxidized OLCs to introduce hydrophobic functional groups which improved OLCs wettability for the use in supercapacitor electrodes [108]. Velásquez *et al.* indirectly functionalized OLCs with pyrene moieties to increase their stability which in turn enhanced their potential on use as a capacitor material [109]. Zheng *et al.* reported that the functionalization of OLCs could increase the specific surface area, improve the degree of graphitization, and introduce a porous structure, which would contribute to an enhanced electrochemical performance of the OLC anode for Lithium-ion batteries [110]. The surface functionalizing of OLCs for bioimaging was also studied by Frasconi *et al.* [111]. They reported that the highly functionalized OLCs displays attractive properties such as high fluorescence and dispersibility in water [111]. The use of π-π interactions for the non-covalent functionalization of carbon nanotubes (CNTs) with molecules bearing extended π-systems is a well-established protocol [112]. In addition, several pyrene–chromophore/CNT hybrids were reported, with prominent examples including pyrene-phthalocyanine and pyrene-porphyrin derivatives [113]. One example of a boron dipyrromethene (BODIPY)-pyrene/CNT hybrid was described by Erbas *et al.* who

immobilized a pyrene-derivatized di-styryl expanded BODIPY derivative on the sidewalls of CNTs [114]. Moreover, an application of functionalized OLCs in environmental remediation was studied by Li *et al.* who revealed that surface oxidized OLCs in aqueous suspensions have a high sorption capacity for heavy metal ions such as Pb^{2+}, Cu^{2+}, Cd^{2+}, Ni^{2+} and Zn^{2+}. The sorption capacity of oxidized OLCs was found to be up to ten times higher than the one of fullerene C_{60} [115].

Recently, heteroatom doping of carbon nanomaterials has proven to be a promising method for the development of carbon-based electrocatalysts. Paraknowitsch *et al.* reported that doping of carbon materials with heteroatoms (such as nitrogen, boron, sulphur, and/or phosphorous) is an effective way to change the physical and chemical properties of OLCs (such as electronic structure, surface chemistry) and, in consequence, the catalytic properties result in a promising approach for their use in various applications. Doping carbon materials with donors or acceptors can improve the electronic properties of OLCs [116]. The inclusion of phosphorus, sulphur and nitrogen atoms results in the formation of electron-rich n-type nanostructures (free electrons). Nitrogen is an n-type dopant that can polarize adjacent carbon atoms and create a charged sites in the carbon skeleton. These charged points act as activation regions on the carbon surface, which are more energy-efficient in their catalytic applications and promote the reductive adsorption of O_2 [117] . This type of activated sites induces catalytic activity and increases the reaction rate. In addition, small particle size, high surface area and improved sp^2 characteristics are essential for carbon materials as particle adsorbents [117] . Modification of nanodiamonds derived carbon nano-onions by forming additional edge- and defect-sites through rupture of surface graphene layers was investigated by Koh *et al.* (**Figure 2.14**) for the application towards oxygen reduction reaction (ORR) in acidic media [118].

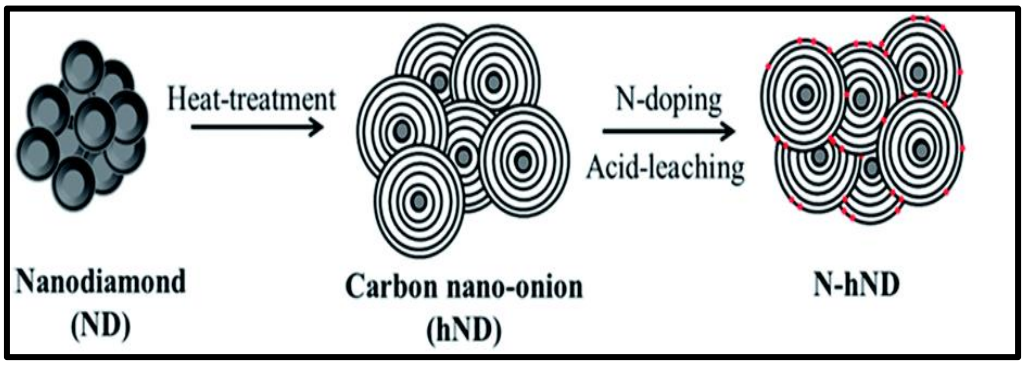

Figure 2.12: Nitrogen doped CNOs derived from nanodiamonds for application in ORR fuel cells [118].

Nitrogen-doped carbon nanostructures may be applied as electrocatalysts in ORR fuel cells, as electrochemical sensors, as a catalyst in ORR, and as anode materials in Li-ion batteries [119]. When it comes to fuel cells, some studies have focused on the use of boron-doped carbon electrocatalysts. For example, Lin *et al*. reported the synthesis of nitrogen-doped OLC (N-OLCs) via nitric acid pretreatment, followed by different temperature calcination treatment under an ammonia atmosphere [120]. Kim *et al*. also reported the production of N-OLCs for their application as a catalyst support for enhanced ORR activity and durability [121]. N-OLCs that were used as electrode for long life LI-O_2 battery were also synthesised by Shu *et al* [122]. High surface area N-OLCs were produced by Pallavolu *et al*. for their application in supercapacitors [123].

2.9 Use of nanoparticles as adsorbents

Recently, nanoparticles adsorbents are being utilized for the purification of water, which has a great scope in water treatment. These desirable nanoparticles are produced with unique properties such as large surface area-to-volume ratios and have surface functional properties to treat the toxic pollutants [39]. Structured nano-carbons such as activated carbon, carbon black, carbon nanotubes, and graphite have also been explored as adsorbents. OLCs could emerge as a promising adsorbent material due to their hydrophobicity, porosity, and has greater surface curvature and strain energy, which leads to higher chemical reactivity [124, 125]. It has been reported that cost-effective production of OLCs improves their feasibility for remediation application. When compared to common adsorbents such as coconut coir, granular activated carbon (GAC), and crab shell powder, which already can be synthesized in large scale, OLCs are expected to possess higher sorption capacity and faster equilibrium rate as reported for other carbonaceous nanosorbents [126].

2.9.1 Use of OLCs and other carbon-based materials as adsorbents

In recent years, various materials have been used as adsorbents for water restoration [127]. These include activated carbon, bentonite, peat, sand, charcoal, fiberglass, polypropylene, amberite, organoclay, and attapulgite [128]. Activated carbon is an adsorbent that is commonly used to remove a variety of organic compounds including oil from water, and it has been proven to be technically feasible [129]. Research on the use of activated carbon to

remediate groundwater contaminated by petroleum hydrocarbons has shown that powdered activated carbon is more effective than granular activated carbon (GAC) in groundwater remediation, and thus is recommended to use [130] . The United States Environmental Protection Agency has recommended activated carbon adsorption as one of the best available technologies for the removal of organic compounds [131].

Carbonaceous nanomaterials, such as fullerene C_{60} and carbon nanotubes (CNTs), and their functionalized derivatives have been demonstrated to possess high adsorption capacity. Further, C_{60} fullerene was found to be able to adsorb a large number of organic contaminants [135]. CNTs, after surface modification, has very high adsorption capacity for heavy metals [136] . Comparing with traditional adsorbents, carbonaceous nano-adsorbents showed rapid equilibrium rates, high adsorption capacity and effectiveness over a broad pH range, due to their high surface area to volume ratio, controlled pore size distribution, and manipulatable surface chemistry [136].

Unfortunately, both C_{60} and CNT are expensive, preventing extensive research, and applications for environmental remediation. [137] . Cost-effective production of CNOs improves their feasibility for remediation application. When compared to common adsorbents such as coconut coir, GAC, and crab shell powder, which already can be synthesized in large scale, CNOs are expected to possess higher adsorption capacity and faster equilibrium rate as reported for other carbonaceous nanosorbents [138].

In literature, CNOs have been used in studies as potential adsorbents. The removal of Cr (III) and (VI) by CNOs has been reported by several studies. Young-Jin *et al.* reported that the Cr (VI) adsorption capacity of the CNOs is superior to those of the commercial GAC and coconut activated carbon [139]. Ntuli *et al.* reported the synthesis of oxygen-rich OLCs for the removal of Cr (VI) from aqueous solutions [140]. The maximum adsorption capacity of 47.62 mg/g at a pH of 2 and a contact time of 360 min was achieved. Venkatesan *et al.* also synthesized CNOs for the removal of industrial dye from wastewater. The CNOs exhibited excellent dye adsorption characteristics with high removal capacity of 1397.35 mg/g and rapid adsorption kinetics with a minimal adsorbent dosage of 10 mg/L, for a low concentration of 20 mg/L methylene blue dye [141]. A scalable and cost-effective approach was developed by Zhou *et al.* for the synthesis of magnetic carbon nano-onions (MCNOs) to apply them as adsorbents for the removal of bisphenol A (BPA) from aqueous solutions

[142] . It was reported that the high adsorption capacities and magnetic properties of the MCNOs offered them great application potential for the fast and efficient removal of BPA from large volumes of wastewater [142] . Sakulthaew *et al.* also reported that the combination of ozone and CNOs provides means for quick removal of polycyclic aromatic hydrocarbons (PAHs) from runoff waters or waste streams. PAHs in urban runoff were transformed by ozone within minutes in a flow through reactor and the ozone-treated PAHs were 100% adsorbed to the CNOs [143].

An ideal adsorbent material must be readily reusable, be of low cost, and contaminant recovery from it must be straightforward. Carbon nanomaterials such as CNTs, graphene and CNOs show high sorption capacity and reusability, while being environmentally friendly [144]. For example, Krishnappa *et al.* synthesized recyclable porous nano-carbons (PNCs) to remove textile dyes from an aqueous environment. Due to their high surface area and mesoporous nature, PNCs exhibited extremely fast and efficient adsorption behaviour [145].

In this study the use of OLCs and the effect of various adsorption parameters such as adsorbent concentration, contact time, and solution pH, will be investigated and to determine the optimum parameters for maximum removal of tartrazine dye from water.

REFERENCES

[1] S. Hugh, "NATIONAL WATER INVESTMENT FRAMEWORK."

[2] World Health Organisation, *State of the World's Drinking Water : An Urgent Call to Action to Accelerate Progress on Ensuring Safe Drinking Water for All*. : http://www.who.int/news-room/fact-sheets/detail/drinking-water, 2018.

[3] A. Krishnakumar, R. Das, and S. Puthalath, "Assessment of the quality of water resources in coastal urban lands of two small catchment rivers, Southwest India," *Management of Environmental Quality: An International Journal*, vol. 28, no. 3, pp. 444–459, 2017, doi: 10.1108/MEQ-01-2015-0002.

[4] A. Maddocks, Y. R. Samuel, and P. Reig, "Ranking the World's Most Water-Stressed Countries in 2040," https://www.wri.org.

[5] R. Eberhard, "Cape is no exception: water crisis risks are systemic and affect all of SA," businesslive.co.za.

[6] G. Ziervogel, B. Franklin, and J. Thorson, "UNPACKING THE CAPE TOWN DROUGHT:LESSONS LEARNED Report for Cities Support Programme Undertaken by African Centre for Cities," 2019.

[7] P. J. Oberholster, P. J. Ashton, P. J. Oberholster, and P. J. Ashton, "Parliamentary Grant Deliverable-March 2008 State of the Nation Report An Overview of the Current Status of Water Quality and Eutrophication in South African Rivers and Reservoirs".

[8] M. Elhneiti and M. Al-Hussami, "Predicting Risk Factors of Heart Disease among Jordanian Patients," *Health N Hav*, vol. 09, no. 02, pp. 237–251, 2017, doi: 10.4236/health.2017.92016.

[9] R. S. Gambhir, V. Kapoor, A. Nirola, R. Sohi, and V. Bansal, "Water Pollution: Impact of Pollutants and New Promising Techniques in Purification Process," *Journal of Human Ecology*, vol. 37, no. 2, pp. 103–109, Feb. 2012, doi: 10.1080/09709274.2012.11906453.

[10] T. H. Mongwe, B. J. Matsoso, B. K. Mutuma, N. J. Coville, and M. S. Maubane, "Synthesis of chain-like carbon nano-onions by a flame assisted pyrolysis technique using different collecting plates," *Diam Relat Mater*, vol. 90, pp. 135–143, Nov. 2018, doi: 10.1016/J.DIAMOND.2018.10.002.

[11] P. J. Oberholster, P. J. Ashton, P. J. Oberholster, and P. J. Ashton, "Parliamentary Grant Deliverable-March 2008 State of the Nation Report An Overview of the Current Status of Water Quality and Eutrophication in South African Rivers and Reservoirs."

[12] S. Thangaraj, P. O. Bankole, and S. K. Sadasivam, "Microbial degradation of azo dyes by textile effluent adapted, Enterobacter hormaechei under microaerophilic condition," *Microbiol Res*, vol. 250, Sep. 2021, doi: 10.1016/j.micres.2021.126805.

[13] L. Ayed, A. Mahdhi, A. Cheref, and A. Bakhrouf, “Decolorization and degradation of azo dye Methyl Red by an isolated Sphingomonas paucimobilis: Biotoxicity and metabolites characterization,” *Desalination*, vol. 274, no. 1–3, pp. 272–277, Jul. 2011, doi: 10.1016/J.DESAL.2011.02.024.

[14] K. T. Chung, “The significance of azo-reduction in the mutagenesis and carcinogenesis of azo dyes,” *Mutation Research/Reviews in Genetic Toxicology*, vol. 114, no. 3, pp. 269–281, Apr. 1983, doi: 10.1016/0165-1110(83)90035-0.

[15] K. Singha, P. Pandit, S. Maity, and S. R. Sharma, “Harmful environmental effects for textile chemical dyeing practice,” *Green Chemistry for Sustainable Textiles: Modern Design and Approaches*, pp. 153–164, Jan. 2021, doi: 10.1016/B978-0-323-85204-3.00005-1.

[16] A. D. McNaught and A. Wilkinson, *Compendium of Chemical Terminology The Gold Book, Second Edition*, Second Edition. Blackwell Science, 1997.

[17] H. S. Freeman and G. N. Mock, *Dye Application, Manufacture of Dye Intermediates and Dyes*. Springer, Boston, MA, 2007.

[18] T. , C. A. M. , H. R. M. , and N. J. , Eds. , A. P. Lesinger, “Biodegradation of systemic organic colorants,” *Microbial Degradation of Xenobiotics and Recalcitrant Compounds*, vol. Vol.12., 1981.

[19] S. Asad, M. A. Amoozegar, A. A. Pourbabaee, M. N. Sarbolouki, and S. M. M. Dastgheib, “Decolorization of textile azo dyes by newly isolated halophilic and halotolerant bacteria,” *Bioresour Technol*, vol. 98, no. 11, pp. 2082–2088, Aug. 2007, doi: 10.1016/J.BIORTECH.2006.08.020.

[20] G. Singh, S. K. Dwivedi, and J. Mishra, “Role of Fungal Enzymes in the Removal of Azo Dyes,” 2020, pp. 231–257. doi: 10.1007/978-981-15-1710-5_9.

[21] A. M. Elgarahy, K. Z. Elwakeel, S. H. Mohammad, and G. A. Elshoubaky, “A critical review of biosorption of dyes, heavy metals and metalloids from wastewater as an efficient and green process,” Oct. 01, 2021, *Elsevier Ltd*. doi: 10.1016/j.clet.2021.100209.

[22] P. Manickam and D. Vijay, “Chemical hazards in textiles,” *Chemical Management in Textiles and Fashion*, pp. 19–52, Jan. 2021, doi: 10.1016/B978-0-12-820494-8.00002-2.

[23] K. Kadirvelu, M. Kavipriya, C. Karthika, M. Radhika, N. Vennilamani, and S. Pattabhi, “Utilization of various agricultural wastes for activated carbon preparation and application for the removal of dyes and metal ions from aqueous solutions,” *Bioresour Technol*, vol. 87, no. 1, pp. 129–132, Mar. 2003, doi: 10.1016/S0960-8524(02)00201-8.

[24] J. Feng, C. E. Cerniglia, and H. Chen, “Toxicological significance of azo dye metabolism by human intestinal microbiota,” *Front Biosci (Elite Ed)*, vol. 4, no. 1, p. 568, Jan. 2012, doi: 10.2741/400.

[25] S. Nikfar and M. Jaberidoost, "Dyes and Colorants," *Encyclopedia of Toxicology: Third Edition*, pp. 252–261, Jan. 2014, doi: 10.1016/B978-0-12-386454-3.00602-3.

[26] A. Gičević, L. Hindija, and A. Karačić, "Toxicity of azo dyes in pharmaceutical industry," *IFMBE Proc*, vol. 73, pp. 581–587, 2020, doi: 10.1007/978-3-030-17971-7_88/COVER.

[27] T Shibamoto and LF Bjeldanes, *Introduction to food toxicology*. Elsevier, 2009.

[28] S. Banerjee and M. C. Chattopadhyaya, "Adsorption characteristics for the removal of a toxic dye, tartrazine from aqueous solutions by a low cost agricultural by-product," *Arabian Journal of Chemistry*, vol. 10, pp. S1629–S1638, May 2017, doi: 10.1016/J.ARABJC.2013.06.005.

[29] A. K. Sharma, M. Bhasker, and P. Choudhary, "JOURNAL OF CRITICAL REVIEWS TARTRAZINE SYNTHESIS, APPLICATIONS AND ISSUES: A CASE STUDY."

[30] L. Wu, "Analysis of food Additives," *Innovative Food Analysis*, pp. 157–180, Jan. 2021, doi: 10.1016/B978-0-12-819493-5.00007-8.

[31] I. Moutinho, L. C. Bertges, and R. Assis, "Prolonged use of the food dye tartrazine (FD&C yellow n°5) and its effects on the gastric mucosa of Wistar rats," 2007.

[32] F. M. D. Chequer *et al.*, "Analyses of the genotoxic and mutagenic potential of the products formed after the biotransformation of the azo dye Disperse Red 1," *Toxicology in Vitro*, vol. 25, no. 8, pp. 2054–2063, Dec. 2011, doi: 10.1016/J.TIV.2011.05.033.

[33] O. Demirkol, X. Zhang, and N. Ercal, "Oxidative effects of Tartrazine (CAS No. 1934-21-0) and New Coccin (CAS No. 2611-82-7) azo dyes on CHO cells," *Journal fur Verbraucherschutz und Lebensmittelsicherheit*, vol. 7, no. 3, pp. 229–236, Sep. 2012, doi: 10.1007/s00003-012-0782-z.

[34] T. Tanaka, "Reproductive and neurobehavioural toxicity study of tartrazine administered to mice in the diet," *Food and Chemical Toxicology*, vol. 44, no. 2, pp. 179–187, Feb. 2006, doi: 10.1016/J.FCT.2005.06.011.

[35] A. K. Bansal, M. Bansal, G. Soni, and D. Bhatnagar, "Modulation of N-nitrosodiethylamine (NDEA) induced oxidative stress by vitamin E in rat erythrocytes," *Hum Exp Toxicol*, vol. 24, no. 6, pp. 297–302, Jun. 2005, doi: 10.1191/0960327105ht533oa.

[36] M. Asgher and H. N. Bhatti, "Evaluation of thermodynamics and effect of chemical treatments on sorption potential of Citrus waste biomass for removal of anionic dyes from aqueous solutions," *Ecol Eng*, vol. 38, no. 1, pp. 79–85, Jan. 2012, doi: 10.1016/J.ECOLENG.2011.10.004.

[37] P. V. Nidheesh, R. Gandhimathi, and S. T. Ramesh, "Degradation of dyes from aqueous solution by Fenton processes: a review," *Environmental Science and Pollution Research 2013 20:4*, vol. 20, no. 4, pp. 2099–2132, Jan. 2013, doi: 10.1007/S11356-012-1385-Z.

[38] T. A. Khan, S. A. Chaudhry, and I. Ali, "Equilibrium uptake, isotherm and kinetic studies of Cd(II) adsorption onto iron oxide activated red mud from aqueous solution," *J Mol Liq*, vol. 202, pp. 165–175, Feb. 2015, doi: 10.1016/J.MOLLIQ.2014.12.021.

[39] N. Tara, S. I. Siddiqui, G. Rathi, S. A. Chaudhry, Inamuddin, and A. M. Asiri, "Nano-engineered Adsorbent for the Removal of Dyes from Water: A Review," *Curr Anal Chem*, vol. 16, no. 1, pp. 14–40, Jan. 2019, doi: 10.2174/1573411015666190117124344.

[40] T. Sasaki, A. Iizuka, M. Watanabe, T. Hongo, and A. Yamasaki, "Preparation and performance of arsenate (V) adsorbents derived from concrete wastes," *Waste Management*, vol. 34, no. 10, pp. 1829–1835, Oct. 2014, doi: 10.1016/J.WASMAN.2014.01.001.

[41] H. Ali, "Biodegradation of synthetic dyes - A review," *Water Air Soil Pollut*, vol. 213, no. 1–4, pp. 251–273, Nov. 2010, doi: 10.1007/S11270-010-0382-4/METRICS.

[42] "Revew".

[43] C. S. Umpierres *et al.*, "Microwave-activated carbons from tucumã (Astrocaryum aculeatum) seed for efficient removal of 2-nitrophenol from aqueous solutions," *Environ Technol*, vol. 39, no. 9, pp. 1173–1187, May 2018, doi: 10.1080/09593330.2017.1323957.

[44] C. Saucier, P. Karthickeyan, V. Ranjithkumar, E. C. Lima, G. S. dos Reis, and I. A. S. de Brum, "Efficient removal of amoxicillin and paracetamol from aqueous solutions using magnetic activated carbon," *Environmental Science and Pollution Research*, vol. 24, no. 6, pp. 5918–5932, Feb. 2017, doi: 10.1007/S11356-016-8304-7/METRICS.

[45] S. Álvarez-Torrellas, A. Rodríguez, G. Ovejero, and J. García, "Comparative adsorption performance of ibuprofen and tetracycline from aqueous solution by carbonaceous materials," *Chemical Engineering Journal*, vol. 283, pp. 936–947, Jan. 2016, doi: 10.1016/J.CEJ.2015.08.023.

[46] Y. He, N. B. Sutton, H. H. H. Rijnaarts, and A. A. M. Langenhoff, "Degradation of pharmaceuticals in wastewater using immobilized TiO2 photocatalysis under simulated solar irradiation," *Appl Catal B*, vol. 182, pp. 132–141, Mar. 2016, doi: 10.1016/J.APCATB.2015.09.015.

[47] X. Xu, Y. Cheng, T. Zhang, F. Ji, and X. Xu, "Treatment of pharmaceutical wastewater using interior micro-electrolysis/Fenton oxidation-coagulation and biological degradation," *Chemosphere*, vol. 152, pp. 23–30, Jun. 2016, doi: 10.1016/J.CHEMOSPHERE.2016.02.100.

[48] R. Al-Tohamy *et al.*, "A critical review on the treatment of dye-containing wastewater: Ecotoxicological and health concerns of textile dyes and possible remediation approaches for environmental safety," *Ecotoxicol Environ Saf*, vol. 231, p. 113160, Feb. 2022, doi: 10.1016/J.ECOENV.2021.113160.

[49] R. Sivaranjanee, P. S. Kumar, and S. Mahalaxmi, "A review on agro-based materials on the separation of environmental pollutants from water system," *Chemical Engineering Research and Design*, vol. 181, pp. 423–457, May 2022, doi: 10.1016/J.CHERD.2022.04.002.

[50] O. Sahu and N. Singh, “Significance of bioadsorption process on textile industry wastewater,” *The Impact and Prospects of Green Chemistry for Textile Technology*, pp. 367–416, Jan. 2018, doi: 10.1016/B978-0-08-102491-1.00013-7.

[51] E. Hadjittofis, S. C. Das, G. G. Z. Zhang, and J. Y. Y. Heng, “Interfacial Phenomena,” *Developing Solid Oral Dosage Forms: Pharmaceutical Theory and Practice: Second Edition*, pp. 225–252, Jan. 2017, doi: 10.1016/B978-0-12-802447-8.00008-X.

[52] H. Hu and K. Xu, “Physicochemical technologies for HRPs and risk control,” *High-Risk Pollutants in Wastewater*, pp. 169–207, Jan. 2020, doi: 10.1016/B978-0-12-816448-8.00008-3.

[53] E. Rápó and S. Tonk, “Factors Affecting Synthetic Dye Adsorption; Desorption Studies: A Review of Results from the Last Five Years (2017–2021),” *Molecules 2021, Vol. 26, Page 5419*, vol. 26, no. 17, p. 5419, Sep. 2021, doi: 10.3390/MOLECULES26175419.

[54] N. M. Mubarak, J. N. Sahu, E. C. Abdullah, and N. S. Jayakumar, “Removal of Heavy Metals from Wastewater Using Carbon Nanotubes,” *Separation & Purification Reviews*, vol. 43, no. 4, pp. 311–338, Oct. 2014, doi: 10.1080/15422119.2013.821996.

[55] M. Hema and S. Arivoli, “Comparative study on the adsorption kinetics and thermodynamics of dyes onto acid activated low cost carbon,” *International Journal of Physical Sciences*, vol. 2, no. 1, pp. 10–017, 2007, Accessed: Nov. 29, 2023. [Online]. Available: http://www.academicjournals.org/IJPS

[56] Z. Eren and F. N. Acar, “Adsorption of Reactive Black 5 from an aqueous solution: equilibrium and kinetic studies,” *Desalination*, vol. 194, no. 1–3, pp. 1–10, Jun. 2006, doi: 10.1016/J.DESAL.2005.10.022.

[57] L. J. Yu, S. S. Shukla, K. L. Dorris, A. Shukla, and J. L. Margrave, “Adsorption of chromium from aqueous solutions by maple sawdust,” *J Hazard Mater*, vol. 100, no. 1–3, pp. 53–63, Jun. 2003, doi: 10.1016/S0304-3894(03)00008-6.

[58] B. H. Hameed, A. T. M. Din, and A. L. Ahmad, “Adsorption of methylene blue onto bamboo-based activated carbon: Kinetics and equilibrium studies,” *J Hazard Mater*, vol. 141, no. 3, pp. 819–825, Mar. 2007, doi: 10.1016/J.JHAZMAT.2006.07.049.

[59] G. Atun, G. Hisarli, W. S. Sheldrick, and M. Muhler, “Adsorptive removal of methylene blue from colored effluents on fuller’s earth,” *J Colloid Interface Sci*, vol. 261, no. 1, pp. 32–39, May 2003, doi: 10.1016/S0021-9797(03)00059-6.

[60] N. Graham, X. G. Chen, and S. Jayaseelan, “The potential application of activated carbon from sewage sludge to organic dyes removal,” *Water Science and Technology*, vol. 43, no. 2, pp. 245–252, Jan. 2001, doi: 10.2166/WST.2001.0096.

[61] S. Karaca, A. Gürses, M. Açikyildiz, and M. Ejder (Korucu), “Adsorption of cationic dye from aqueous solutions by activated carbon,” *Microporous and Mesoporous Materials*, vol. 115, no. 3, pp. 376–382, Nov. 2008, doi: 10.1016/J.MICROMESO.2008.02.008.

[62] S. Wang, Z. H. Zhu, A. Coomes, F. Haghseresht, and G. Q. Lu, "The physical and surface chemical characteristics of activated carbons and the adsorption of methylene blue from wastewater," *J Colloid Interface Sci*, vol. 284, no. 2, pp. 440–446, Apr. 2005, doi: 10.1016/J.JCIS.2004.10.050.

[63] "Explain how the adsorption of a gas on solid varies with the nature of adsorbate and adsorbent. - Chemistry | Shaalaa.com." Accessed: Jul. 08, 2024. [Online]. Available: https://www.shaalaa.com/question-bank-solutions/explain-how-the-adsorption-of-a-gas-on-solid-varies-with-the-nature-of-adsorbate-and-adsorbent-factors-affecting-adsorption-of-gases-on-solids_172766

[64] "Major Factors Affecting Adsorption." Accessed: Jul. 08, 2024. [Online]. Available: https://unacademy.com/content/cbse-class-11/study-material/chemistry/major-factors-affecting-adsorption/

[65] S. Karimi, M. Tavakkoli Yaraki, and R. R. Karri, "A comprehensive review of the adsorption mechanisms and factors influencing the adsorption process from the perspective of bioethanol dehydration," *Renewable and Sustainable Energy Reviews*, vol. 107, pp. 535–553, Jun. 2019, doi: 10.1016/J.RSER.2019.03.025.

[66] K. Okiel, M. El-Sayed, and M. Y. El-Kady, "Treatment of oil–water emulsions by adsorption onto activated carbon, bentonite and deposited carbon," *Egyptian Journal of Petroleum*, vol. 20, no. 2, pp. 9–15, Jun. 2011, doi: 10.1016/J.EJPE.2011.06.002.

[67] D. Saha and H. A. Grappe, "Adsorption properties of activated carbon fibers," *Activated Carbon Fiber and Textiles*, pp. 143–165, Jan. 2017, doi: 10.1016/B978-0-08-100660-3.00005-5.

[68] F. Banat, S. Al-Asheh, and L. Makhadmeh, "Preparation and Examination of Activated Carbons from Date Pits Impregnated with Potassium Hydroxide for the Removal of Methylene Blue from Aqueous Solutions," *http://dx.doi.org/10.1260/026361703771953613*, vol. 21, no. 6, pp. 597–606, Jul. 2003, doi: 10.1260/026361703771953613.

[69] B. C. Pan *et al.*, "Application of an effective method in predicting breakthrough curves of fixed-bed adsorption onto resin adsorbent," *J Hazard Mater*, vol. 124, no. 1–3, pp. 74–80, Sep. 2005, doi: 10.1016/J.JHAZMAT.2005.03.052.

[70] M. Pooresmaeil and H. Namazi, "Application of polysaccharide-based hydrogels for water treatments," *Hydrogels Based on Natural Polymers*, pp. 411–455, Jan. 2020, doi: 10.1016/B978-0-12-816421-1.00014-8.

[71] Y. S. Ho and G. McKay, "A Comparison of Chemisorption Kinetic Models Applied to Pollutant Removal on Various Sorbents," *Process Safety and Environmental Protection*, vol. 76, no. 4, pp. 332–340, Nov. 1998, doi: 10.1205/095758298529696.

[72] N. T. Coleman, A. C. Mcclung, and D. P. Moore, "Formation constants for Cu(II)-peat complexes [8]," *Science (1979)*, vol. 123, no. 3191, pp. 330–331, Feb. 1956, doi:

10.1126/SCIENCE.123.3191.330/ASSET/D055B4C1-8676-49A5-B5A7-C047C6C8C13F/ASSETS/SCIENCE.123.3191.330.FP.PNG.

[73] Y. S. Ho, "Review of second-order models for adsorption systems," *J Hazard Mater*, vol. 136, no. 3, pp. 681–689, Aug. 2006, doi: 10.1016/J.JHAZMAT.2005.12.043.

[74] Y. S. Ho, "Review of second-order models for adsorption systems," *J Hazard Mater*, vol. 136, no. 3, pp. 681–689, Aug. 2006, doi: 10.1016/J.JHAZMAT.2005.12.043.

[75] S. Al-Asheh, F. Banat, and A. Masad, "Kinetics and equilibrium sorption studies of 4-nitrophenol on pyrolyzed and activated oil shale residue," *Environmental Geology*, vol. 45, no. 8, pp. 1109–1117, Jun. 2004, doi: 10.1007/S00254-004-0969-4/METRICS.

[76] M. Alkan, Ö. Demirbaş, and M. Doğan, "Adsorption kinetics and thermodynamics of an anionic dye onto sepiolite," *Microporous and Mesoporous Materials*, vol. 101, no. 3, pp. 388–396, Apr. 2007, doi: 10.1016/J.MICROMESO.2006.12.007.

[77] M. Hussein, A. A. Amer, and I. I. Sawsan, "Oil spill sorption using carbonized pith bagasse: 1. Preparation and characterization of carbonized pith bagasse," *J Anal Appl Pyrolysis*, vol. 82, no. 2, pp. 205–211, Jul. 2008, doi: 10.1016/J.JAAP.2008.03.010.

[78] A. Kushwaha *et al.*, "Polyhydroxyalkanoates production from biowastes: A route towards environmental sustainability," *Bio-Based Materials and Waste for Energy Generation and Resource Management: Present and Emerging Waste Management Practices: Volume 5 of Advanced Zero Waste Tools*, pp. 143–182, Jan. 2023, doi: 10.1016/B978-0-323-91149-8.00013-2.

[79] H. Singh, N. Bhardwaj, S. K. Arya, and M. Khatri, "Environmental impacts of oil spills and their remediation by magnetic nanomaterials," *Environ Nanotechnol Monit Manag*, vol. 14, p. 100305, Dec. 2020, doi: 10.1016/J.ENMM.2020.100305.

[80] T. H. Mongwe, B. J. Matsoso, B. K. Mutuma, N. J. Coville, and M. S. Maubane, "Synthesis of chain-like carbon nano-onions by a flame assisted pyrolysis technique using different collecting plates," *Diam Relat Mater*, vol. 90, pp. 135–143, Nov. 2018, doi: 10.1016/J.DIAMOND.2018.10.002.

[81] B. Shaku, T. P. Mofokeng, T. H. Mongwe, N. J. Coville, K. I. Ozoemena, and M. S. Maubane-Nkadimeng, "Physicochemical Properties of Nitrogen Doped Carbon Nano-onions Grown by Flame Pyrolysis from Grapeseed Oil for Use in Supercapacitors," *Electroanalysis*, vol. 32, no. 12, pp. 2946–2957, Dec. 2020, doi: 10.1002/ELAN.202060383.

[82] L. L. Sikeyi *et al.*, "Microwave assisted synthesis of nitrogen doped and oxygen functionalized carbon nano onions supported palladium nanoparticles as hybrid anodic electrocatalysts for direct alkaline ethanol fuel cells," *Int J Hydrogen Energy*, vol. 46, no. 18, pp. 10862–10875, Mar. 2021, doi: 10.1016/J.IJHYDENE.2020.12.154.

[83] S. Jung *et al.*, “Carbon nano-onions from waste oil for application in energy storage devices,” *New Journal of Chemistry*, vol. 44, no. 18, pp. 7369–7375, May 2020, doi: 10.1039/D0NJ00699H.

[84] J. Ahlawat, S. Masoudi Asil, G. Guillama Barroso, M. Nurunnabi, and M. Narayan, “Application of carbon nano onions in the biomedical field: recent advances and challenges,” *Biomater Sci*, vol. 9, no. 3, pp. 626–644, Feb. 2021, doi: 10.1039/D0BM01476A.

[85] O. Mykhailiv, H. Zubyk, and M. E. Plonska-Brzezinska, “Carbon nano-onions: Unique carbon nanostructures with fascinating properties and their potential applications,” *Inorganica Chim Acta*, vol. 468, pp. 49–66, Nov. 2017, doi: 10.1016/J.ICA.2017.07.021.

[86] R. Bacon, “Growth, Structure, and Properties of Graphite Whiskers,” *J Appl Phys*, vol. 31, no. 2, pp. 283–290, Feb. 1960, doi: 10.1063/1.1735559.

[87] M. Zeiger, N. Jäckel, M. Aslan, D. Weingarth, and V. Presser, “Understanding structure and porosity of nanodiamond-derived carbon onions,” *Carbon N Y*, vol. 84, no. 1, pp. 584–598, Apr. 2015, doi: 10.1016/J.CARBON.2014.12.050.

[88] C. T. Cioffi *et al.*, “A Carbon Nano-Onion–Ferrocene Donor–Acceptor System: Synthesis, Characterization and Properties,” *Chemistry – A European Journal*, vol. 15, no. 17, pp. 4419–4427, Apr. 2009, doi: 10.1002/CHEM.200801818.

[89] D. Malgorzata Bobrowska, O. Butsyk, L. Echegoyen, and M. E. Plonska-Brzezinska, “Carbon Nano-Onions Nanoonions Carbon Nanoonions,” 2007, doi: 10.1201/b19679-14.

[90] T. H. Mongwe, B. J. Matsoso, B. K. Mutuma, N. J. Coville, and M. S. Maubane, “Synthesis of chain-like carbon nano-onions by a flame assisted pyrolysis technique using different collecting plates,” *Diam Relat Mater*, vol. 90, pp. 135–143, Nov. 2018, doi: 10.1016/J.DIAMOND.2018.10.002.

[91] M. Zeiger, N. Jäckel, V. N. Mochalin, and V. Presser, “Review: carbon onions for electrochemical energy storage,” *J Mater Chem A Mater*, vol. 4, no. 9, pp. 3172–3196, Feb. 2016, doi: 10.1039/C5TA08295A.

[92] M. Bartkowski and S. Giordani, “Supramolecular chemistry of carbon nano-onions,” *Nanoscale*, vol. 12, no. 17, pp. 9352–9358, May 2020, doi: 10.1039/D0NR01713B.

[93] R. A. Venkatesan and M. Balachandran, “Novel carbon nano-onions from paraffinum liquidum for rapid and efficient removal of industrial dye from wastewater,” *Environmental Science and Pollution Research*, vol. 27, no. 35, pp. 43845–43864, Dec. 2020, doi: 10.1007/S11356-020-09981-W/METRICS.

[94] “(16) Daniel Bourassa.” Accessed: Feb. 10, 2024. [Online]. Available: https://www.researchgate.net/profile/Daniel-Bourassa

[95] D. Mohapatra, M. S. Sayed, and J. J. Shim, "Co-doped In-Situ Engineered Carbon Nano-Onions Enabled High-Performance Supercapacitors," *Nanomaterials 2023, Vol. 13, Page 19*, vol. 13, no. 1, p. 19, Dec. 2022, doi: 10.3390/NANO13010019.

[96] V. L. Kuznetsov, A. L. Chuvilin, Y. V. Butenko, I. Y. Mal'kov, and V. M. Titov, "Onion-like carbon from ultra-disperse diamond," *Chem Phys Lett*, vol. 222, no. 4, pp. 343–348, May 1994, doi: 10.1016/0009-2614(94)87072-1.

[97] A. Palkar *et al.*, "Reactivity Differences between Carbon Nano Onions (CNOs) Prepared by Different Methods," *Chem Asian J*, vol. 2, no. 5, pp. 625–633, May 2007, doi: 10.1002/ASIA.200600426.

[98] N. Sano *et al.*, "Properties of carbon onions produced by an arc discharge in water," *J Appl Phys*, vol. 92, no. 5, pp. 2783–2788, Sep. 2002, doi: 10.1063/1.1498884.

[99] L. L. Sikeyi *et al.*, "Microwave assisted synthesis of nitrogen doped and oxygen functionalized carbon nano onions supported palladium nanoparticles as hybrid anodic electrocatalysts for direct alkaline ethanol fuel cells," *Int J Hydrogen Energy*, vol. 46, no. 18, pp. 10862–10875, Mar. 2021, doi: 10.1016/J.IJHYDENE.2020.12.154.

[100] T. D. Ntuli *et al.*, "Removal of hexavalent chromium via an adsorption coupled reduction mechanism using olive oil derived carbon nano-onions," *Environ Nanotechnol Monit Manag*, vol. 16, p. 100477, Dec. 2021, doi: 10.1016/J.ENMM.2021.100477.

[101] P. K. Kharwar, R. K. Verma, K. Debnath, and A. Singh, "Synthesis of Catalyst-Free Carbon Nano Onions (CNOs) for Advanced Functional Materials," *Trends in Fabrication of Polymers and Polymer Composites*, pp. 8-1-8–22, Mar. 2022, doi: 10.1063/9780735423916_008.

[102] J. Bartelmess and S. Giordani, "Carbon nano-onions (multi-layer fullerenes): chemistry and applications," *Beilstein Journal of Nanotechnology 5:207*, vol. 5, no. 1, pp. 1980–1998, Nov. 2014, doi: 10.3762/BJNANO.5.207.

[103] Y. Zheng and P. Zhu, "Carbon nano-onions: large-scale preparation, functionalization and their application as anode material for rechargeable lithium ion batteries," *RSC Adv*, vol. 6, no. 95, pp. 92285–92298, Sep. 2016, doi: 10.1039/C6RA19060J.

[104] "Sci-Hub | Carbon nano-onions: Unique carbon nanostructures with fascinating properties and their potential applications. Inorganica Chimica Acta, 468, 49–66 | 10.1016/j.ica.2017.07.021." Accessed: Jan. 15, 2024. [Online]. Available: https://sci-hub.se/10.1016/j.ica.2017.07.021

[105] M. Á. Herranz and N. Martín, "Noncovalent Functionalization of Carbon Nanotubes," *Carbon Nanotubes and Related Structures: Synthesis, Characterization, Functionalization, and Applications*, pp. 103–134, Mar. 2010, doi: 10.1002/9783527629930.CH5.

[106] M. Frasconi, V. Maffeis, J. Bartelmess, L. Echegoyen, and S. Giordani, “Highly surface functionalized carbon nano-onions for bright light bioimaging,” *Methods Appl Fluoresc*, p. 044005, 2015, doi: 10.1088/2050-6120/3/4/044005.

[107] M. Frasconi, V. Maffeis, J. Bartelmess, L. Echegoyen, and S. Giordani, “Highly surface functionalized carbon nano-onions for bright light bioimaging,” *Methods Appl Fluoresc*, p. 044005, 2015, doi: 10.1088/2050-6120/3/4/044005.

[108] R. Borgohain, J. Li, J. P. Selegue, and Y. T. Cheng, “Electrochemical study of functionalized carbon nano-onions for high-performance supercapacitor electrodes,” *Journal of Physical Chemistry C*, vol. 116, no. 28, pp. 15068–15075, Jul. 2012, doi: 10.1021/JP301642S/ASSET/IMAGES/MEDIUM/JP-2012-01642S_0007.GIF.

[109] J. D. Velásquez, M. Tomczykowa, M. E. Plonska-Brzezinska, and M. N. Chaur, “Evaluation of the Covalent Functionalization of Carbon Nano-Onions with Pyrene Moieties for Supercapacitor Applications,” *Materials 2020, Vol. 13, Page 1141*, vol. 13, no. 5, p. 1141, Mar. 2020, doi: 10.3390/MA13051141.

[110] Y. Zheng and P. Zhu, “Carbon nano-onions: large-scale preparation, functionalization and their application as anode material for rechargeable lithium ion batteries,” *RSC Adv*, vol. 6, no. 95, pp. 92285–92298, Sep. 2016, doi: 10.1039/C6RA19060J.

[111] M. Frasconi, V. Maffeis, J. Bartelmess, L. Echegoyen, and S. Giordani, “Highly surface functionalized carbon nano-onions for bright light bioimaging,” *Methods Appl Fluoresc*, vol. 3, no. 4, p. 044005, Oct. 2015, doi: 10.1088/2050-6120/3/4/044005.

[112] J. Bartelmess and S. Giordani, “Carbon nano-onions (multi-layer fullerenes): chemistry and applications,” *Beilstein Journal of Nanotechnology 5:207*, vol. 5, no. 1, pp. 1980–1998, Nov. 2014, doi: 10.3762/BJNANO.5.207.

[113] J. Bartelmess *et al.*, “Phthalocyanine-pyrene conjugates: A powerful approach toward carbon nanotube solar cells,” *J Am Chem Soc*, vol. 132, no. 45, pp. 16202–16211, Nov. 2010, doi: 10.1021/JA107131R/SUPPL_FILE/JA107131R_SI_001.PDF.

[114] S. Erbas, A. Gorgulu, M. Kocakusakogullari, and E. U. Akkaya, “Non-covalent functionalized SWNTs as delivery agents for novel Bodipy-based potential PDT sensitizers,” *Chemical Communications*, no. 33, pp. 4956–4958, Aug. 2009, doi: 10.1039/B908485A.

[115] M. B. Seymour, C. Su, Y. Gao, Y. Lu, and Y. Li, “Characterization of carbon nano-Onions for heavy metal ion remediation,” *Journal of Nanoparticle Research*, vol. 14, no. 9, pp. 1–13, Sep. 2012, doi: 10.1007/S11051-012-1087-Y/METRICS.

[116] “Sci-Hub | Doping carbons beyond nitrogen: an overview of advanced heteroatom doped carbons with boron, sulphur and phosphorus for energy applications. Energy & Environmental Science, 6(10), 2839 | 10.1039/c3ee41444b.” Accessed: Jan. 14, 2024. [Online]. Available: https://sci-hub.se/10.1039/c3ee41444b

[117] “Sci-Hub | Recent progress in doped carbon nanomaterials as effective cathode catalysts for fuel cell oxygen reduction reaction. Journal of Power Sources, 236, 238–249 | 10.1016/j.jpowsour.2013.02.057.” Accessed: Jan. 14, 2024. [Online]. Available: https://sci-hub.se/10.1016/j.jpowsour.2013.02.057

[118] J. Koh, S. H. Park, M. W. Chung, S. Y. Lee, and S. I. Woo, “Diamond@carbon-onion hybrid nanostructure as a highly promising electrocatalyst for the oxygen reduction reaction,” *RSC Adv*, vol. 6, no. 33, pp. 27528–27534, Mar. 2016, doi: 10.1039/C5RA28066D.

[119] O. Mykhailiv *et al.*, “Improvement of the Structural and Chemical Properties of Carbon Nano-onions for Electrocatalysis,” *ChemNanoMat*, vol. 3, no. 8, pp. 583–590, Aug. 2017, doi: 10.1002/CNMA.201700161.

[120] Y. Lin, X. Pan, W. Qi, B. Zhang, and D. S. Su, “Nitrogen-doped onion-like carbon: A novel and efficient metal-free catalyst for epoxidation reaction,” *J Mater Chem A Mater*, vol. 2, no. 31, pp. 12475–12483, Aug. 2014, doi: 10.1039/C4TA01611D.

[121] S. M. Kim, Y. K. Heo, K. T. Bae, Y. T. Oh, M. H. Lee, and S. Y. Lee, “In situ formation of nitrogen-doped onion-like carbon as catalyst support for enhanced oxygen reduction activity and durability,” *Carbon N Y*, vol. 101, pp. 420–430, May 2016, doi: 10.1016/J.CARBON.2016.02.022.

[122] C. Shu, Y. Lin, and D. Su, “N-doped onion-like carbon as an efficient oxygen electrode for long-life Li–O2 battery,” *J Mater Chem A Mater*, vol. 4, no. 6, pp. 2128–2136, Feb. 2016, doi: 10.1039/C5TA09539E.

[123] M. R. Pallavolu *et al.*, “Design and synthesis of highly efficient nitrogen-doped carbon nano-onions for asymmetric supercapacitors,” *J Alloys Compd*, vol. 918, p. 165609, Oct. 2022, doi: 10.1016/J.JALLCOM.2022.165609.

[124] C. M. Hussain, “Carbon Nanomaterials as Adsorbents for Environmental Analysis,” *Nanomaterials for Environmental Protection*, vol. 9781118496978, pp. 217–236, Jan. 2015, doi: 10.1002/9781118845530.CH14.

[125] O. Mykhailiv, H. Zubyk, and M. E. Plonska-Brzezinska, “Carbon nano-onions: Unique carbon nanostructures with fascinating properties and their potential applications,” *Inorganica Chim Acta*, vol. 468, pp. 49–66, Nov. 2017, doi: 10.1016/J.ICA.2017.07.021.

[126] “Sci-Hub | Characterization of carbon nano-onions for heavy metal ion remediation. Journal of Nanoparticle Research, 14(9) | 10.1007/s11051-012-1087-y.” Accessed: Jan. 15, 2024. [Online]. Available: https://sci-hub.se/10.1007/s11051-012-1087-y

[127] M. H. Dehghani *et al.*, “Recent advances on sustainable adsorbents for the remediation of noxious pollutants from water and wastewater: A critical review,” *Arabian Journal of Chemistry*, vol. 16, no. 12, p. 105303, Dec. 2023, doi: 10.1016/J.ARABJC.2023.105303.

[128] T. D. Reynolds and P. A. Richards, “Unit operations and processes in environmental engineering,” p. 798, 1996, Accessed: Jan. 21, 2024. [Online]. Available: https://thuvienso.hoasen.edu.vn/handle/123456789/9759

[129] M. J. Ayotamuno, R. B. Kogbara, S. O. T. Ogaji, and S. D. Probert, “Petroleum contaminated ground-water: Remediation using activated carbon,” *Appl Energy*, vol. 83, no. 11, pp. 1258–1264, Nov. 2006, doi: 10.1016/J.APENERGY.2006.01.004.

[130] P. C. Nicholas, *Handbook of Water and Wastewater Treatment Technology. Boston: Butterworth and Heinemann.* 2002.

[131] F. Cadena, “Use of Tailored Bentonite for Selective Removal of Organic Pollutants,” *Journal of Environmental Engineering*, vol. 115, no. 4, pp. 756–767, Aug. 1989, doi: 10.1061/(ASCE)0733-9372(1989)115:4(756).

[132] M. B. , P. T. J. , & M. M. M. McBride, “Adsorption of aromatic molecules by clays in aqueous suspension.,” 1977.

[133] H. Moazed and T. Viraraghavan, “Organo-clay/anthracite filtration for oil removal,” *Journal of Canadian Petroleum Technology*, vol. 40, no. 9, pp. 37–42, Sep. 2001, doi: 10.2118/01-09-03/30135/ORGANO-CLAY-ANTHRACITE-FILTRATION-FOR-OIL-REMOVAL.

[134] K. Okiel, M. El-Sayed, and M. Y. El-Kady, “Treatment of oil–water emulsions by adsorption onto activated carbon, bentonite and deposited carbon,” *Egyptian Journal of Petroleum*, vol. 20, no. 2, pp. 9–15, Jun. 2011, doi: 10.1016/J.EJPE.2011.06.002.

[135] K. Yang, L. Zhu, and B. Xing, “Adsorption of polycyclic aromatic hydrocarbons by carbon nanomaterials,” *Environ Sci Technol*, vol. 40, no. 6, pp. 1855–1861, Mar. 2006, doi: 10.1021/ES052208W/SUPPL_FILE/ES052208WSI20060120_051443.PDF.

[136] K. Yang, L. Zhu, and B. Xing, “Adsorption of polycyclic aromatic hydrocarbons by carbon nanomaterials,” *Environ Sci Technol*, vol. 40, no. 6, pp. 1855–1861, Mar. 2006, doi: 10.1021/ES052208W/SUPPL_FILE/ES052208WSI20060120_051443.PDF.

[137] D. Ugarte, “Formation mechanism of quasi-spherical carbon particles induced by electron bombardment,” *Chem Phys Lett*, vol. 207, no. 4–6, pp. 473–479, May 1993, doi: 10.1016/0009-2614(93)89032-D.

[138] M. S. Mauter and M. Elimelech, “Environmental Applications of Carbon-Based Nanomaterials,” *Environ Sci Technol*, vol. 42, no. 16, pp. 5843–5859, Aug. 2008, doi: 10.1021/ES8006904.

[139] Y. J. Ko *et al.*, “Chromate adsorption mechanism on nanodiamond-derived onion-like carbon,” *J Hazard Mater*, vol. 320, pp. 368–375, Dec. 2016, doi: 10.1016/J.JHAZMAT.2016.08.041.

[140] T. D. Ntuli *et al.*, “From waste cooking oil to oxygen-rich onion-like nanocarbons for the removal of hexavalent chromium from aqueous solutions,” *S Afr J Sci*, vol. 119, no. 9–10, pp. 1–11, 2023, doi: 10.17159/SAJS.2023/14006.

[141] R. A. Venkatesan and M. Balachandran, “Novel carbon nano-onions from paraffinum liquidum for rapid and efficient removal of industrial dye from wastewater,” *Environmental Science and Pollution Research*, vol. 27, no. 35, pp. 43845–43864, Dec. 2020, doi: 10.1007/S11356-020-09981-W/METRICS.

[142] M. Zhou, Q. Li, S. Zhong, J. Chen, H. Lin, and X. L. Wu, “Facile large scale fabrication of magnetic carbon nano-onions for efficient removal of bisphenol A,” *Mater Chem Phys*, vol. 198, pp. 186–192, Sep. 2017, doi: 10.1016/J.MATCHEMPHYS.2017.05.020.

[143] C. Sakulthaew, S. D. Comfort, C. Chokejaroenrat, X. Li, and C. E. Harris, “Removing PAHs from urban runoff water by combining ozonation and carbon nano-onions,” *Chemosphere*, vol. 141, pp. 265–273, Dec. 2015, doi: 10.1016/J.CHEMOSPHERE.2015.08.002.

[144] T. H. Ibrahim, M. A. Sabri, and M. I. Khamis, “Application of multiwalled carbon nanotubes and its magnetite derivative for emulsified oil removal from produced water,” *Environ Technol*, vol. 40, no. 25, pp. 3337–3350, Nov. 2019, doi: 10.1080/09593330.2018.1472302.

[145] B. Krishnappa, S. Saravu, J. M. Shivanna, M. Naik, and G. Hegde, “Fast and effective removal of textile dyes from the wastewater using reusable porous nano-carbons: a study on adsorptive parameters and isotherms,” *Environmental Science and Pollution Research*, vol. 29, no. 52, pp. 79067–79081, Nov. 2022, doi: 10.1007/S11356-022-21251-5/METRICS.

CHAPTER 3

Physicochemical properties of onion-like carbon nanoparticles synthesized using different waste oils

3.1 Introduction

Carbon allotropes such as fullerenes, nanotubes, and graphene are among the most investigated CNMs due to their unique chemical, electrical, and morphological properties [1]. Ugarte studied the curling and graphitization of amorphous carbon in 1992 using an electron beam [2] . This resulted in the formation of multi-layered fullerenes known as onion-like graphitic nanoparticles, which exhibited intriguing physicochemical features such as the ability to reversibly receive electrons [3] . These nanoparticles are now known as carbon nano-onions (CNOs), due to their onion-like structural design.

As mentioned in **Section 2.7.1**, OLCs can be produced using a variety of techniques, including thermal annealing of nano diamonds [4] , arc discharge [5] , pyrolysis [6] , ion implantation [7], and chemical vapour deposition (CVD) [8]. Among the techniques available to produce OLCs, the flame pyrolysis (FP) technique to produce carbon nanomaterials has been widely researched due to its advantages over alternative generation strategies that need complex setups and high temperature. The flame pyrolysis process produces OLCs with many layers connected to each other, giving a partially spherical shape. Flame pyrolysis is a low-cost process for producing OLCs that do not require further purifying stages because the material produced is free of other forms of carbon [9] . The flame pyrolysis approach produces highly stable OLCs with no byproducts [9] . Functionalization and doping can be used to change their structure and increase their conductivity. According to a report [10] , conductive carbon materials are necessary for energy storage because they increase capacitance values, which increase the quantity of energy stored.

Recently, oil has become the most reported precursor for the production OLCs using FP. This is because oil is readily available and attractive as a carbon and oxygen-rich source for the synthesis of OLCs using FP [11] . For example, Lei *et al*. used heavy oil to produce OLCs with tuneable sizes (5–200 nm), shapes (spherical and polyhedral), and types of cores (hollow and dense) [12] . In another study, Wang *et al.* OLCs from castor oil were posing unique surface properties suitable for the use in electrochemical performances [13]. Mohapatra *et al*. also synthesized high quality hydrophobic OLCs from ghee oil [14].

However, these studies employed pure oils. To develop a more competitive carbon material, carbon materials derived from renewable resources should be considered. One of the methods to derive renewable resource is the conversion of waste substances to energy [15]. Das *et al.* reported that the synthesis of OLCs using FP does not only provide a cost-effective synthesis approach, but also can offer waste management if waste oil is used as a precursor [16]. There has been a lot of interest in using waste biomass, such as natural oil or vegetable ghee, as a sustainable feedstock for nano-carbon synthesis as a cost and environmentally friendly synthesis [17] . Thus, this study describes a straightforward, ecologically friendly, and commercially feasible synthesis of OLCs from various waste oils for their uses as adsorbents.

3.2 Experimental Procedure

3.2.1 Materials

OLCs were prepared using the following carbon precursors without any further treatment: restaurant waste oil collected from a local restaurant, waste paraffin oil collected from our laboratory (University of the Witwatersrand, School of Chemistry, Johannesburg, South Africa), household waste oil a mixture of household fried foods collected from a home in Centurion, South Africa, and engine waste oil collected from a local mechanic in Centurion. A cotton wick and ignition lighter purchased from a local retailer, a scotch bottle from our laboratory (University of the Witwatersrand, School of Chemistry), a polished brass collecting plate (BCP) from the University of the Witwatersrand, School of Physics workshop), and a steel-tube stand (University of the Witwatersrand School of Physics workshop).

3.2.2 Synthesis of OLCs using the flame pyrolysis method

The wick soaked into the scotch bottle containing waste oil (50 mL) was ignited on its tip to produce a flame under ambient air conditions [18] . In a typical experiment, the flame was made to contact a BCP at a 30 mm distance from the tip of the flame, where the black soot was collected, and the collected as prepared material was labelled onion-like carbons (OLCs). Namely Household pristine OLCs (H-pOLCs), Engine pristine OLCs (E-pOLCs), Restaurant pristine OLCs (R-pOLCs), and Paraffin pristine OLCs (P-pOLCs). The as-synthesized OLCs were collected from the surface of BCP at hourly intervals. The schematic representation of the flame pyrolysis is given in Scheme 1. The percentage conversion of the oil was determined using **Equation 1:**

$$\%\textbf{Conversion} = \frac{OLCs\ Produced\ (g)}{Waste\ oil\ used\ (g)} \times 100 \quad (1)$$

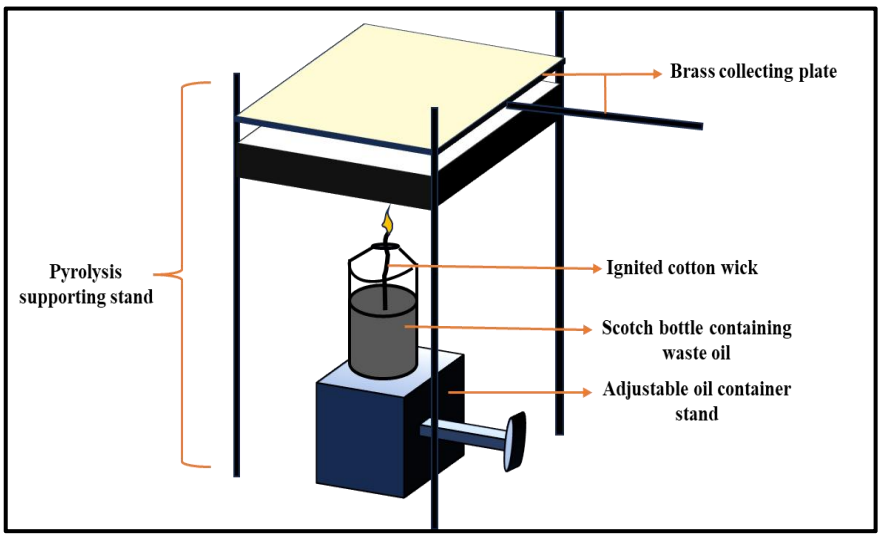

Scheme 3.1: Schematic representation of flame pyrolysis set-up used during the synthesis of pristine OLCs.

3.3 Characterization of OLCs

The structural properties of pristine OLCs (pOLCs) including their morphology, crystallographic nature, and size were determined using the listed techniques. The XRD technique was used to identify and determine the crystalline phase of the synthesized materials based on their diffraction patterns. A Bruker D2 phaser at an operating voltage of 30 kV and current of 10 mA was used. The fine powders were packed into a XRD zero-background sample holder, the measurements were collected at 2θ = 10-90 °. The crystallinity of pOLCs was also investigated by Raman spectroscopy using a Jobin-Yvon T6400 micro-Raman spectrometer. Excitation was provided by a 532 nm green laser with spectral resolution of 3-5 cm^{-1}. Morphological properties and particle sizes of pOLCs were determined using FEI G2 TECNAI Spirit T12. The samples were dispersed in ethanol and then placed on a copper grid coated with a carbon film. The samples were dried before carrying out TEM analysis at an accelerating voltage of 120 kV. Morphological properties and particle sizes of pOLCs were also determined by ZEISS GeminiSEM 560 scanning electron microscopy (SEM) utilizing sub 1 kV resolution below 1 nm. The surface area and porosity of the as-synthesized materials was determined using the Micromeritics Tristar II plus analyser. TGA was used to study and compare the thermal stability of pOLCs using the TA Q50 instrument. Approximately 10.0 mg of the solid samples was weighed and heated

from 35-900 °C at the rate of 20 °C/min in air/ Nitrogen purged at a flow rate of 20 mL/min. Both the derivative thermal gravimetric (DTG) and weight loss (TG) were obtained and analysed.

3.4 Results and discussion

The pOLCs were synthesized using wick-flame pyrolysis method, with different waste oils (Engine, Household, Restaurant, and paraffin oil) as carbon precursors. The percentage conversion of the oils to soot are shown in **Table 3.1**. The as-synthesized pristine were produced in relatively low yield percentages. The observed low OLC yields are usually the result of carbon and hydrogen radicals formed during pyrolysis reacting with oxygen in ambient air to produce carbon dioxide (CO_2) and water (H_2O) or the hydrogen radicals reacting among themselves to produce hydrogen atoms or molecules [19, 20]. Sikeyi *et al.* [21], Shaku *at al.* [22] and Ntuli *et al.* [23] also produced low yields of OLCs using wick-flame pyrolysis. The differences in yield percentages can be attributed to inconsistences during the synthesis process and the nature of waste oils which includes the conversion rate of oil to soot.

Table 3.1: The percentage yield of as-synthesized carbon materials

	Waste oil Carbon Precursor			
	Engine	**Household**	**Restaurant**	**Paraffin**
%Yield	5.34	5.53	7.28	7.07

3.4.1 Morphological analysis TEM and SEM

The SEM images of the H-pOLCs, R-pOLCs, O-pOLCs, and E-pOLCs are shown in **Figure 3.1**. The SEM micrograph of the pOLCs from the all-different precursor oils shows that the materials are quasi-spherical and closely packed together with average particle sizes of 43 ± 3.4, 42 ± 2.2, 43 ± 4.4 and 46 ± 4.7 nm for E-pOLCs, H-pOLCs, O-pOLCs, and R-pOLCs respectively. The identified morphological characteristics from the obtained SEM micrographs of all pOLCs produced are similar to those reported by Mongwe *et al.* [20], Singh *et al.*[24], and Castano *et al.*[25]. Thus, it was observed that the quasi-spherical OLCs

are always conglomerated irrespective of the organic hydrocarbon oil used to synthesize them through the flame pyrolysis process.

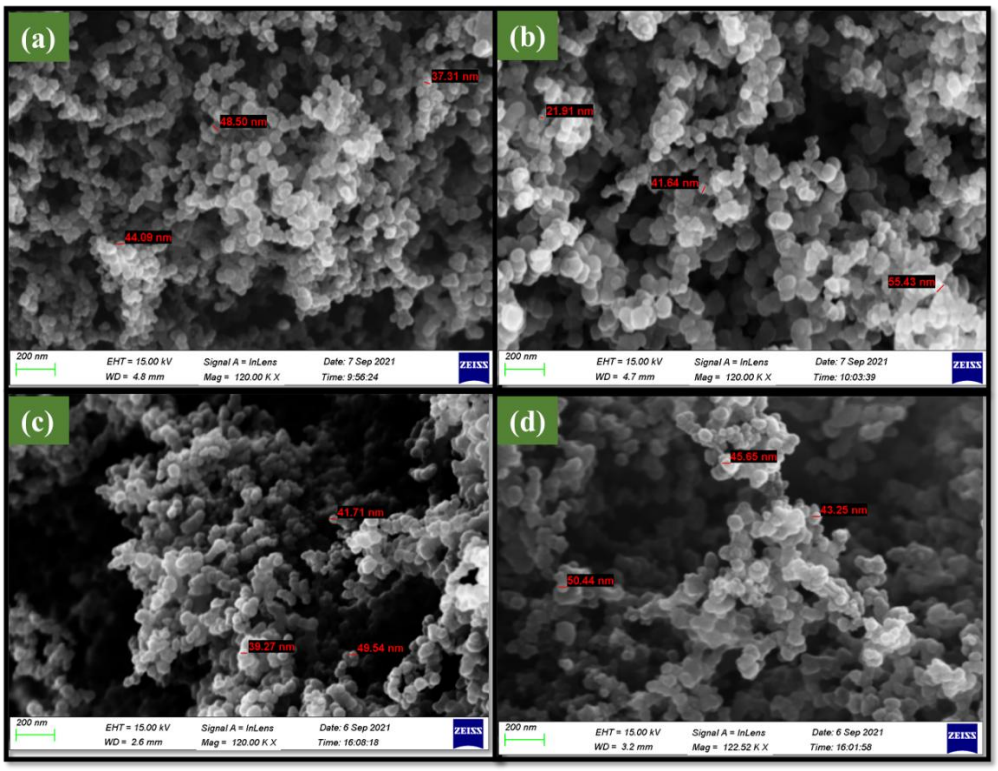

Figure 3.1: SEM images of (a) E-pOLCs, (b) H-pOLCs, (c) O-pOLCs, and (d) R-pOLCs nano materials.

The low magnification TEM micrograph in **Figure 3.2** shows an overview of pOLCs particles. These images revealed that all the pOLCs exhibited typical agglomerated particles with average sizes of ca. 48 ± 3.1 nm, 43± 2.5 nm, 47 ± 3.4 nm, and 42 ± 2.8 nm for E-pOLCs, H-pOLCs, O-pOLCs, and R-pOLCs respectively (**Figure 3.2 (a-d)).** It is notable that R-pOLCs exhibited the smallest particle size and this is explained by the reactive poly-aromatic radicals, which, depending on the chemical characteristics of the oil, react to grow varied particle sizes [26]. This data is in congression with data reported by authors such as Luo *et al.*[27], Parida *et al.*[28], and Ramya *et al.* [29] who also displayed low magnified TEM images of OLCs.

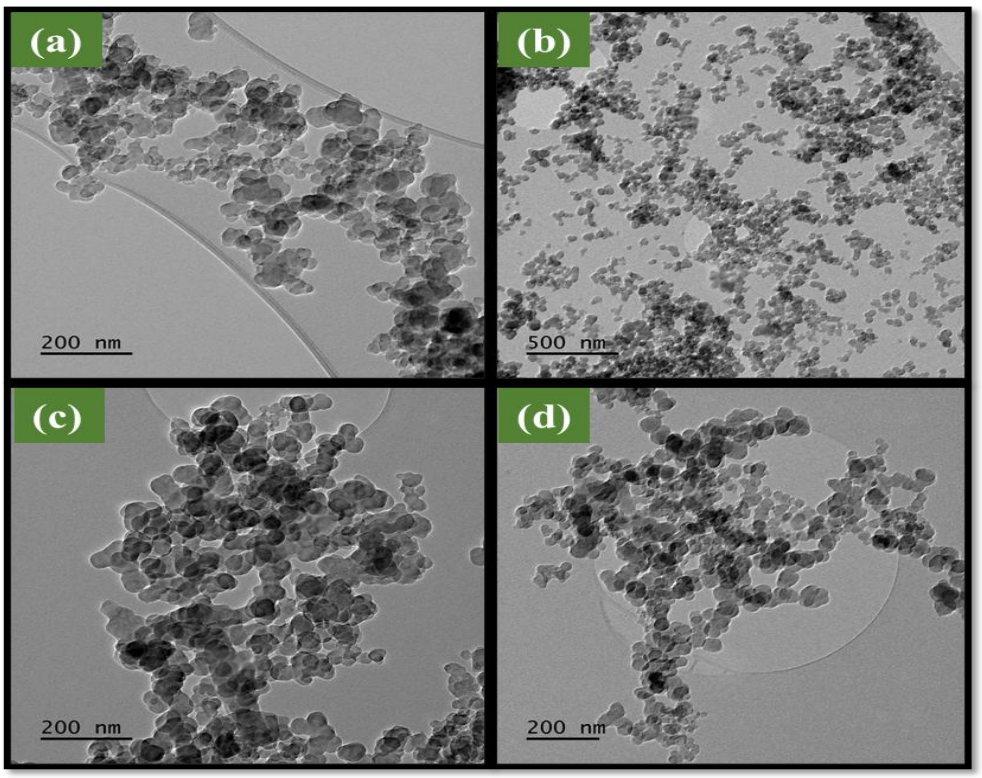

Figure 3.2: Low magnification HRTEM micrographs of the produced OLCs using different oils; (a) E-pOLCs, (b) H-pOLCs, (c) O-pOLCs, and (d) R-pOLCs.

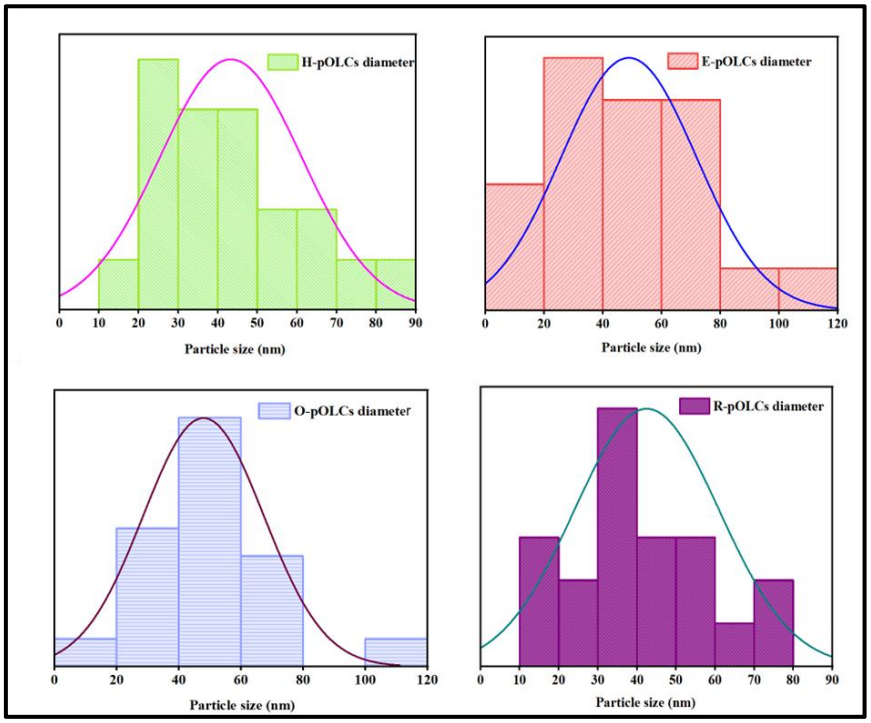

Figure 3.3: Particle size distribution of E-pOLCs, H-pOLCs, O-pOLCs, and R-pOLCs.

At higher magnification (**Figure 3.4**), the pOLCs appears to be aggregated (linked in a chain-like arrangement) and have a structure similar to a "fullerene" with numerous graphitic layers. It was found that there was a 0.32 nm distance between the graphitic layers (see **Figure 3b & 3c**).

The Van der Waals forces, which promote the linking of quasi-spherical nanoparticles made up of closed cages, are contributing to this observation. Moreover, it is also clear that the carbon nanoparticles formed during the pyrolysis of various oils group together in a manner resembling a chain and are agglomerated (see yellow markings in **Figure 3.4**). The formed chain-like arranged nanoparticles exhibit multi-layered turbostratic shells. The presence of disordered carbon is indicated by the lattice spacing which is confirmed by both XRD and Raman spec.

Similar results were obtained by Shaku *et al.* [30] . The morphology of the onion-like nanocarbons derived from waste cooking oil that–were produced by Ntuli *et al*. [11] , and Mohapatra *et al*. [31] using wick-oil flame pyrolysis method is also similar to the OLCs produced in this study.

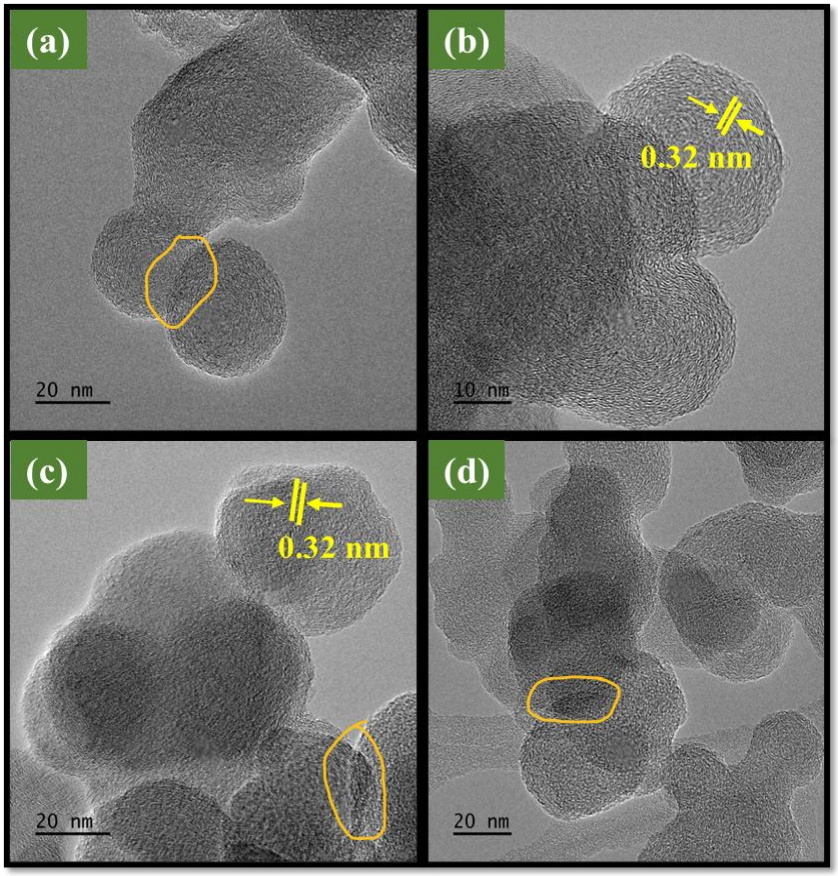

Figure 3.4: High magnification HRTEM micrographs of E-pOLCs, (b) H-pOLCs, (c) O-pOLCs, and (d) R-pOLCs.

3.4.2 X-ray diffraction (XRD) analysis

Using the XRD technique, it was possible to identify and characterize the different polycrystalline phases that the as-synthesised OLCs displayed. This technique was used to investigate the atomic arrangements obtained by X-ray diffraction to comprehend the crystallinity of the OLC. The diffractograms shown in **Figure 3.4** demonstrated that the primary constituents of all the different OLCs were amorphous carbon atom arrangements devoid of any additional contaminants, such as metal inclusion. A broad amorphous peak from all carbons at $2\theta = 25.7^{o}$ is due to the carbon (002) graphitic plane reflection [32]. The broad carbon signal is an indication of small, disordered fragments of a carbon structure in line with the TEM images [33]. All OLCs patterns showed carbon peaks centred at $2\theta = 25.0^{o}$ and 43.5^{o} corresponding to the (002) and (101) planes of carbon. Choucair *et al*. expressed crystallinity of the gram-scale synthesised pure OLCs and obtained same carbon peaks as this study at $2\theta = 25°$ and $45°$ [34]. Similar data was also reported by McDonough *et al*. who

synthesised OLCs through annealing of nanodiamonds [35] . The O-pOLC and E-pOLCs exhibited relatively broader and weak peaks, this is mostly due to the size of the nanoparticles, but it can also be brought on by strains and defects in the amorphous material and by OLC shells which have not been fully formed [24].

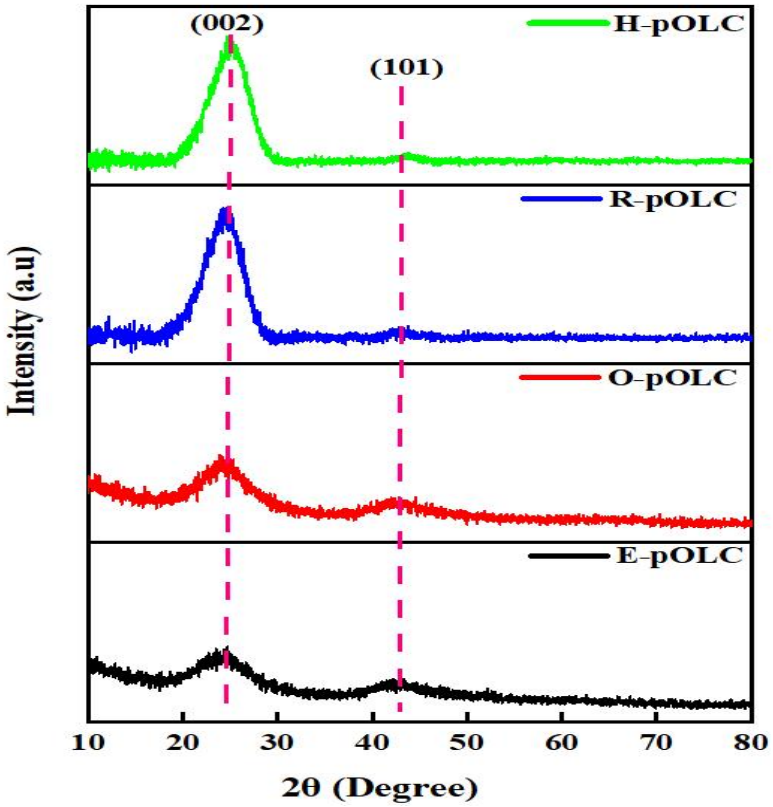

Figure 3.4: X-ray diffractograms for all pOLCs.

3.4.3 Raman spectroscopy analysis

Raman spectroscopy is a technique that can be used to investigate the defects and disorder nature in the structure of as-synthesized carbon nanomaterials. **Figure 3.5** shows the Raman spectra of H-pOLCs, E-pOLCs, O-pOLCs, and R-pOLCs with two dominant peaks (D and G bands) centred around in the 1342 and 1576 cm^{-1} region. Structural defects in the graphitic layers, including as edge defects, sp^3 bonding, dangling bonds, and atomic defects between individual graphitic layers, are the origin of the D band [36] . The sp^2 graphitic carbon's in-plane stretching (c-c) vibrations are responsible for formation of the G-peak. Two intrinsic peaks that were assigned to D and G band were observed in OLCs produced through flame synthesis in studies conducted by Chung *et al.* [37] and Dhand *et al.*[38]. The spectrum was deconvoluted to isolate the D and G band by fitting all possible Lorentzian bands. All The

pristine OLCs showed only one additional band (D3 band), which is found between 1500 and 1600 cm^{-1} and results from amorphous carbon. Mutuma *et al*. [39] evaluated the ratio of the relative intensity of the D-band to that of the G-band (I_D/I_G) to measure the degree of graphitization of OLCs generated. This is because the disorder density ratio (I_D/I_G) is directly related to the extent of disorder in the form of sp^3 hybridized carbons and the presence of shorter graphitic fragments [40], [41]. The I_{D1}/ I_G ratio was calculated based on the area under the curve and values for H-pOLCs, E-pOLCs, O-pOLCs, and R-pOLCs were 3.8, 7.8, 3.9, and 5.8 respectively (Table 3.2). The E-pOLCs had the highest disorder ratio indicating that the carbon material poses the highest degree of defects.

Table 3.2: Raman data of all pOLCs.

Material	**D-band**	**G-band**	**I_{D1}/I_G**
H-pOLCs	1342.3	1588.7	3.8
E-pOLCs	1342.5	1526.9	7.8
O-pOLCs	1341.8	1588.5	3.9
R-pOLCs	1341.7	1596.5	5.8

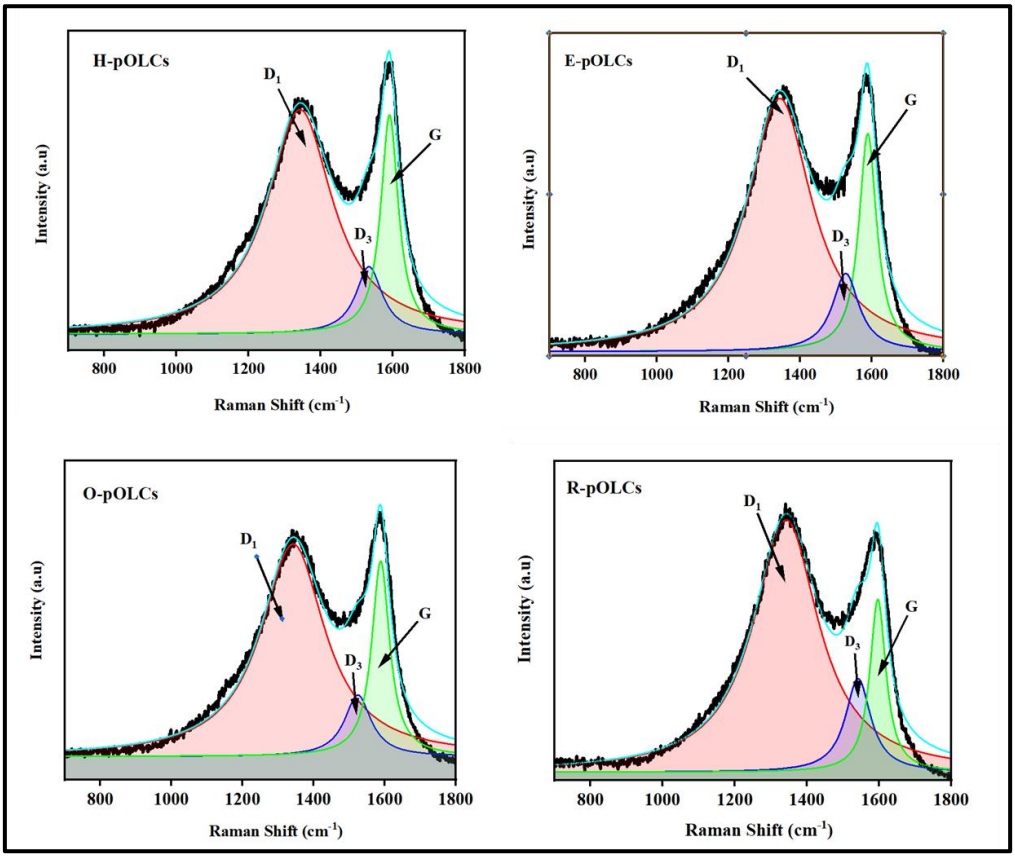

Figure 3.5: Raman spectra of (a) H-pOLCs, (b) E-pOLCs, (c) O-pOLCs, and (d) R-pOLCs

3.4.4 Surface area and porosity analysis

Nitrogen (N_2) adsorption-desorption isotherms acquired at 77 K have been utilized to evaluate the BET surface area (S_{BET}) analysis. The S_{BET} area (**Table 3.3**) analysis was conducted to measure the surface area, pore volume and pore size of the pOLCs. The obtained S_{BET} values for E-pOLC, H-pOLC, O-pOLC, and R-pOLC were 70.6, 70.3, 55.9, and 65 m^2/g respectively. The E-pOLC had the largest S_{BET} and adsorption pore size values while the O-pOLC showed the lowest S_{BET} value adsorption pore size values. This analysis corresponds to the Raman results in **Table 3.2.** It has been observed that carbon materials with high defects poses higher surface area. For example, Mongwe *et al.* [20] compared OLCs that were synthesized using different collecting plates, the material with higher Raman I_D/I_G ratio showed higher S_{BET} value.

Figure 3.6 shows a selected adsorption–desorption isotherms of N_2 at 77 K for all pristine carbons. They give illustrative examples for the shape and behaviour of the N_2 adsorption isotherms for these carbons. All the isotherms belong to Type IV in the IUPAC classification. The knee of the isotherms is wide, no clear plateau is attained, and a certain hysteresis loop

can be observed at high pressure. All these facts indicate the presence of large mesopores in the pristine nanoparticles which is described by Type IV isotherm. Closely related data was obtained by Mohapatra *et al*. who synthesized OLCs using flame pyrolysis [42].

Table 3.3: Summarizes BET analysis data of pristine OLCs.

Material	Surface Area (m^2/g)	Pore Size (nm)
E-pOLC	70.6	17.7
H-pOLC	70.3	14.6
O-pOLC	55.9	13.3
R-pOLC	65	17.3

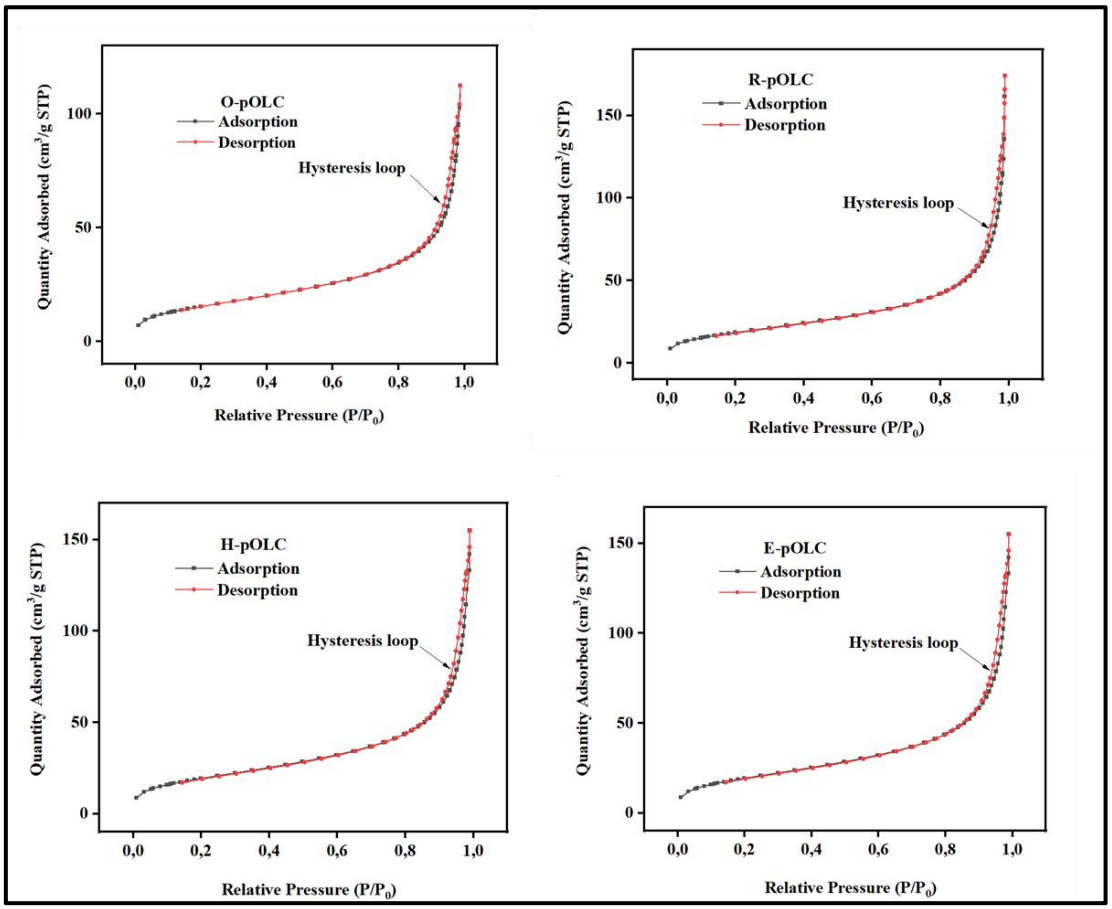

Figure 3.6: N_2 adsorption and desorption isothermal curves of all the pOLCs

3.4.5 Thermal stability

TGA was used to compare the thermal stability and purity of the synthesized materials. **Figure**

3.7 depicts the TGA and derivative curve of OLCs synthesized using wick-oil flame pyrolysis. The TGA results provides an indication of the impurity levels (residual mass) after the completion of decomposition for the OLCs. The obtained TGA profiles show varying slopes of all the profiles obtained which suggest varying degradation of multi-layered OLCs [43]. **Figure 3.7a** shows that the H-pOLC sample presented a higher on-set decomposition temperature as compared to the other OLCs as shown by values of 532.7 °C, 531.2°C, 531.6 °C and 530.2 °C for H-pOLC, R-pOLC, O-pOLC, and E-pOLC respectively. The difference in decomposition temperatures can be attributed to the inconsistent synthesis temperatures. It is also notable on **Figure 3.7a** that H-pOLCs did not completely decompose, and this be attributed to the impurities which might be present. The number of peaks observed in DTA data represents the number of decomposition stages, and the temperature of the peak in DTA corresponds to the temperature at which maximum decomposition occurs [44]. Thus, a single peak for all pOLCs is showed in **Figure 3.7b** suggesting that all pOLCs decomposes once as there are no major impurities incorporated in the materials. Tripathi *et al*. OLCs that were produced by wick-flame pyrolysis exhibited a similar TGA profile as the presented in this study [45]. This data provides evidence that there is no significant difference in the thermal stabilities of the pOLCs. This is supported by the notable difference between the lowest and highest decomposition temperature is 2.5 °C. Similarly, pristine chain-like CNOs from four different oils were synthesized by Mongwe *et al.* [46] and exhibited no variation in thermal stability.

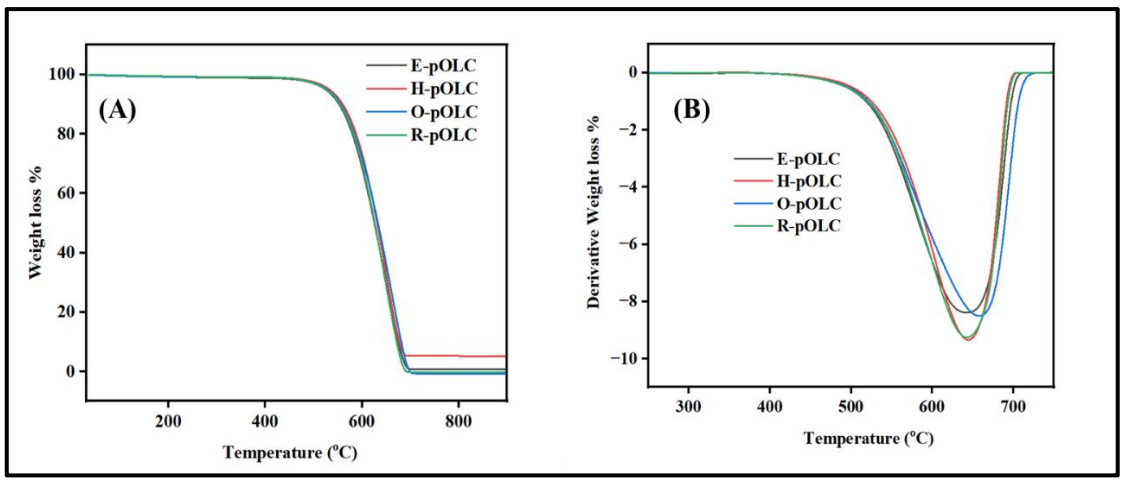

Figure 3.7: (a) TGA and (b) the corresponding derivative (DTGA) curves of pOLCs.

3.5 Conclusion

The synthesized OLCs are mainly found as non-metallic quasi-spherical, and closely packed together nanoparticles. This carbon allotrope has nanoparticles that have particle sizes less than 80 nm and exhibit concentric multi-layers. These carbon nanoparticles are mostly connected like chains in which they have surface fragmentations as shown by HRTEM results. OLCs synthesized by wick-oil flame pyrolysis process are mainly amorphous nanomaterial as presented by the two broad peaks appearing in the XRD diffractograms. The pOLCs presented similar thermal strength properties. Overall, the OLCs synthesised using flame pyrolysis of waste oils showed similar characteristics to those of OLCs produced from pure oils such as olive oil, castor oil etc. This study also indicated that the OLCs properties such as surface area and pore volume also depend on the type of precursor oil used. Notably, the highest surface area among the four OLCs materials was obtained from E-pOLCs, followed by H-pOLCs. This is an important property for application purposes, as such, in further studies, the OLCs obtained from waste engine and household oils were used, due to their outstanding physicochemical properties.

REFERENCES

[1] M. Y. Gao, F. Wang, Z. G. Gu, D. X. Zhang, L. Zhang, and J. Zhang, "Fullerene-like Polyoxotitanium Cage with High Solution Stability," *J Am Chem Soc*, vol. 138, no. 8, pp. 2556–2559, Mar. 2016, doi: 10.1021/JACS.6B00613/SUPPL_FILE/JA6B00613_SI_002.CIF.

[2] D. Ugarte, "Curling and closure of graphitic networks under electron-beam irradiation," *Nature 1992 359:6397*, vol. 359, no. 6397, pp. 707–709, 1992, doi: 10.1038/359707a0.

[3] B. S. Xu and S. I. Tanaka, "Formation of giant onion-like fullerenes under Al nanoparticles by electron irradiation," *Acta Mater*, vol. 46, no. 15, pp. 5249–5257, Sep. 1998, doi: 10.1016/S1359-6454(98)00221-3.

[4] E. Koudoumas *et al.*, "Onion-like carbon and diamond nanoparticles for optical limiting," *Chem Phys Lett*, vol. 357, no. 5–6, pp. 336–340, May 2002, doi: 10.1016/S0009-2614(02)00557-2.

[5] X. H. Chen *et al.*, "New method of carbon onion growth by radio-frequency plasma-enhanced chemical vapor deposition," *Chem Phys Lett*, vol. 336, no. 3–4, pp. 201–204, Mar. 2001, doi: 10.1016/S0009-2614(01)00085-9.

[6] E. Sohouli *et al.*, "A glassy carbon electrode modified with carbon nanoonions for electrochemical determination of fentanyl," *Materials Science and Engineering: C*, vol. 110, p. 110684, May 2020, doi: 10.1016/J.MSEC.2020.110684.

[7] J. Wang and S. Kaskel, "KOH activation of carbon-based materials for energy storage," *J Mater Chem*, vol. 22, no. 45, pp. 23710–23725, Oct. 2012, doi: 10.1039/C2JM34066F.

[8] N. Sano, H. Wang, M. Chhowalla, I. Alexandrou, and G. A. J. Amaratunga, "Synthesis of carbon 'onions' in water," *Nature 2001 414:6863*, vol. 414, no. 6863, pp. 506–507, Nov. 2001, doi: 10.1038/35107141.

[9] W. Merchan-Merchan, A. Saveliev, L. A. Kennedy, and A. Fridman, "Formation of carbon nanotubes in counter-flow, oxy-methane diffusion flames without catalysts," *Chem Phys Lett*, vol. 354, no. 1–2, pp. 20–24, Mar. 2002, doi: 10.1016/S0009-2614(02)00027-1.

[10] G. Luo, L. Liu, J. Zhang, G. Li, B. Wang, and J. Zhao, "Hole defects and nitrogen doping in graphene: Implication for supercapacitor applications," *ACS Appl Mater Interfaces*, vol. 5, no. 21, pp. 11184–11193, Nov. 2013, doi: 10.1021/AM403427H/SUPPL_FILE/AM403427H_SI_001.PDF.

[11] T. D. Ntuli *et al.*, "From waste cooking oil to oxygen-rich onion-like nanocarbons for the removal of hexavalent chromium from aqueous solutions," *S Afr J Sci*, vol. 119, no. 9–10, pp. 1–11, 2023, doi: 10.17159/SAJS.2023/14006.

[12] J. Lei *et al.*, "Novel Gram-Scale Synthesis of Carbon Nano-Onions from Heavy Oil for Supercapacitors," *Adv Mater Interfaces*, vol. 8, no. 19, p. 2101208, Oct. 2021, doi: 10.1002/ADMI.202101208.

[13] Q. Wang, X. Sun, D. He, and J. Zhang, “Preparation and study of carbon nano-onion for lithium storage,” *Mater Chem Phys*, vol. 139, no. 1, pp. 333–337, Apr. 2013, doi: 10.1016/J.MATCHEMPHYS.2013.02.002.

[14] D. Mohapatra, S. Badrayyana, and S. Parida, “Facile wick-and-oil flame synthesis of high-quality hydrophilic onion-like carbon nanoparticles,” *Mater Chem Phys*, vol. 174, pp. 112–119, May 2016, doi: 10.1016/J.MATCHEMPHYS.2016.02.057.

[15] C. Quan, A. Li, and N. Gao, “Synthesis of carbon nanotubes and porous carbons from printed circuit board waste pyrolysis oil,” *J Hazard Mater*, vol. 179, no. 1–3, pp. 911–917, Jul. 2010, doi: 10.1016/J.JHAZMAT.2010.03.092.

[16] G. S. Das, R. Panigrahi, S. Ghosh, and K. M. Tripathi, “Waste frying oil derived carbon nano-onions as a cost-effective cathode material for high-voltage zinc-ion hybrid supercapacitors,” *Materials Today Sustainability*, vol. 25, p. 100656, Mar. 2024, doi: 10.1016/J.MTSUST.2023.100656.

[17] Y. Wang *et al.*, “3D graphene-like oxygen and sulfur-doped porous carbon nanosheets with multilevel ion channels for high-performance aqueous Zn-ion storage,” *Carbon N Y*, vol. 201, pp. 624–632, Jan. 2023, doi: 10.1016/J.CARBON.2022.09.056.

[18] T. D. Ntuli *et al.*, “From waste cooking oil to oxygen-rich onion-like nanocarbons for the removal of hexavalent chromium from aqueous solutions,” *S Afr J Sci*, vol. 119, no. 9–10, 2023, doi: 10.17159/sajs.2023/14006.

[19] D. S. N. Parker, R. I. Kaiser, T. P. Troy, and M. Ahmed, “Hydrogen Abstraction/Acetylene Addition Revealed,” *Angewandte Chemie International Edition*, vol. 53, no. 30, pp. 7740–7744, Jul. 2014, doi: 10.1002/ANIE.201404537.

[20] T. H. Mongwe, B. J. Matsoso, B. K. Mutuma, N. J. Coville, and M. S. Maubane, “Synthesis of chain-like carbon nano-onions by a flame assisted pyrolysis technique using different collecting plates,” *Diam Relat Mater*, vol. 90, pp. 135–143, Nov. 2018, doi: 10.1016/J.DIAMOND.2018.10.002.

[21] L. L. Sikeyi *et al.*, “Microwave assisted synthesis of nitrogen doped and oxygen functionalized carbon nano onions supported palladium nanoparticles as hybrid anodic electrocatalysts for direct alkaline ethanol fuel cells,” *Int J Hydrogen Energy*, vol. 46, no. 18, pp. 10862–10875, Mar. 2021, doi: 10.1016/J.IJHYDENE.2020.12.154.

[22] B. Shaku, T. P. Mofokeng, T. H. Mongwe, N. J. Coville, K. I. Ozoemena, and M. S. Maubane-Nkadimeng, “Physicochemical Properties of Nitrogen Doped Carbon Nano-onions Grown by Flame Pyrolysis from Grapeseed Oil for Use in Supercapacitors,” *Electroanalysis*, vol. 32, no. 12, pp. 2946–2957, Dec. 2020, doi: 10.1002/ELAN.202060383.

[23] T. D. Ntuli *et al.*, “Removal of hexavalent chromium via an adsorption coupled reduction mechanism using olive oil derived carbon nano-onions,” *Environ Nanotechnol Monit Manag*, vol. 16, p. 100477, Dec. 2021, doi: 10.1016/J.ENMM.2021.100477.

[24] V. Singh, “Natural source derived carbon nano-onions as electrode material for sensing applications,” *Diam Relat Mater*, vol. 87, pp. 202–207, Aug. 2018, doi: 10.1016/J.DIAMOND.2018.06.007.

[25] J. A. Castaño, J. G. Betancourth, D. L. Caicedo, R. Visbal, and M. N. Chaur, “Synthesis and Electrochemical Applications of Carbon Nano-onions,” *Curr Nanosci*, vol. 20, no. 1, pp. 47–73, Mar. 2023, doi: 10.2174/1573413719666230329134840.

[26] “Comprehensive Assessment of Soot Particles from Waste Cooking Oil Biodiesel and Diesel in a Compression Ignition Engine on JSTOR.” Accessed: Mar. 04, 2024. [Online]. Available: https://www.jstor.org/stable/26273087

[27] N. Luo, J. X. Xiang, T. Shen, H. L. Liang, and S. Xin, “One-step gas-liquid detonation synthesis of carbon nano-onions and their tribological performance as lubricant additives,” *Diam Relat Mater*, vol. 97, p. 107448, Aug. 2019, doi: 10.1016/J.DIAMOND.2019.107448.

[28] D. Mohapatra, S. Badrayyana, and S. Parida, “Facile wick-and-oil flame synthesis of high-quality hydrophilic onion-like carbon nanoparticles,” *Mater Chem Phys*, vol. 174, pp. 112–119, May 2016, doi: 10.1016/J.MATCHEMPHYS.2016.02.057.

[29] A. V. Ramya, R. Thomas, and M. Balachandran, “Mesoporous onion-like carbon nanostructures from natural oil for high-performance supercapacitor and electrochemical sensing applications: Insights into the post-synthesis sonochemical treatment on the electrochemical performance,” *Ultrason Sonochem*, vol. 79, p. 105767, Nov. 2021, doi: 10.1016/J.ULTSONCH.2021.105767.

[30] B. Shaku, T. P. Mofokeng, T. H. Mongwe, N. J. Coville, K. I. Ozoemena, and M. S. Maubane-Nkadimeng, “Physicochemical Properties of Nitrogen Doped Carbon Nano-onions Grown by Flame Pyrolysis from Grapeseed Oil for Use in Supercapacitors,” *Electroanalysis*, vol. 32, no. 12, pp. 2946–2957, Dec. 2020, doi: 10.1002/ELAN.202060383.

[31] D. Mohapatra, S. Badrayyana, and S. Parida, “Facile wick-and-oil flame synthesis of high-quality hydrophilic onion-like carbon nanoparticles,” *Mater Chem Phys*, vol. 174, pp. 112–119, May 2016, doi: 10.1016/J.MATCHEMPHYS.2016.02.057.

[32] Z. Q. Li, C. J. Lu, Z. P. Xia, Y. Zhou, and Z. Luo, “X-ray diffraction patterns of graphite and turbostratic carbon,” *Carbon N Y*, vol. 45, no. 8, pp. 1686–1695, Jul. 2007, doi: 10.1016/J.CARBON.2007.03.038.

[33] J. K. McDonough and Y. Gogotsi, “Carbon onions: Synthesis and electrochemical applications,” *Electrochemical Society Interface*, vol. 22, no. 3, pp. 61–66, Jan. 2013, doi: 10.1149/2.F05133IF/XML.

[34] M. Choucair and J. A. Stride, “The gram-scale synthesis of carbon onions,” *Carbon N Y*, vol. 50, no. 3, pp. 1109–1115, Mar. 2012, doi: 10.1016/J.CARBON.2011.10.023.

[35] J. K. McDonough and Y. Gogotsi, "Carbon onions: Synthesis and electrochemical applications," *Electrochemical Society Interface*, vol. 22, no. 3, pp. 61–66, Jan. 2013, doi: 10.1149/2.F05133IF/XML.

[36] D. Roy *et al.*, "Characterisation of carbon nano-onions using Raman spectroscopy," *Chem Phys Lett*, vol. 373, no. 1–2, pp. 52–56, May 2003, doi: 10.1016/S0009-2614(03)00523-2.

[37] D. H. Chung, T. H. Lin, and S. S. Hou, "Flame synthesis of carbon nano-onions enhanced by acoustic modulation," *Nanotechnology*, vol. 21, no. 43, p. 435604, Oct. 2010, doi: 10.1088/0957-4484/21/43/435604.

[38] V. Dhand, J. S. Prasad, M. V. Rao, S. Bharadwaj, Y. Anjaneyulu, and P. K. Jain, "Flame synthesis of carbon nano onions using liquefied petroleum gas without catalyst," *Materials Science and Engineering: C*, vol. 33, no. 2, pp. 758–762, Mar. 2013, doi: 10.1016/J.MSEC.2012.10.029.

[39] B. K. Mutuma, B. J. Matsoso, K. Ranganathan, J. M. Keartland, D. Wamwangi, and N. J. Coville, "Generation of radical species in CVD grown pristine and N-doped solid carbon spheres using H 2 and Ar as carrier gases," *RSC Adv*, vol. 7, no. 34, pp. 21187–21195, Apr. 2017, doi: 10.1039/C7RA03142D.

[40] Y. Lin, X. Pan, W. Qi, B. Zhang, and D. S. Su, "Nitrogen-doped onion-like carbon: a novel and efficient metal-free catalyst for epoxidation reaction," *J Mater Chem A Mater*, vol. 2, no. 31, pp. 12475–12483, Jul. 2014, doi: 10.1039/C4TA01611D.

[41] A. V. Gubarevich, J. Kitamura, S. Usuba, H. Yokoi, Y. Kakudate, and O. Odawara, "Onion-like carbon deposition by plasma spraying of nanodiamonds," *Carbon N Y*, vol. 41, no. 13, pp. 2601–2606, Jan. 2003, doi: 10.1016/S0008-6223(03)00338-5.

[42] D. Mohapatra, G. Dhakal, M. S. Sayed, B. Subramanya, J. J. Shim, and S. Parida, "Sulfur Doping: Unique Strategy To Improve the Supercapacitive Performance of Carbon Nano-onions," *ACS Appl Mater Interfaces*, vol. 11, no. 8, pp. 8040–8050, Feb. 2019, doi: 10.1021/ACSAMI.8B21534/SUPPL_FILE/AM8B21534_SI_001.PDF.

[43] E. N. Nxumalo, P. J. Letsoalo, L. M. Cele, and N. J. Coville, "The influence of nitrogen sources on nitrogen doped multi-walled carbon nanotubes," *J Organomet Chem*, vol. 695, no. 24, pp. 2596–2602, Nov. 2010, doi: 10.1016/J.JORGANCHEM.2010.08.030.

[44] "(16) How can I interpret a TGA/DTA data? | ResearchGate," Goonoo, Nowsheen. (2015). Accessed: Mar. 10, 2024. [Online]. Available: https://www.researchgate.net/post/How_can_I_interpret_a_TGA_DTA_data/1

[45] K. M. Tripathi *et al.*, "From the traditional way of pyrolysis to tunable photoluminescent water soluble carbon nano-onions for cell imaging and selective sensing of glucose," *RSC Adv*, vol. 6, no. 44, pp. 37319–37329, Apr. 2016, doi: 10.1039/C6RA04030F.

[46] T. H. Mongwe, B. J. Matsoso, B. K. Mutuma, N. J. Coville, and M. S. Maubane, "Synthesis of chain-like carbon nano-onions by a flame assisted pyrolysis technique using different

collecting plates," *Diam Relat Mater*, vol. 90, pp. 135–143, Nov. 2018, doi: 10.1016/j.diamond.2018.10.002.

CHAPTER 4

Physicochemical properties of nitrogen doped and oxidised onion-like carbons

4.1 Introduction

Chemical surface modification of OLCs was extensively researched after their discovery [1]. Their edges with highly curved surfaces display relatively high chemical reactivity as compared to other graphitic nanostructures. It is commonly recognized that as fullerene-like structures get larger, their reactivity decreases because the surface's curvature and related strain decreases [2]. High chemical resistance is exhibited by several carbon nanostructures. Similarly, OLCs aggregate due to strong intermolecular interactions such as van der Waals forces, which results in poor solubility in organic and inorganic solvents [3].

Doping of OLCs has been recently studied and widely used by researchers to improve the physicochemical properties of carbon materials [4]. It has been observed that doping carbon materials with heteroatoms including nitrogen, boron, sulfur, and phosphorus is an efficient way to alter their surface chemistry, electrical structure, and catalytic characteristics. [5] . Incorporation of heteroatoms onto nanoparticle structures has also been shown to increase the surface area of nanoparticles [6] . This is an important feature for an ideal adsorbent. For example, Tovar *et al*. [7] and Mykhailiv *et al*. [8] synthesized nitrogen doped OLCs (N-OLCs) that exhibited higher structural defects and surface areas.

Among the techniques available to produce heteroatom doped OLCs, chemical vapour deposition (CVD) is viewed as a promising strategy to make these materials. The advantage of using CVD is that it does not require extremely high vacuum levels and can typically process substrates in bigger batches. The liquids used that flow into the process chamber from external reservoirs that can be refilled without contaminating the growth environment [9] . Studies has shown successful synthesis of heteroatom doped OLCs via CVD. For instance, a boron-rich graphitic material was synthesized via the CVD of BCl_3 and C_6H_6 by Lin *et al*. [10]. Raghu *et al*. synthesized highly surface-active phosphorus doped OLCs using a CVD method [11]. Shaku *et al*. also produced boron doped OLCs via a CVD method [12].

On the other hand, both ex-situ covalent and non-covalent reactions can occur on OLCs to attach multiple groups on their surfaces to also improve solubility and change physicochemical properties of OLCs [13]. Often, the oxidation reaction serves as the initial

step in the further functionalization of carbons, since it increases the solubility of carbon nanoparticles in aqueous solutions. The functionalization approach employed should be effective enough to deagglomerate the material into individual primary particles and increase the surface available for further chemical reactions [14]. Chen *et al*. showed that sulfuric acid oxidation of single-walled carbon nanotubes (SWCNTs) produced ultra-short SWCNTs, with oxygen-containing functional groups, that were soluble in polar solvents [15]. Sarkar *et al.* also oxidised CNOs through the standard method while Rettenbacher *et al*. oxidized CNOs that improved their solubility for further decoration with complex organic compounds [16].

Several oxidation approaches implemented for the functionalization of OLCs include refluxing with nitric acid [16], using a mixture of sulfuric and nitric acid [17], oxidation by laser ablation [18], and ozonolysis [19]. Of the above-mentioned purification methods, refluxing with nitric acid has been employed most often. For example, Sreeramoju *et al.* oxidized N-CNOs that were synthesized through annealing of nanodiamonds [14], and Hu *et al.* used refluxing nitric acid to purify single-walled carbon nanotubes generated by an electric arc discharge method [20]. In this study, we optimized the nitric acid oxidation method for functionalizing N-OLCs that were produced using the CVD method.

4.2 Experimental procedure

4.2.1 Materials

N-OLCs and oxidised OLCs were prepared using the following reagents without any further treatment: Synthesized E-pOLCs and H-pOLCs, argon, Ar(g) ≥ 99% from Afrox, Johannesburg, South Africa. Ammonia, NH3(g) ≥ 10 % from Afrox, nitric acid, and NH_3 (l) > 32% from Sigma-Aldrich, Johannesburg, South Africa.

4.2.2 Nitrogen doping of the p-OLCs.

The pOLCs were synthesized as described in **section 3.2.2**. N-OLCs were prepared by using a chemical vapor deposition method using argon as carrier gas and ammonia 10% HN_3(g) as nitrogen source [21]. Two grams of the p-OLCs were transferred into a quartz boat which was placed at the center of the quartz tube and mounted inside an electric furnace and the system flushed with argon. The furnace temperature was raised to 600 °C under argon and the p-OLCs were then heated at 600 °C under a stream of dilute gases (100 mL/min argon and 150 mL/min ammonia) for 60 min. The N-OLCs formed were permitted to cool at ambient temperature under argon. After the heat-treatment at 600 °C, the N-OLCs yield was

1.6 g. The decrease in mass is due to loss of sample resulted from prolonged overheating of the sample in the furnace. The schematic representation of the flame pyrolysis method is given in **Scheme 1**.

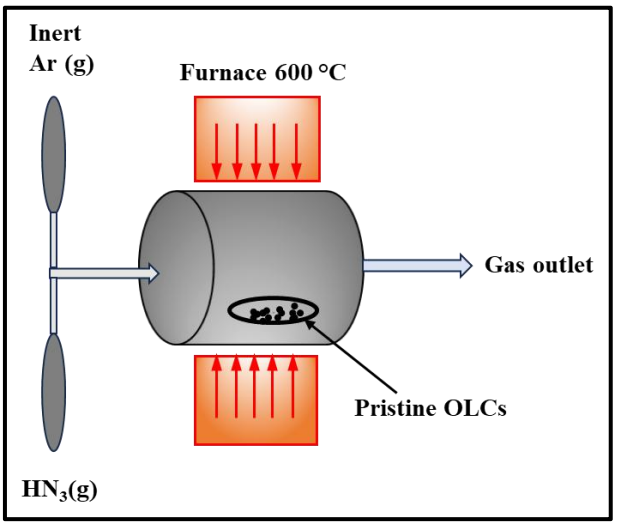

Scheme 1: The schematic representation of N-OLCs synthesis using the CVD method.

4.2.3 Oxidation of the N-OLCs

The p-OLCs were oxidized using 32% nitric acid as described by Hu *et al*. [20]. The p-OLCs (2 g) were transferred to a round bottom flask containing 50 mL of 32% HNO_3. The mixture was refluxed for 6 h. The acidified carbon nano-onions mixture was cooled at room temperature and was separated using a centrifuge (15 000 rpm) for 15 min. The supernatant was removed, and the precipitate was washed twice with about 15 mL distilled water. The sediment was then dried in an oven at 100 °C overnight to obtain the oxidized onion-like carbons (ox-OLCs).

4.3 Characterization of N-OLCs and ox-OLCs

The structural properties of the N-OLCs and ox-OLCs including their morphology, crystallographic nature, and size were determined using XRD, Raman spectroscopy, HRTEM, FTIR, BET, and TGA. All these techniques were employed using the same standard conditions as mentioned in **section 3.3.**

4.4 Results and discussion

4.4.1 Morphological analysis by high magnification TEM

The TEM analysis was conducted to observe possible morphological chances that could occur due to nanoparticle surface modification of the pOLCs. The HRTEM images of the N-OLCs and ox-OLCs from waste household and engine oil are shown in **Figure 4.1 and 4.3.** These micrographs reveals that there were no noticeable changes observed in the morphology of the N-OLCs and ox-OLCs indicating that nitrogen doping and functionalizing of the carbon spheres through the oxidation reaction did not alter the structure of the OLCs. HRTEM images of N-OLCs and ox-OLCs at low magnification are represented in **Figure 4.1 (a – d)**. Studies in literature suggest that functionalisation of the carbon surface with oxygen-rich species can promote carbon de-agglomeration [13] . However, the low magnification images indicate that OLCs from both waste oils are still agglomerated, as expected, after surface modification. **Figure 4.1** shows the average particle sizes of the E-N-OLCs, E-ox-OLCs, H-N-OLCs, and H-ox-OLCs were found to be 36 ± 6.2 nm, 29 ± 5.3 nm, 43 ± 5.8 nm, and 34 ± 6.7 nm respectively. The particle sizes decreased upon N-doping and oxidation. However, the H-pOLCs particle size was not altered post doping.

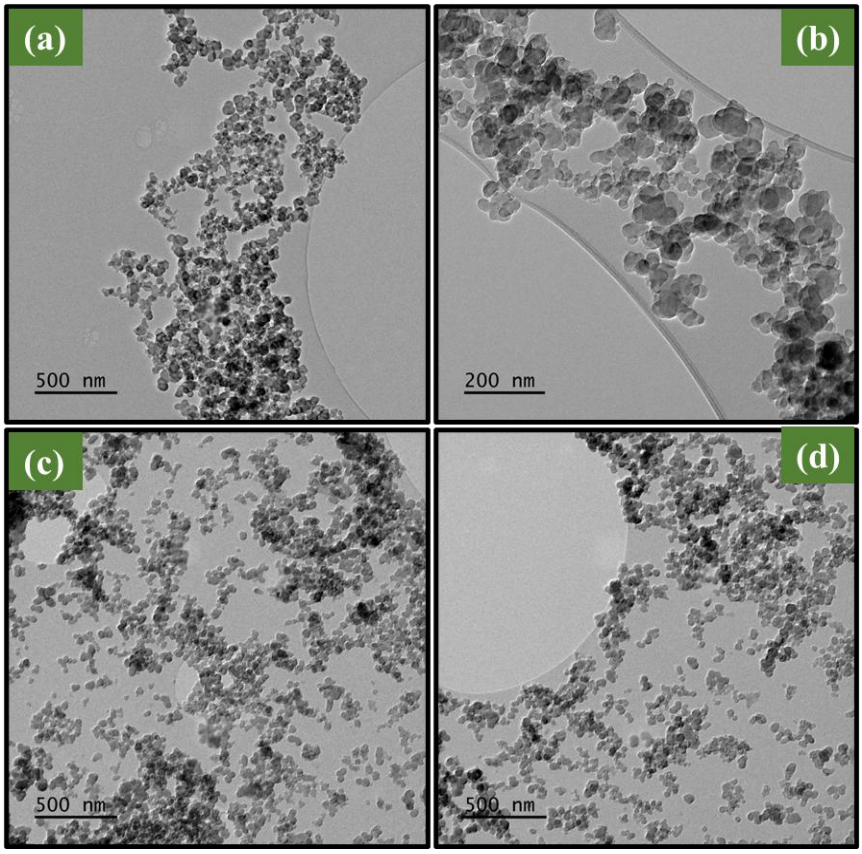

Figure 4.1: Low magnification HRTEM micrographs of the (a) of E-N-OLCs, (b) E-ox-OLCs, (c) H-N-OLCs, and (d) H-ox-OLCs.

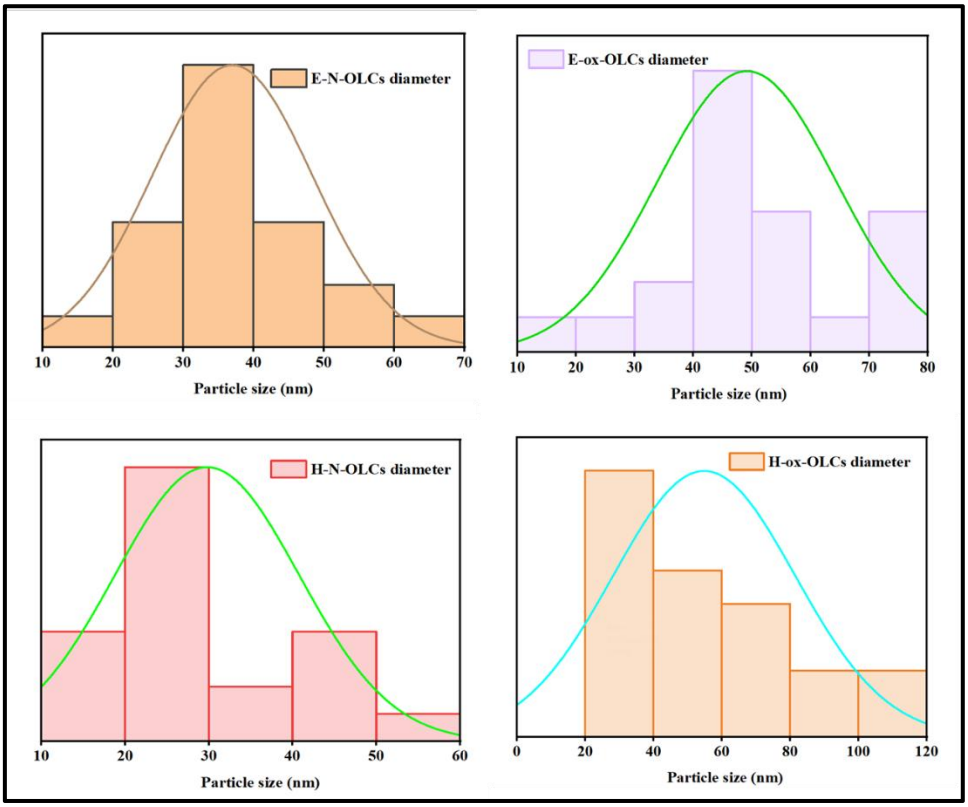

Figure 4.2: Particle size distribution of E-N-OLCs, E-ox-OLCs, H-N-OLCs, and H-ox-OLCs.

Figure 4.3 (a-d) shows high magnification HRTEM images of the ox-CNO, and N-CNO. The images show that these materials are spherical and have an onion-like nanostructure with disconnected shells. As shown in **Figure 4.5**, no conspicuous fracturing in the circular shell of ox-OLCs and N-OLCs was observed, showing the onion-like nanostructure was maintained during the oxidation and nitrogen doping steps. The p-OLCS, ox-OLCs, and N-OLCs were observed to exhibit disordered concentric graphite multi-shells, all with an interplanar spacing close to 0.32 nm [22] . Similar results were observed by Shaikh *et al.* where N-doping of the surface of OLCs made by in-situ doping of OLCs synthesized by flame pyrolysis of castor oil using acetonitrile did not alter the structure of their carbon material [23]. Sikeyi *et al*. also synthesised pOLCs, N-OLCs, and ox-OLCs from pure olive oil using wick-oil frame pyrolysis and the material's morphology remained unchanged post N-doping and oxidation of the material [21].

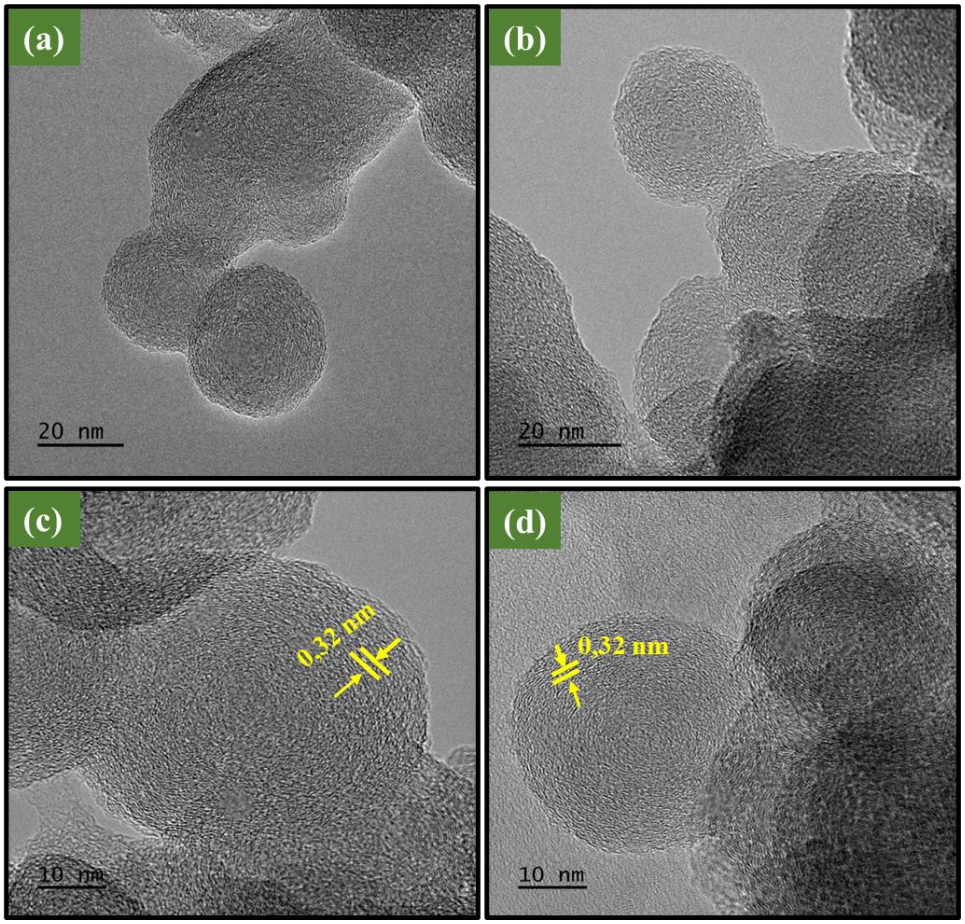

Figure 4.3: High magnification TEM micrographs of (a) E-N-OLCs, (b) E-ox-OLCs, (c) H-N-OLCs, and (d) H-ox-OLCs.

4.4.2 X-ray diffraction (XRD) analysis

The crystallinity of the modified materials was studied using XRD. **Figure 4.4** shows the diffractogram of the N-OLCs and ox-OLCs for both household and engine oil. The diffraction patterns of both oxidised and N-doped materials show an intrinsic carbon peak centred at around 2θ=25.42°, whereas the E-ox-OLCs diffractogram shows an additional weak peak at 2θ = 44.6°. The observed carbon peaks correspond to (002) and (101) planes (**Figure 4.4**) of a disordered carbon structure [24]. The full width at half maximum (FWHM) values of the intense (002) peak were found to be 5.2 and 5.4 for E-N-OLCs and E-ox-OLCs, while H-N-OLCs and H-ox-OLC were found to be 4.7 and 4.8 respectively. This shows that the FWHM of the 002 peak of E-OLCs increased from 4.2 (of E-pOLCs) to 5.2 and H-OLCs slightly increased from 4.5 to 4.7 after nitrogen doping. This is evidence that the incorporation of nitrogen into the carbon matrix creates structural disorder and renders the material to be more amorphous, which broadens the 002 peak. Chatterjee *et al*. showed that

nitrogen-rich OLCs exhibited a similar behaviour [25]. A similar phenomenon is observed on FWHM's of ox-OLCs of both engine and household as shown on **Table 4.1**. This can be assigned to the introduction of hydroxyl functional groups on to the surface of the materials. Fluorinated OLCs made by Frasconi *et al*. showed an increase in FWHM of 002 peak after fictionalisation [26].

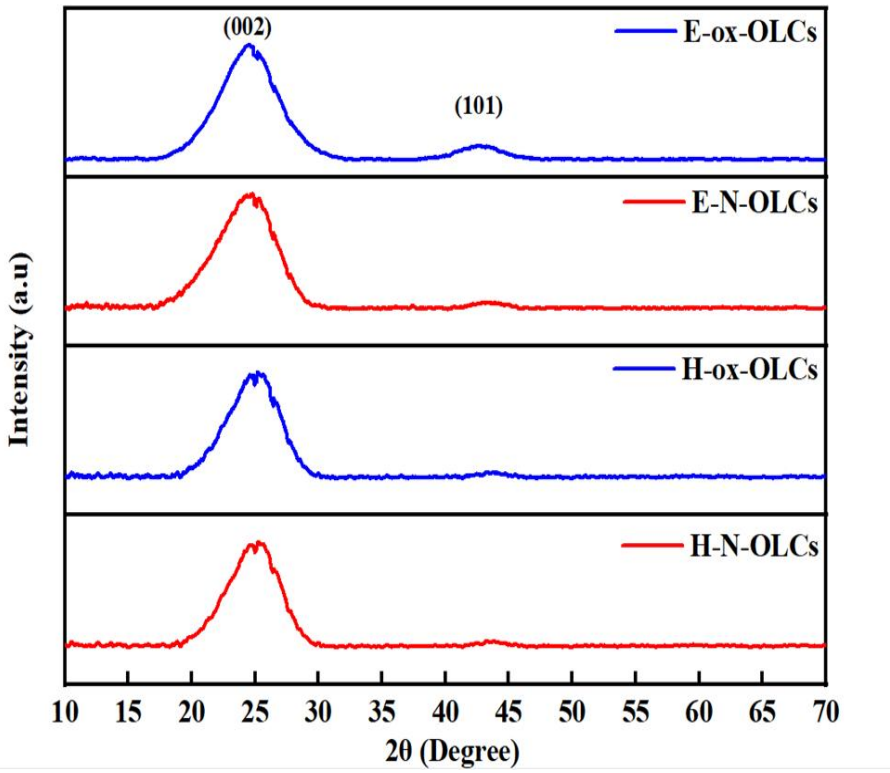

Figure 4.4: X-ray diffractograms for N-OLCs and ox-OLCs from Engine and Household waste oils.

It is noteworthy to mention that the broadening of (002) diffraction peak after doping and functionalising also corresponds to an increase in interlayer spacing (d 002) values which are higher than the d-spacing of graphite material (3.36 Å). **Table 4.1** shows that the interlayer spacing of E-N-OLCs, E-ox-OLCs, H-N-OLCs, and H-ox-OLCs were calculated to be 3.57 Å, 3.66 Å, 3.80 Å, and 3,82 Å respectively. The presence of structural defects in the materials after doping and functionalising resulted in a larger d-spacing than found in the graphite material.

Table 4.1: Summary of FWHM and Interlayer values of N-OLCs and ox-OLCs obtained.

Carbon material	FWHM value	Interlayer spacing (Å)
E-N-OLCs	5.2	3.6
E-ox-OLCs	5.4	3.6
H-N-OLCs	4.7	3.8
H-ox-OLCs	4.8	3.8

4.4.3 Raman spectroscopy analysis

The defects and disorders of the N-doped and functionalised OLCs were further studied using Raman spectroscopy. **Figure 4.5** shows the expected two major peaks (D and G bands) cantered around the 1340 cm^{-1} and 1550 cm^{-1} region for both N-doped and ox-OLCs of engine and household oils. The D and G bands were deconvoluted to reveal additional peaks after OLC modification. The Lorentz G, D_1, D_2, and D_3 bands were fitted for the N-OLCs and ox-OLCs and the disordered graphitic lattice peaks ($A1_g$ symmetry) are observed at D_3 (~1200 cm^{-1}) and D_2 (~1500 cm^{-1}) [27] . It is notable that the pOLCs showed only one additional band (D_3 band), which results from amorphous carbon. On the other hand, the N-doped and ox-OLCs showed two additional bands (see **Figure 4.5**). The two additional bands are due to structural disorder created after nitrogen doping and oxidation of the carbon material. The I_D/ I_G ratio was calculated based on the area under the curves of the major bands (D_1/G). The ratio increased upon N-doping and after oxidation. The increase in I_{D1}/I_G ratio in N-OLCs can be attributed to the presence of more structural defects in the N-OLCs (**Table 4.2**), possibly due to the shorter carbon-nitrogen bond that is formed in the carbon matrix [28]. Likewise, oxidising OLCs caused damage and structural changes on the carbon surfaces by disrupting the graphene sheet structure [13] . It has also been reported that oxidising OLCs usually leads to an increase of the D-band intensity, due to the increase of sp^3-hybridized carbon atoms [29] . The N-OLCs data is similar to that of N-doped OLCs made by Liu *et al.*. This data also corelates to the factionalized OLCs reported by Yu Liu *et al*. which exhibited increased I_D/I_G ratios after functionalization. Sreeramoju *et al*. also

functionalized pristine OLCs through an oxidation reaction and the value of the I_D/I_G ratio increased upon introduction of hydroxyl groups onto the carbon surface [30].

Table 4.2: Raman data showing peak positions, intensities, and intensity ratios for

N-OLCs, and ox-OLCs

Material	**D_1-band position**	**G-band position**	**I_{D1}/I_G**
E-N-OLCs	1340.6	1588.7	4.7
E-ox-OLCs	1340.3	1587.4	4.8
H-N-OLCs	1348.2	1589.8	4.1
H-ox-OLCs	1347.7	1588.2	4.4

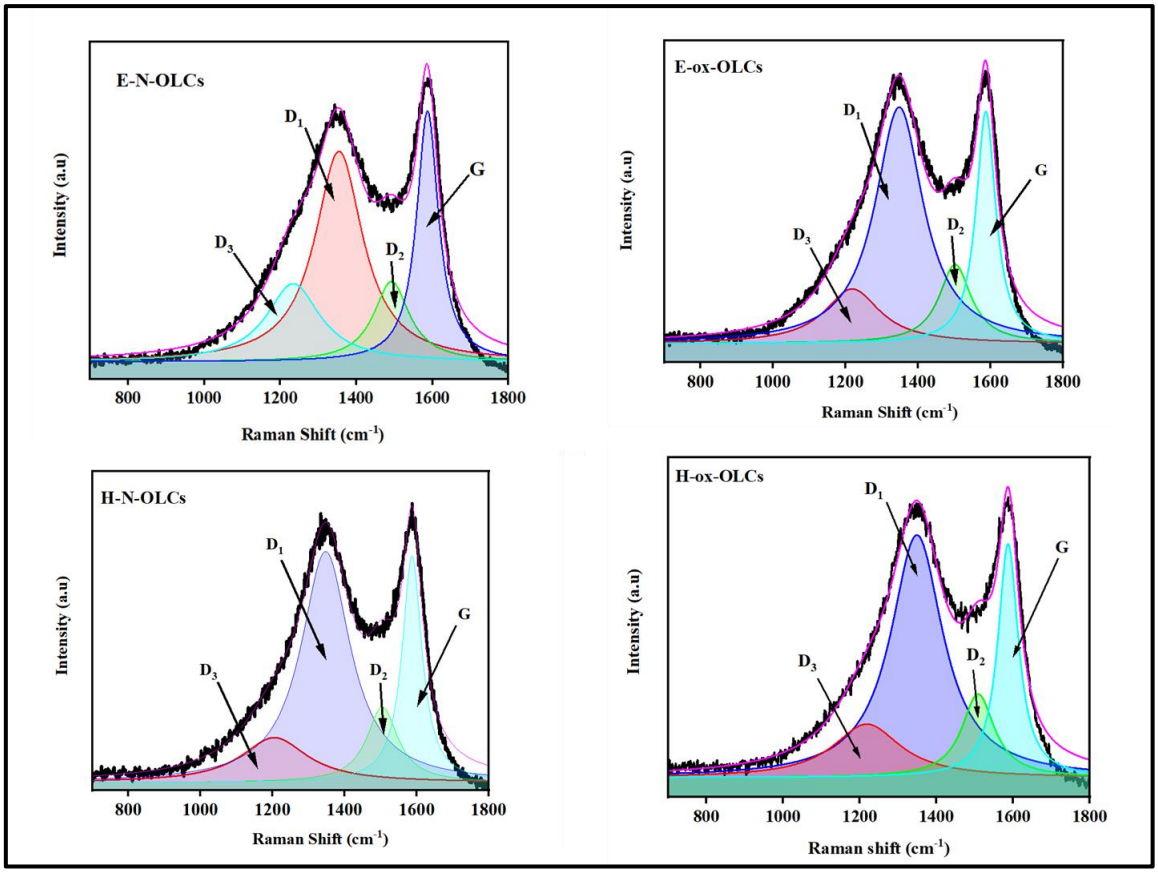

Figure 4.5: Raman spectra of E-N-OLCs, E-ox-OLCs, H-N-OLCs, and H-ox-OLCs.

4.4.5. Thermal gravimetric analysis

TGA analysis was conducted to compare the thermal stabilities of N-OLCs and ox-OLCs to support and provide evidence of successful nitrogen incorporation onto the carbon material matrix and attachment of hydroxyl groups onto to carbon surface. **Figure 4.5** presents the TGA and derivative curves of N-OLCs and ox-OLCs. **Figure 4.5a** shows that after doping the OLCs with nitrogen, H-N-OLCs exhibited the highest onset decomposition temperature (572.2 °C) compared to E-N-OLCs (537.81 °C). It is also notable that the decomposition temperatures of these materials increased after doping as the decomposition temperatures of E-pOLCs and H-pOLCs were found to be 532.7 °C and 530.2 °C respectively. The increase in decomposition temperatures after doping pOLC can be assigned to the presence of nitrogen in the carbon matrix while their differences can be attributed to the heteroatom content present in the material. **Figure 4.5a** also shows that the E-ox-OLCs decomposed at a higher temperatures (598.1 °C) as compared to E-N-OLCs. This is possibly due to the impurities present in the carbon material after oxidising the OLCs. However, H-ox-OLCs decomposed at a lower temperature (537.9 °C) as compared to H-N-OLCs (572.2 °C). This can be assigned to the oxygen-containing functional groups present in the carbon material. Similar findings were reported by Sikeyi *et al*. who synthesized N-doped and oxygen functionalised OLCs [21].

Figure 4.5b represents the DTA curves of N-OLCs and ox-OLCs OLCs and shows their decomposition peaks. It is notable that H-ox-OLCs presented two prominent peaks at temperature 108.4 °C and at 643.31 °C, while the other OLCs showed one peak at temperatures 677.8 °C, 694.5 °C, and 666.0 °C for E-ox-OLCs, E-N-OLCs, and H-N-OLCs respectively. The peak at temperature 114.4 °C is assigned to the loss of water in the H-ox-OLCs. A weak peak can be observed at 83 °C in DTA profile of E-ox-OLCs which suggests that E-ox-OLCs is also due to loss of water. A thermal stability study that was conducted by Li *et al*. showed that oxygen-containing function groups decompose at temperatures below 126.8 °C [31].

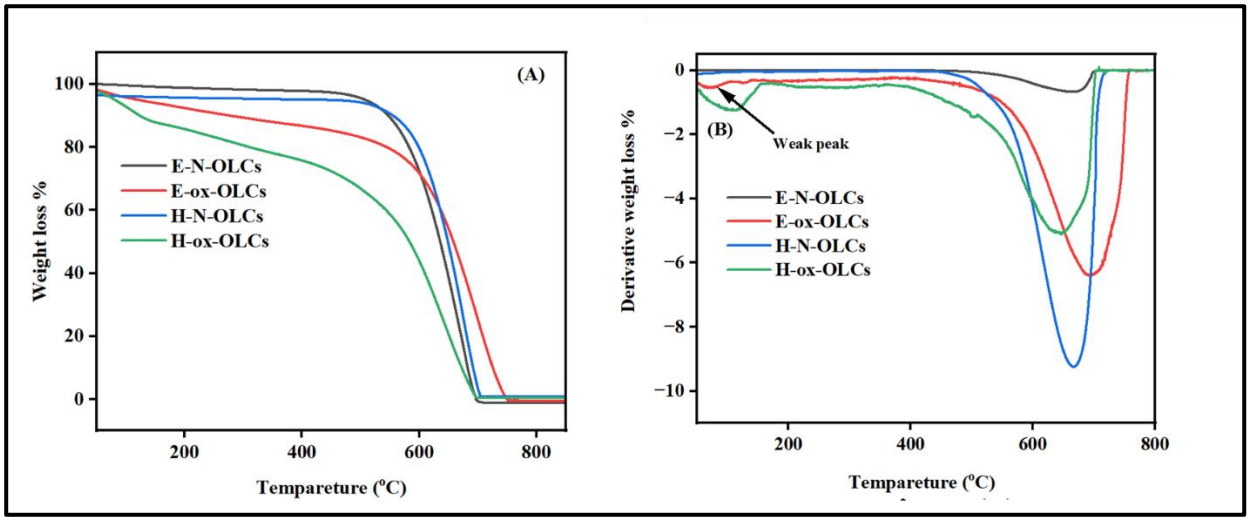

Figure 4.6: (a) TGA and (b) the corresponding derivative (DTGA) curves of N-OLCs and ox-OLCs.

4.4.4. Surface area and porosity analysis

The BET surface area analysis was conducted to measure the surface area and pore size of the N-OLCs and ox-OLCs. The interpretation of the results was based on the adsorption-desorption of liquid N_2 at 77 K. [32]. As shown in **Table 4.1**, the S_{BET} value obtained for E-N-OLCs and H-N-OLCs were 169.9 m^2/g and 179.3 m^2/g respectively. A study conducted by Shi *et al*. revealed that the modification of OLCs surface may result in defects on the carbon lattice thereby leading to formation of inter and intra-particle pores. [33]. The S_{BET} values of OLCs have increased upon doping due to increased defects and disorder as revealed by Raman analysis in **Section 4.4.3.** **Table 4.3** also shows the increase of S_{BET} values of OLCs after oxidising the N-OLCs. The surface areas of the E-ox-OLCs and H-ox-OLCs were found to be 182.2 m^2/g and 198 m^2/g respectively. Similarly, functionalization does not only introduce the functional groups on the surface of OLCs, but it is also linked to the presence of defects in the carbon lattice and the presence of sp^3-hybridized carbon atoms on the surface of nanoparticles [34]. The BET data of oxidised OLCs also correlates with the Raman and HRTEM data.

Table 4.3: Summarizes BET analysis data of pristine OLCs.

Material	**Surface Area (m^2/g)**	**Pore Size (nm)**
E-N-OLCs	169.9	38.8

E-ox-OLCs	198.2	53.8
H-N-OLCs	176.3	45.1
H-ox-OLCs	182.5	74.9

The plots of adsorption–desorption isotherms of N_2 at 77 K were also conducted for N-OLCs and ox-OLCs and are depicted in **Figure 4.7.** N-OLCs and ox-OLCs from both engine oil and household oil exhibited similar plots that resembles isotherm type IV. All the hysteresis loops show a type IV isothermal behaviour, and this is due to the presence of both mesopores and micropores [35]. This data provides evidence that the nanoparticle pores of both N-OLCs and ox-OLCs are mesopore (2-50 nm), except for H-ox-OLCs which was found to be 74.9 nm indicating the presence of macropores. This can be attributed to the intense damage and structural changes on the carbon surfaces post oxidation.

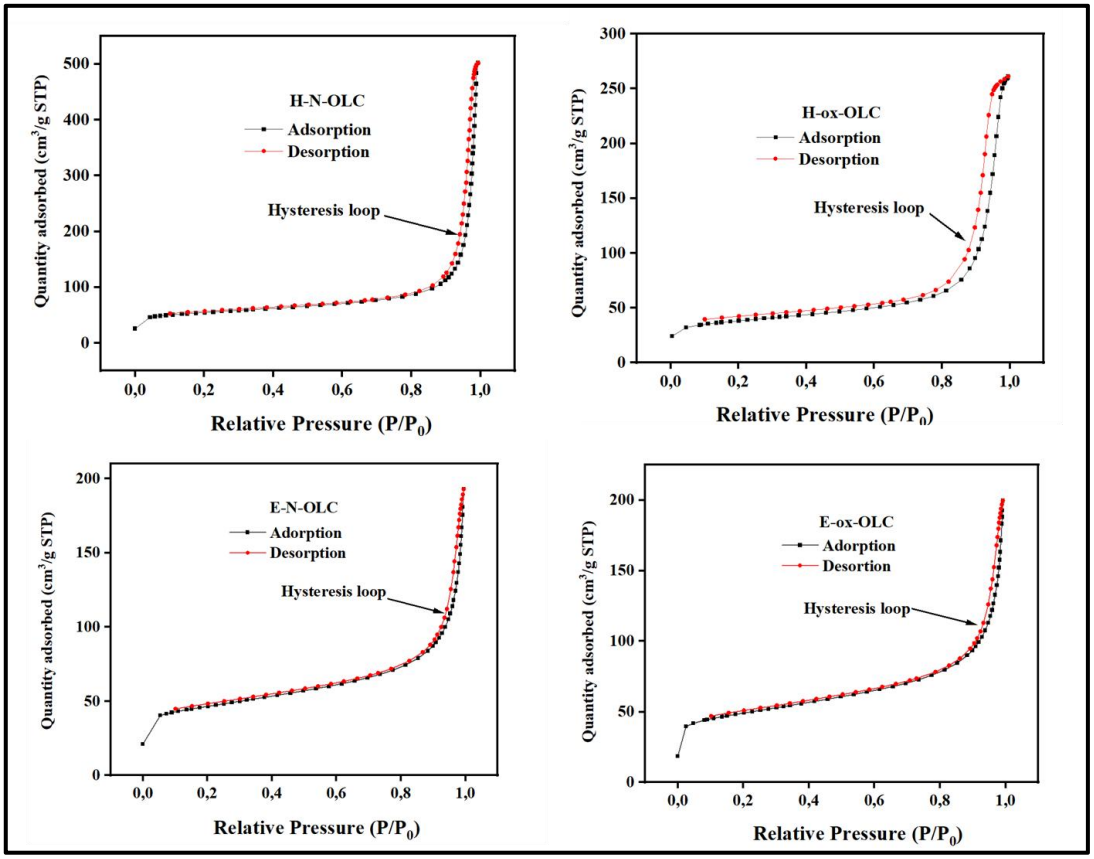

Figure 4.7: N_2 adsorption and desorption isothermal curves of N-OLCs and ox-OLCs.

4.5 Conclusion

The simple synthesis of quasi-spherical N-OLCs and ox-OLCs with particle sizes between ca. 29-60 nm was successfully achieved using a CVD method and an oxidation reaction. The HRTEM analysis revealed that the properties of N-OLCs and ox-OLCs such as shape and structure remained the same as those of pOLCs, while the particle size decreased post modification. Raman and XRD analysis results indicated that the incorporation of nitrogen and the introduction of hydroxyl groups caused stress and minor structural disorders which is linked with increasing particle surface area. The TGA-DTA profiles indicated oxygen-containing groups in E-ox-OLCs and the presence of impurities in H-ox-OLCs.

REFERENCES

[1] Y. Zheng and P. Zhu, “Carbon nano-onions: large-scale preparation, functionalization and their application as anode material for rechargeable lithium ion batteries,” *RSC Adv*, vol. 6, no. 95, pp. 92285–92298, Sep. 2016, doi: 10.1039/C6RA19060J.

[2] A. Hirsch, “Fullerenes and related structures”.

[3] J. Bartelmess and S. Giordani, “Carbon nano-onions (multi-layer fullerenes): chemistry and applications,” *Beilstein Journal of Nanotechnology 5:207*, vol. 5, no. 1, pp. 1980–1998, Nov. 2014, doi: 10.3762/BJNANO.5.207.

[4] M. Boshir Ahmed *et al.*, “General Doping Chemistry of Carbon Materials,” *ChemNanoMat*, vol. 9, no. 4, p. e202200482, Apr. 2023, doi: 10.1002/CNMA.202200482.

[5] Y. Lin, Y. Zhu, B. Zhang, Y. A. Kim, M. Endo, and D. S. Su, “Boron-doped onion-like carbon with enriched substitutional boron: the relationship between electronic properties and catalytic performance,” *J Mater Chem A Mater*, vol. 3, no. 43, pp. 21805–21814, Oct. 2015, doi: 10.1039/C5TA03141A.

[6] B. Shaku, T. P. Mofokeng, T. H. Mongwe, N. J. Coville, K. I. Ozoemena, and M. S. Maubane-Nkadimeng, “Physicochemical Properties of Nitrogen Doped Carbon Nano-onions Grown by Flame Pyrolysis from Grapeseed Oil for Use in Supercapacitors,” *Electroanalysis*, vol. 32, no. 12, pp. 2946–2957, Dec. 2020, doi: 10.1002/ELAN.202060383.

[7] E. Tovar-Martinez, J. V. Cabrera-Salazar, D. Hernandez-Arriaga, M. Reyes-Reyes, L. F. Chazaro-Ruiz, and R. López-Sandoval, “Nitrogen doped carbon nanotubes decorated with iron carbide nanoparticles and their electrochemical capacitance,” *Mater Today Commun*, vol. 21, p. 100667, Dec. 2019, doi: 10.1016/J.MTCOMM.2019.100667.

[8] O. Mykhailiv *et al.*, “Improvement of the Structural and Chemical Properties of Carbon Nano-onions for Electrocatalysis,” *ChemNanoMat*, vol. 3, no. 8, pp. 583–590, Aug. 2017, doi: 10.1002/CNMA.201700161.

[9] “Chemical Vapor Deposition,” *The Materials Science of Semiconductors*, pp. 573–609, 2008, doi: 10.1007/978-0-387-68650-9_12.

[10] Y. Lin, Y. Zhu, B. Zhang, Y. A. Kim, M. Endo, and D. S. Su, “Boron-doped onion-like carbon with enriched substitutional boron: the relationship between electronic properties and catalytic performance,” *J Mater Chem A Mater*, vol. 3, no. 43, pp. 21805–21814, Oct. 2015, doi: 10.1039/C5TA03141A.

[11] A. V. Raghu, K. K. Karuppanan, and B. Pullithadathil, “Highly Surface Active Phosphorus-Doped Onion-Like Carbon Nanostructures: Ultrasensitive, Fully Reversible, and Portable NH3Gas Sensors,” *ACS Appl Electron Mater*, vol. 1, no. 11, pp. 2208–2219, Nov. 2019, doi: 10.1021/ACSAELM.9B00412/SUPPL_FILE/EL9B00412_SI_001.PDF.

[12] B. Shaku, M. S. Maubane-Nkadimeng, N. J. Coville, and K. I. Ozoemena, “Synthesis and application of boron-nitrogen doped carbon nano-onions in supercapacitors”.

[13] O. Mykhailiv, H. Zubyk, and M. E. Plonska-Brzezinska, “Carbon nano-onions: Unique carbon nanostructures with fascinating properties and their potential applications,” *Inorganica Chim Acta*, vol. 468, pp. 49–66, Nov. 2017, doi: 10.1016/J.ICA.2017.07.021.

[14] M. K. Sreeramoju, J. P. Selegue, R. Podila, and A. M. Rao, “Surface functional group investigation of oxidized, nanodiamond-derived carbon nano-onions,” *Mater Today Commun*, vol. 26, p. 101966, Mar. 2021, doi: 10.1016/J.MTCOMM.2020.101966.

[15] Z. Chen *et al.*, “Soluble ultra-short single-walled carbon nanotubes,” *J Am Chem Soc*, vol. 128, no. 32, pp. 10568–10571, Aug. 2006, doi: 10.1021/JA063283P/SUPPL_FILE/JA063283PSI20060620_113159.PDF.

[16] A. S. Rettenbacher, B. Elliott, J. S. Hudson, A. Amirkhanian, and L. Echegoyen, “Preparation and Functionalization of Multilayer Fullerenes (Carbon Nano-Onions),” *Chemistry – A European Journal*, vol. 12, no. 2, pp. 376–387, Jan. 2006, doi: 10.1002/CHEM.200500517.

[17] R. Borgohain, J. Li, J. P. Selegue, and Y. T. Cheng, “Electrochemical study of functionalized carbon nano-onions for high-performance supercapacitor electrodes,” *Journal of Physical Chemistry C*, vol. 116, no. 28, pp. 15068–15075, Jul. 2012, doi: 10.1021/JP301642S/ASSET/IMAGES/MEDIUM/JP-2012-01642S_0007.GIF.

[18] R. L. Calabro, D. S. Yang, and D. Y. Kim, “Liquid-phase laser ablation synthesis of graphene quantum dots from carbon nano-onions: Comparison with chemical oxidation,” *J Colloid Interface Sci*, vol. 527, pp. 132–140, Oct. 2018, doi: 10.1016/J.JCIS.2018.04.113.

[19] M. E. Plonska-Brzezinska *et al.*, “The synthesis and characterization of carbon nano-onions produced by solution ozonolysis,” *Carbon N Y*, vol. 49, no. 15, pp. 5079–5089, Dec. 2011, doi: 10.1016/J.CARBON.2011.07.027.

[20] H. Hu, B. Zhao, M. E. Itkis, and R. C. Haddon, “Nitric Acid Purification of Single-Walled Carbon Nanotubes,” *Journal of Physical Chemistry B*, vol. 107, no. 50, pp. 13838–13842, Dec. 2003, doi: 10.1021/JP035719I.

[21] L. L. Sikeyi *et al.*, “Microwave assisted synthesis of nitrogen doped and oxygen functionalized carbon nano onions supported palladium nanoparticles as hybrid anodic electrocatalysts for direct alkaline ethanol fuel cells,” *Int J Hydrogen Energy*, vol. 46, no. 18, pp. 10862–10875, Mar. 2021, doi: 10.1016/J.IJHYDENE.2020.12.154.

[22] K. Chatterjee *et al.*, “Nitrogen-rich carbon nano-onions for oxygen reduction reaction,” *Carbon N Y*, vol. 130, pp. 645–651, Apr. 2018, doi: 10.1016/J.CARBON.2018.01.052.

[23] A. Shaikh, B. K. Singh, D. Mohapatra, and S. Parida, “Nitrogen-Doped Carbon Nano-Onions as a Metal-Free Electrocatalyst,” *Electrocatalysis*, vol. 10, no. 3, pp. 222–231, May 2019, doi: 10.1007/S12678-019-00514-9/METRICS.

[24] J. K. McDonough and Y. Gogotsi, “Carbon onions: Synthesis and electrochemical applications,” *Electrochemical Society Interface*, vol. 22, no. 3, pp. 61–66, Jan. 2013, doi: 10.1149/2.F05133IF/XML.

[25] K. Chatterjee *et al.*, “Nitrogen-rich carbon nano-onions for oxygen reduction reaction,” *Carbon N Y*, vol. 130, pp. 645–651, Apr. 2018, doi: 10.1016/J.CARBON.2018.01.052.

[26] M. Frasconi, V. Maffeis, J. Bartelmess, L. Echegoyen, and S. Giordani, “Highly surface functionalized carbon nano-onions for bright light bioimaging,” *Methods Appl Fluoresc*, vol. 3, no. 4, p. 044005, Oct. 2015, doi: 10.1088/2050-6120/3/4/044005.

[27] T. P. Mofokeng, Z. N. Tetana, and K. I. Ozoemena, “Defective 3D nitrogen-doped carbon nanotube-carbon fibre networks for high-performance supercapacitor: Transformative role of nitrogen-doping from surface-confined to diffusive kinetics,” *Carbon N Y*, vol. 169, pp. 312–326, Nov. 2020, doi: 10.1016/J.CARBON.2020.07.049.

[28] L. S. Panchakarla *et al.*, “Synthesis, Structure, and Properties of Boron- and Nitrogen-Doped Graphene,” *Advanced Materials*, vol. 21, no. 46, pp. 4726–4730, Dec. 2009, doi: 10.1002/ADMA.200901285.

[29] J. Bartelmess and S. Giordani, “Carbon nano-onions (multi-layer fullerenes): chemistry and applications,” *Beilstein Journal of Nanotechnology 5:207*, vol. 5, no. 1, pp. 1980–1998, Nov. 2014, doi: 10.3762/BJNANO.5.207.

[30] M. K. Sreeramoju, J. P. Selegue, R. Podila, and A. M. Rao, “Surface functional group investigation of oxidized, nanodiamond-derived carbon nano-onions,” *Mater Today Commun*, vol. 26, p. 101966, Mar. 2021, doi: 10.1016/J.MTCOMM.2020.101966.

[31] L. Li, X. Yao, H. Li, Z. Liu, W. Ma, and X. Liang, “Thermal Stability of Oxygen-Containing Functional Groups on Activated Carbon Surfaces in a Thermal Oxidative Environment,” *JOURNAL OF CHEMICAL ENGINEERING OF JAPAN*, vol. 47, no. 1, pp. 21–27, Jan. 2014, doi: 10.1252/JCEJ.13WE193.

[32] O. Y. Bakather, A. Kayvani Fard, Ihsanullah, M. Khraisheh, M. S. Nasser, and M. A. Atieh, “Enhanced Adsorption of Selenium Ions from Aqueous Solution Using Iron Oxide Impregnated Carbon Nanotubes,” *Bioinorg Chem Appl*, vol. 2017, 2017, doi: 10.1155/2017/4323619.

[33] K. Shi, J. Liu, and R. Chen, “Nitrogen-Doped nano-carbon onion rings for energy storage in Lithium-ion capacitors,” *J Energy Storage*, vol. 31, p. 101609, Oct. 2020, doi: 10.1016/J.EST.2020.101609.

[34] “Sci-Hub | Carbon nano-onions: Unique carbon nanostructures with fascinating properties and their potential applications. Inorganica Chimica Acta, 468, 49–66 | 10.1016/j.ica.2017.07.021.” Accessed: Jan. 15, 2024. [Online]. Available: https://sci-hub.se/10.1016/j.ica.2017.07.021

[35] L. Huang *et al.*, “Recovery of lanthanum cations by functionalized magnetic multi-walled carbon nanotube bundles,” *RSC Adv*, vol. 11, no. 8, pp. 4751–4759, Jan. 2021, doi: 10.1039/D0RA09902C.

CHAPTER 5

Application of onion-like carbons as adsorbents for the removal of tartrazine dye in water

5.1 Introduction

Wastewater-containing dyes present a serious environmental problem because of its high toxicity and possible accumulation in the environment [1]. Most of these dyes are synthetic and are classified as triphenylmethane and phthalocyanine derivatives. Most of these dyes contain aromatic rings, which make them carcinogenic and mutagenic [2]. Dyes containing –N═N– group, are known as azo dyes. Due to the extensive use of these dyes in industries, they become an integral part of industrial wastewater. Therefore, the removal of dyes from textile effluents is currently of great interest [3]. Adsorption is extensively used for decontamination because it has a facile operation procedure, greater removal efficiency, and low processing cost and generates no by-product [4]. Nanostructured materials, on the other hand, possess a comparatively greater specific surface area and corresponding adsorption sites in addition to tunable surface features (pore volume and surface functionalities) which bestow on them high adsorption efficiency, quick adsorption rates, and efficacious in a broad range of pH [5].

In the recent times, OLCs have transpired as attractive adsorbents because of their unique structure and chemistry [6,7,8]. OLCs are a constituent of carbon nanostructures, consisting of distinct concentric shells of graphitic carbon. Pristine OLCs have a fully available outer surface with large surface area and curved edges, easing the attachment of multiple functional groups to their surface, thereby improving the solubility [9]. OLCs possess relatively higher chemical reactivity compared with other nanocarbon materials owing to the nature of their chemical bonds and higher strain.

Onions-like carbons have previously been explored as adsorbents [10]. For example, Kumari *et al*. studied the adsorption capacities of OLCs for the removal of norfloxacin (NOR) and hydrochloride (TCH) antibiotics in water. The OLCs showed good adsorption efficiency with maximum adsorption capacity (qmax) was found to be 416.66 and 344.82 mg g^{-1} for TCH and NOR, respectively [11]. Tripathi *et al*. used OLCs for the adsorption of ox-onions in drinking water and concluded that OLCs provide high adsorption efficiency for the removal of MnO_4^- (99.9%) from aqueous system at ambient temperature, neutral pH in 70 min [12].

In another study Gupta *et al*. studied the biomass-derived OLCs as adsorbents for the removal of organic pollutants and oils from water and found that the OLCs exhibit the promising potential to be used in practical applications for oil-polluted water treatment. These studies demonstrated the compatibility of OLCs as adsorbents. However, OLCs in these studies were used as received without any modifications and were not sourced from any waste. Studies showed that modification of carbons enhances their adsorption capacity [13]. Hence in this study, we present an innovative approach to investigate the adsorption capacity of surface modified OLCs produced from waste materials. Our goal is to interpret and understand the interactions and adsorption capacities between differently modified OLCs derived from different waste materials, and the dye, to optimize nanocarbons as adsorbent.

5.2 Experimental procedures

5.2.1 Materials

Tartrazine dye (trisodium;5-oxo-1-(4-sulfonatophenyl)-4-[(4-sulfonatophenyl)diazenyl]-4*H*-pyrazole-3-carboxylate, $C_{16}H_9N_4Na_3O_9S_2$), Hydrochloric acid (HCl), Sodium hydroxide (NaOH) were purchased from Sigma Aldrich (Johannesburg, South Africa) and employed without further purification. The stock solutions were prepared using distilled water.

5.2.2. Batch adsorption experiments

5.2.2.1 Preparation of dye stock solution

The stock solution of the tartrazine dye was prepared by dissolving tartrazine dye (1 g) and transfer to a 1000 mL volumetric flask, followed by filling the flask to the mark with distilled water, to achieve a 1000 mg/L concentrated tartrazine solution. The appropriate concentrations needed for adsorption studies were prepared from the stock solution. Ultraviolet – visible spectroscopy (UV-vis Spec) calibration standards were obtained using 5, 10, 13, 15, and 20 mg/L solutions prepared from the stock solution through series of dilutions.

5.2.2.2. Adsorption experiments

The batch adsorption experiments of OLCs were carried out at room temperature using 5 - 25mg/L initial dye concentrations (shaked for 24 h at 220 rpm). The amount of the adsorbent was kept constant at 30 mg through all the experiments. Parameters such as pH, initial dye solution concentration, and contact time were varied to establish the optimum conditions for the removal of the dye. The pH of the dye solution was regulated with pH meter using 0,1M

of HCl(aq) and NaOH(aq). Typically, a desired amount of OLCs as adsorbent was mixed with the dye solution and shaken using an obit shaker. Thereafter, carbons were filtered out using 0.22µm syringe microfilters. UV-vis Spectrometer with wavelength range of 200 – 500 nm was used to determine the final concentration of the dye solution at 256nm. The adsorption (mg/g) capacity of the OLCs was calculated using Equation 5.1:

$$q_e = \frac{(C_i - C_{eq})V}{m} \qquad \textbf{5.1}$$

where q_e is the adsorption capacity (mg/g), C_i is the initial concentration and C_{eq} is the

equilibrium concentration (mg/L), m is the mass of the adsorbent (g) and V is the volume of the solutions (L). The removal percentage of the dye (% R) was be calculated as:

$$\%R = \left(\frac{C_i - C_{eq}}{C_i}\right) x100 \qquad \textbf{5.2}$$

where C_i is the initial concentration of adsorbate (mg/L) and C_{eq} is the equilibrium

concentration of adsorbate (mg/L)

5.2.2.2.1 Point of zero charge

The point of zero charge (pH_{PZC}) was obtained by measuring the initial pH and final pH in all pH parameter experiments. The initial pH was determined as the pH measured from the water before the experiment, and the final pH was determined as the pH of the solution measured post-experiment after filtering the adsorbent. These values were recorded and a plot of change in pH versus initial pH was deduced from the values. The point at which the curve of the graph crosses the x-intercept was determined as the pH_{PZC} [14].

5.2.2.2.2 Adsorption kinetics

The kinetics of the experimental data were determined using pseudo-first order (PFO), and pseudo-second order (PSO) adsorption models [15].

5.2.2.2.2.1 Pseudo-first order model

The Lagergren pseudo-first-order model proposes that the rate of adsorption is proportional to the number of sites unoccupied by the adsorbate. The pseudo-first-order equation can be written in a non-linear (Equation 5.3) and linear (Equation 5.4) equations as follows:

$$q_t = q_e\left(1 - e^{-tk1}\right) \qquad \textbf{5.3}$$

$$\frac{dq_t}{dt} = k_{pl}(q_e - q_t), \quad \textbf{5.4}$$

where qt is the adsorption capacity (mg/g) at any present time interval (t), qe is the adsorption capacity at equilibrium and k_1 is the pseudo-first-order rate constant (1/min).

5.2.2.2.2.2 Pseudo-second order model

The adsorption data can be analysed using the pseudo-second-order kinetic model. The pseudo-second-order kinetic model can be written in a non-linear (Equation 5.5) and linear (Equation 5.6) as follows:

$$q_t = \frac{q_e^2 k_2}{1 + k_2 q_e t} \quad \textbf{5.5}$$

$$log(q_e - q_t) = \frac{k_1}{2{,}303} + log(q_e) \quad \textbf{5.6}$$

where q_t is the adsorption capacity (mg/g) at any present time interval (t), q_e is adsorption capacity at equilibrium and k_1 is the pseudo-second order rate constant (min^{-1}). The parameters q_e, k_2 and h were obtained from the slope and intercept of the t/q_t versus time. In which the initial adsorption rate was calculated from the equation below:

$$h = k_2 q_2^2 \quad \textbf{5.7}$$

where h is the initial adsorption rate (mg/g/min), q_e is adsorption capacity at equilibrium and k_2 is the second-order rate constant (g/mg min)

5.2.2.2.3 Adsorption isotherms

The adsorption isotherms are significant as they give data about the adsorption capacity and how the adsorbate cooperates with the adsorbents, which are basic in optimizing the use of an adsorbent. Herein, Langmuir and Freundlich models were employed to determine the best descriptor of the study [16]. They were calculated manually and with Ky plot software.

5.2.2.2.3.1. Langmuir isotherm model

The Langmuir isotherm is projected to describe the gas-solid phase, although it is used in this study to describe the liquid-solid interaction and assumes monolayer adsorption on a uniform surface with the same affinity and has no lateral interaction [17]. This isotherm is governed by Equation 5.8 non-linear and Equation 5.9 linear below.

$$q_e = \frac{Q^0_{max} K_L C_e}{1 + K_L C_e} \quad \textbf{5.8}$$

$$\frac{C_e}{q_e} = \left(\frac{1}{Q^0_{max}}\right) C_e + \frac{1}{Q^0_{max} K_L} \quad \textbf{5.9}$$

where C_e is a concentration of the adsorbate at equilibrium (mg/g), q_e is the quantity or maximum adsorption capacity (mg/g), q_{max} is the maximum amount of the adsorbate adsorbed (mg/g), K_f is the Langmuir constant related to the energy of the adsorption. The crucial characteristic of the Langmuir isotherm can be achieved by a constant called equilibrium parameter or separation factor (R_L) calculated by Equation 5.10:

$$R_L = \frac{1}{1 + K_L C_0} \quad \textbf{5.10}$$

where, K_L is the Langmuir constant (mg/g), C_o is initial concentration of initial adsorbate (mg/g), R_L lies within 0 and 1 when adsorption is favourable: when R_L >1- unfavourable, R_L =1- linear, RL =0 - irreversible and R_L <1- favourable.

5.2.2.2.3.2. Freundlich isotherm model

The Freundlich model is an observational relationship depicting the uptake of adsorbate particles on a heterogeneous surface. The model assumes multi-layer adsorption and accepts the existence of various sites with different energies on the surface of the adsorbent [17]. This isotherm is governed by Equation 5.11 non-linear and Equation 5.12 linear below.

$$q_e = K_F C_e^{\frac{1}{n}} \quad \textbf{5.11}$$

$$log q_e = \frac{1}{n} log C_e + log K_f \quad \textbf{5.12}$$

where, K_f is a constant adsorption capacity (L/mg), q_e is the concentration at equilibrium (mg/L), Ce is the equilibrium concentration (mg/L), n is a constant adsorption intensity. Furthermore, to determine the best-suited model, the chi-squared χ 2 of the experimental data can be calculated using the equation:

$$\chi^2 = \frac{(q_{e,exp} - q_{e,cal})^2}{q_{e,cal}} \quad \textbf{5.13}$$

where, $q_{e,exp}$ and $q_{e,calc}$ (mg/g) are the amount of adsorbate uptake at equilibrium and achieved, respectively. In which the χ^2 value that is close to zero or 1 is best fitted to the model.

5.3. Results and Discussions

5.3.1. Adsorption studies

5.3.1.1. Effect of pH solution

5.3.1.1.1 Effect of pH solution on pristine OLCs

pH of the solution plays a vital role in the adsorption of dyes, as it affects the surface bonding sites of the adsorbent [18]. The effect of pH was investigated using E-pOLCs, H-pOLCs, R-pOLCs, and O-pOLCs. **Figure 5.1** depicts the experimental data for the effect of pH (1-9) for the pristine carbons derived from all waste oils. Based on the data, it is evident that at pH 1, there is maximum adsorption removal percentage of the dye for all carbons. This due to the presence of H^+ ions in the solution which results to the surface of the carbons being protonated and hence higher affinity to bind with the anionic tartrazine dye [19]. Huisien S *et al*. reported that it is commonly observed that adsorbent adsorbs anions favorably at lower pH due to the presence of H^+ ions, where at higher pH, it is active for adsorption of cations due to the deposition of OH^- ions [19]. It is also notable that pristine carbon materials from engine waste oil and household waste oil have the highest percentage removal of 65% and 54% respectively. This can be attributed to surface chemistry of the materials, household and engine waste oil carbons having the highest BET surface areas of 70.3296 m^2/g and 70.5668 m^2/g respectively. However, there was a significant decrease in removal percentage at pH 3 – 9 for all the OLCs. This can be associated to the presence of OH^- in the surface of the carbons which repel the anionic adsorbate dye [20].

The point of zero charge (pH_{PZC}) values were the values of the x-intercepts from the plot of change in pH against initial pH. The pH_{PZC} values of E-pOLCs, H-pOLCs, R-pOLCs, and O-pOLCs were found to be 2.5, 1.3, 1.7, and 1.5 respectively. The plots that support this data are provided on **Figure S1 and S2** of the appendix of the document. The avareage pH_{PZC} of all carbons was found to be 1.8. This suggests that below these values the surface of the carbons will be positively charged while above this values the surface will be negatively charged [18]. A similar observation has been discussed by Gunture *et al* in their study of adsorption of organic dyes by diesel soot derived OLCs [21]. This provides evidence to the results we obtained for all carbons which suggested that the highest removal capacity of the carbon materials on the tartrazine dye is achieved at protonated media pH (below 1.8). However, the minimal capacity is found when the solution pH is above 1.8. From this

experiment, it was deduced that E-OLCs and H-OLCs exhibit the highest removal percentage at pH below 1.8 than all other OLCs and thus was furtherly used in adsorption experiments.

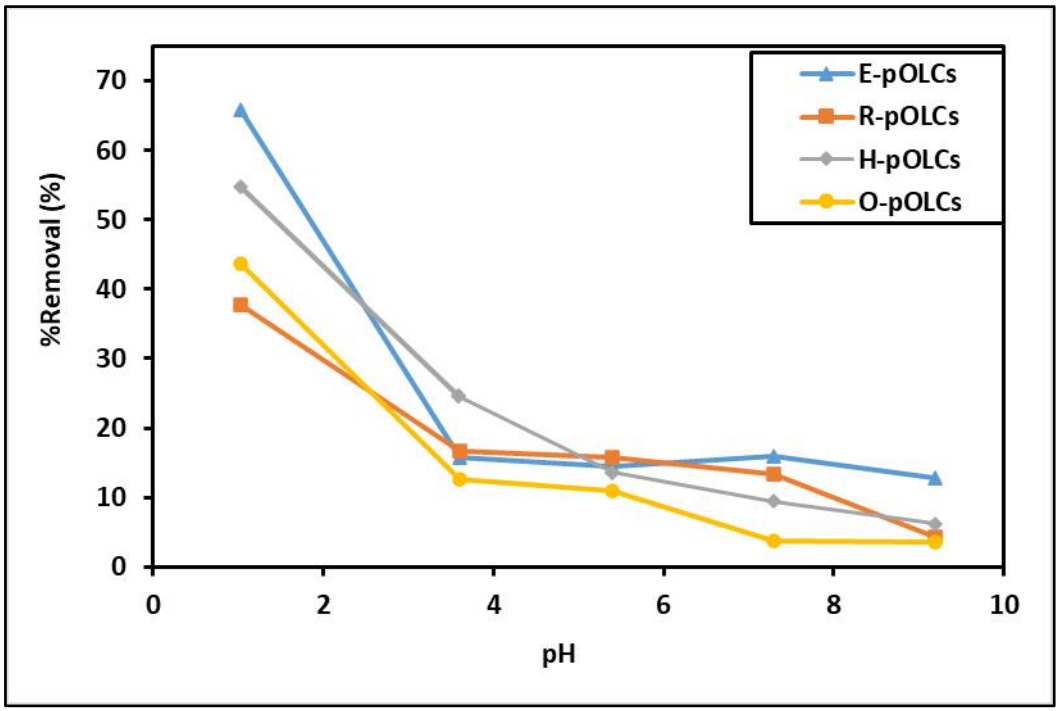

Figure 5.1: Effect of initial pH on tartrazine dye removal using E-pOLCs, R-pOLCs, H-pOLCs, H-pOLCs, and O-pOLCs (initial concentration: 20 mg/L, adsorbent mass: 0.03 g, contact time = 6 h, shaking speed: 220 rpm, and at room temperature).

5.3.1.1.2 Effect of pH solution on N-OLCs and ox-OLCs

The properties of OLCs can be enhanced through surface modifications. Not only does functionalization introduce the functional groups on the surface of OLCs but it is also linked to the presence of defects in the carbon lattice and the presence of sp^3-hybridized carbon atoms on the surface of nanoparticles [22]. Li *et al*. reported that CNT supported amorphous alumina had higher fluoride adsorption capacity which was about 13.5 times higher than that of activated carbon and 4 times higher than that of γ-Al_2O_3, and after oxidation with nitric acid, CNTs also showed exceptional adsorption capability and high adsorption efficiency for lead removal from water [23]. It is also reported that nitrogen atoms replacing the carbon atoms of carbon materials could create many active sites and defects and open the band gap, displaying the similar property with the semiconductor and thus improving the adsorption and electric performance [24]. In this work, the effect of pH was explored on nitrogen incorporated and oxidized OLCs (E-N-OLCs, E-ox-OLCs, H-N-OLCs, and H-ox-OLCs).

Figure 5.2 presents the experimental data for the effect of pH on above mentioned OLCs. Comparing the modified OLCs, the H-N-OLCs and E-N-OLCs had the highest maximum removal percentages of 83% and 72% than the H-ox-OLCs and E-ox-OLCs which had maximum removal percentages of 38% and 39% respectively. This can be attributed to the abundant presence of oxygen-containing groups which induced reduction of electron density on the surface of the carbons, resulting to the surface to being negatively charged and consequently causing a repulsive force for the anionic dye [25] . Xue *et al*, reported that nitrogen is an n-type dopant that can polarize adjacent carbon atoms and create a charged sites in the carbon skeleton. These charged points act as activation regions on the carbon surface, which are more energy-efficient in their catalytic applications and promote the reductive adsorption of O_2 [26]. It also observable that the adsorption capacities decrease with increasing pH in all carbons as discussed on 5.3.1.1. N-OLCs achieved better adsorption results than pOLCs and this is due to higher surface area of the N-OLCs. This is shown by BET results in chapters 3 and 4. This experiment provides evidence that N-OLCs are best suitable carbons for the adsorption of anionic tartrazine dye.

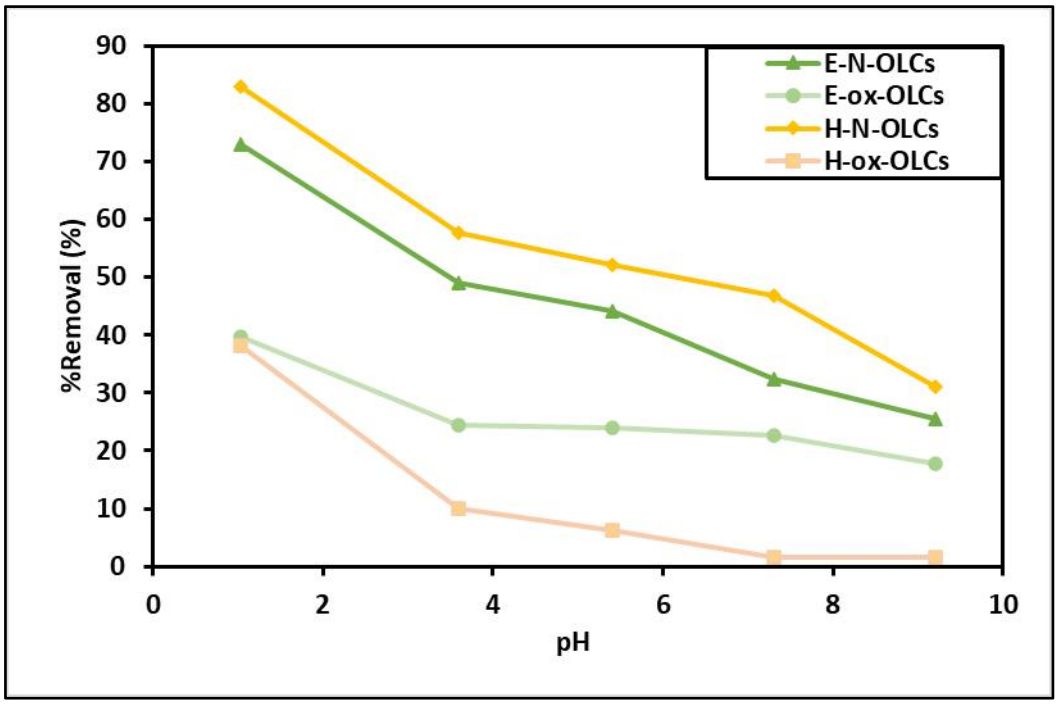

Figure 5.2: Effect of initial pH on tartrazine dye removal using E-N-OLCs, E-ox-OLCs, H-N-OLCs, and H-ox-OLCs (initial concentration: 20 mg/L, adsorbent mass: 0.03 g, contact time = 6 h, shaking speed: 220 rpm, and at room temperature).

5.3.1.4. Effect of contact time

To examine the influence of contact time on adsorption of the dye onto E-N-OLCs and H-N-OLCs, the experiments were conducted at pH 1 with a fixed concentration of 20 mg/L over a period of 5−1440 min. Figure 5.3 shows that at first there is a fast removal of the dye as the contact time between the adsorbents and adsorbate increases, followed by a gentler increase until little increase in removal was noticed between 360 and 1440 minutes. This trend was noticeable for both E-N-OLCs and H-N-OLCs. The availability of an increased number of active sites on the adsorbents results in rapid dye removal at the earliest stages (5−120min) of the reaction. As the contact time increases, saturation of sites increases, resulting in a slow uptake of the dye with time [27]. Such behavior is common adsorption behavior and credited mainly to the reduction in the number of the available uptake active sites under the occupation of them by adsorbed dye ion with increasing the contact time [28]. The uptake of the dye using E-N-OLCs shows abrupt removal percentage reaches 40,6% after only 5 min. After that, the amount of the adsorbed dye increased gradually to 77.1% after 360 min. The equilibrium was achieved after 360 min and the quantity of the adsorbed dye increased only from 77.1% to about 82% with increasing the time from 360 to 1440 min. Similar behavior was detected for the removal of the dye using H-N-OLCs, the uptake appears to be abrupt at the first 5 min achieving 44% removal of the dye. This was followed by a slight but noticeable increase in the uptake from 41% to 74.6% removal with expanding the reaction time from 5 min to 360 min. After that, the changes in the amount of adsorbed dye become nearly fixed and the value increased only from 76.6% to 84.3% with increasing the time from 360 to 1440 min. This experiment shows that the adsorption of tartrazine dye by both E-N-OLCs and H-N-OLCs reaches equilibrium after 360 min.

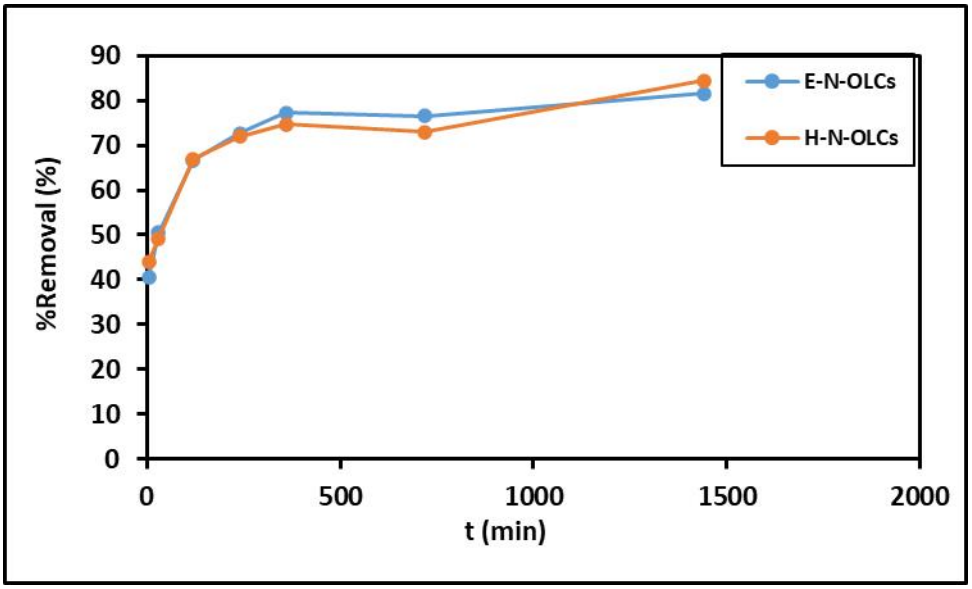

Figure 5.3: Effect of contact time on tartrazine dye uptake onto E-N-OLCs and H-N-OLCs respectively with fixed solution concentration of 20 mg/L (pH: 1, adsorbent mass: 0.03 g, shaking speed: 220 rpm and room temperature).

5.3.1.2. Effect of initial concentration

The initial concentration of the adsorbate plays a vital role, as a given mass of the nano-adsorbent can adsorb a fixed quantity of the solute [29]. The effect of initial concentration (5 to 25 mg/L) for the removal of the dye using N-OLCs was varied, while the other parameters were kept constant. As shown in Figure 5.3, the E-N-OLCs removal percentage of the dye decreases with an increase in the initial concentration from 10 mg/L to 25 mg/L. This was attributed to strong driving forces at higher concentrations, that allows the dye ions to move towards the available binding sites [30, 31] . The H-N-OLCs nano-adsorbents was also investigated under similar conditions. In the case of H-N-OLCs, similar trend was also observed. The removal percentages at low concentrations (5 to 15 mg/L) were higher which might be attributed to high availability of active sites for adsorption. At higher concentrations (20 mg/L to 25 mg/L), it is evident that the removal percentage was decreasing. This was attributed to declining available active sites for adsorption as the adsorbent was kept constant and the adsorbate quantity was increased.

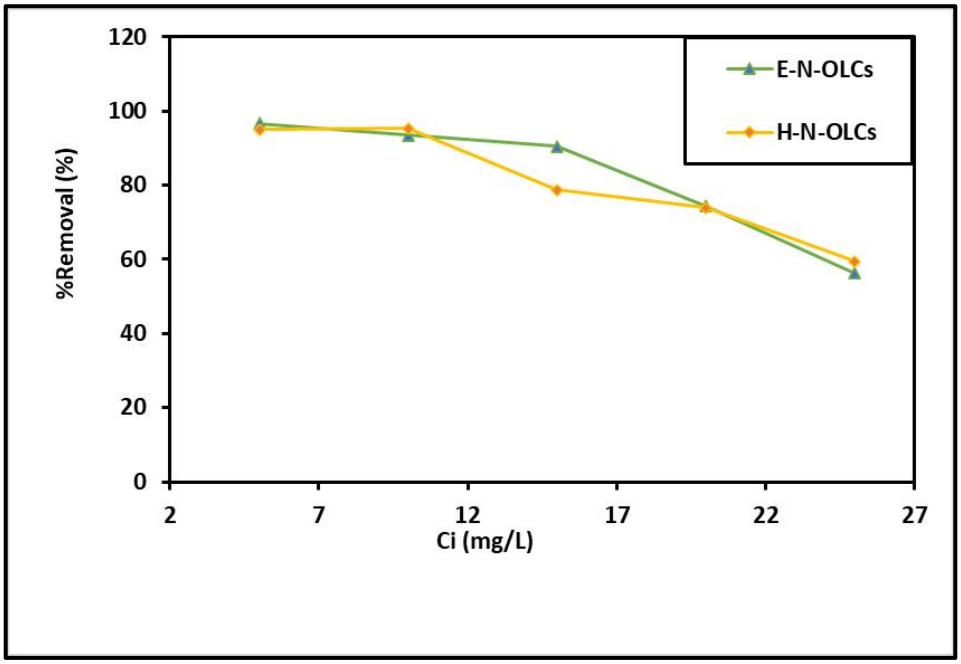

Figure 5.4: Effect of initial tartrazine dye concentration on the removal percentage over E-N-OLCs and H-N-OLCs (adsorbent mass: 0.03 g, time: 6 h, shaking speed: 220 rpm, pH: 1 and room temperature).

5.3.2. Kinetic studies

The kinetics adsorption variables such as the rate constant and equilibrium adsorption capacities are vital for understanding the adsorption processes. The PFO (Pseudo-first order) and PSO (pseudo-second order) kinetic models were used to determine the best model that will best fit the experimental data (**Figure 5.5**). The nonlinear forms of the PFO and PSO for both E-N-OLCs and H-OLCs did not yield any meaningful correlation coefficient (R^2) values. However, the linear forms for E-N-OLCs showed R^2 values of 0,4524 and 0,9959 and the q_e values of 0,998823mg/g and 16,23mg/g for the PFO and PSO models respectively (**Table 5.1**). The calculated q_e of the PSO model (16,23 mg/g) was close to the experimental value of q_e (16,29 mg/g), and the R^2 was close to the value of 1 suggesting that the calculated kinetic parameters attained from the experimental data for E-N-OLCs best fitted the PSO. Therefore, the removal of tartrazine dye appeared to follow a PSO model, indicating a possible chemical bond formation of the dye ions and the surface of the E-N-OLCs (i.e., chemisorption) [32]. A similar phenomenon has been observed in the adsorption of reactive dye (Procion Red MX-5B) onto carbon nanotubes [33], hexavalent chromium using olive oil derived carbon nano-onions [32], and industrial dye (methylene blue) from wastewater using carbon nano-onions

from paraffinum liquidum [34]. Bonelli *et al.,* reported that the best fit for PFO is commonly observed when adsorption occurs through diffusion through the interface and it does not fit well for the whole range of adsorption time, it is usually applicable over the initial 20–30 min of the adsorption process [35]. The H-N-OLCs R^2 and q_e values of linear form PFO and PSO were closely related to those of E-N-OLCs. The R^2 (0,9947) and calculated q_e (16,75mg/g) of PSO also indicated the rate controlling step as being the chemisorption process.

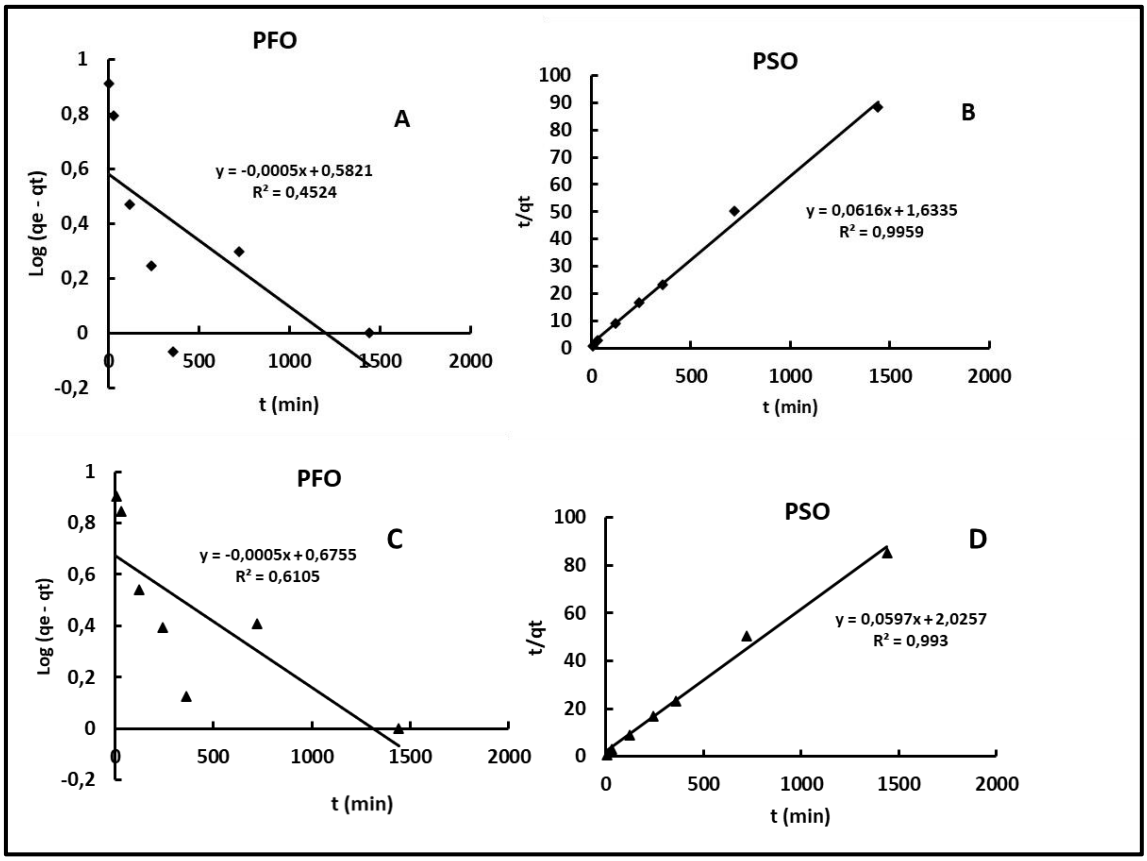

Figure 5.5: Pseudo first and second order plots for the dye removal from aqueous solutions with E-N-OLCs (A&B) and H-NOLCs (C&D), with initial dye concentration Ci = 50 mg/L and pH 1.

Table 5.1: Comparison of experimental and calculated values for the first and the second order adsorption rate constants.

Kinetic Model	Parameter	Sample	
		E-N-OLCs	**H-N-OLCs**
PFO	K_1 (g/mg min)	0.0012	0,0011
	$q_{e,exp}$ (mg/g)	16,29	16,87
	$q_{e,cal}$ (mg/g)	0,998	0,998
	R^2	0.4524	0,6105
	χ^2	234,22	252,26
PSO	K_2 (g/mg min)	0,0023	0,0017
	$q_{e,exp}$ (mg/g)	16,29	16,57
	$q_{e,cal}$ (mg/g)	16,22	16,75
	R^2	0,9959	0,9947
	χ^2	0,000227	0,000886

5.3.3. Isotherm studies

The Langmuir and Freundlich adsorption isotherms were selected to study the progression of the dye removal using the E-N-OLCs and H-N-OLCs (**Table 5.2**). Different model factors were used to establish the best model: the R^2, the maximum adsorption capacity Q_{max} (mg/g) compared to the experimental adsorption capacity (q_e mg/g), and the chi-squared (χ^2) values. The E-N-OLCs R^2 value for the linear Langmuir isotherm was higher than Freundlich's and

closer to 1. The maximum adsorption capacity Q_{max} was found to be 19,61 mg/g which was close to the experimental adsorption capacity (16,24 mg/g). The E-N-OLCs linear Langmuir model showed a value of χ^2 as 0.59 which was fairly close to 1, indicating that the model data were close to the experimental data. Overall, the experimental data was better explained by the linear Langmuir isotherm indicating a monolayer coverage by the dye occurring on a homogeneous surface of E-N-OLCs as nano-adsorbent [36]. However, the R^2 (0,9104) value of Freundlich model in H-N-OLCs was higher than that of Langmuir isotherm (0,8963), indicating that adsorption with H-N-OLCs is best described by Freundlich isotherm which implies that the adsorption mechanisms is related to multilayer properties and of heterogeneous types [27]. In literature, Ntuli T *et al.,* reported that adsorption of hexavalent chromium by polyacrylic acid-grafted *Macadamia* nutshell powder was isothermally best described by linear Langmuir model [37]. Meanwhile, Konicki *et al*., reported the adsorption of anionic dye Direct Red 23 onto magnetic multi-walled carbon nanotubes which favored linear Freundlich model [38]. The separation factor (R_L) values of both E-N-OLCs and H-N-OLCs obtained from the Langmuir isotherm and the Freundlich exponent (n) portrayed values $0 < R_L < 1$ and $0 < n < 1$ respectively, indicated favorable adsorption of dye by the OLCs. The R_L values shown on Table 5.3 decreased as the initial concentration of the dye was increased from 5 mg/L to 25 mg/L. This can be attributed to stronger bond formation between the sorbate ions and the sorbent surface indicating possible chemisorption [32].

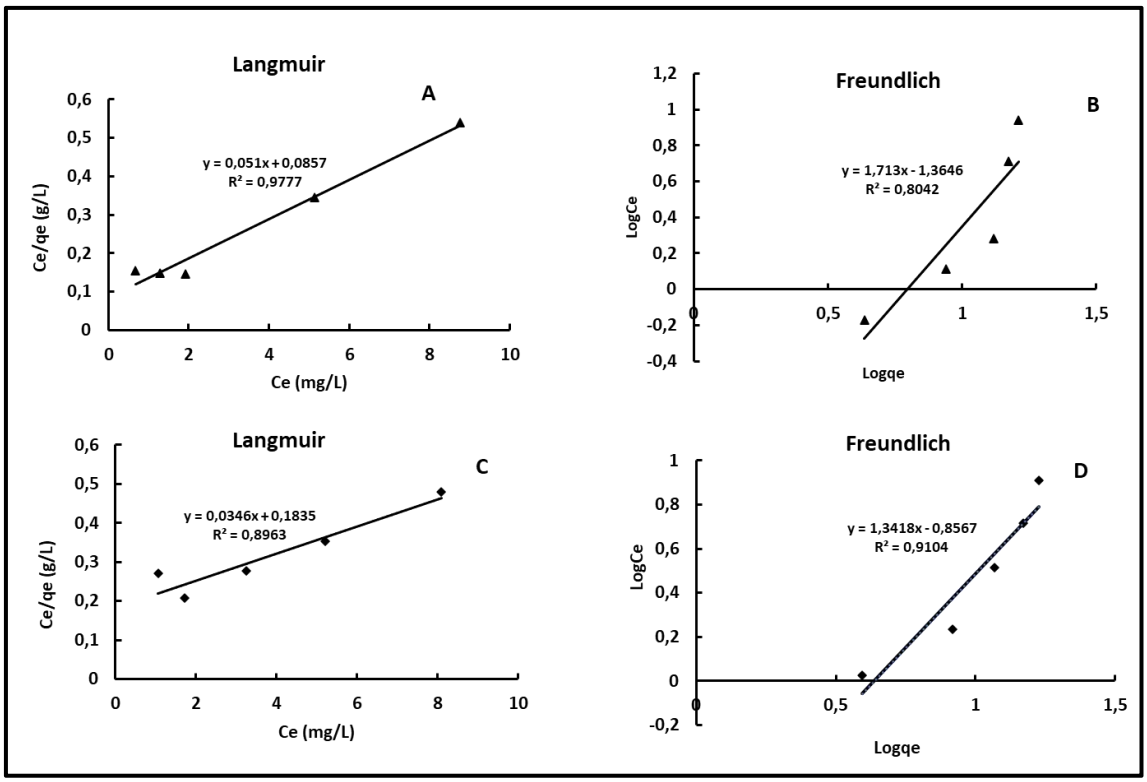

Figure 5.6: Langmuir and Freundlich plots of the dye removal from aqueous solutions with E-N-OLCs (A&B) and H-N-OLCs (C&D). (Time: 6 h and pH 1).

Table 5.2: Langmuir and Freundlich constants for the dye adsorption on E-N-OLCs and H-N-OLCs.

Isotherm	**Parameter**	**Sample**	
		E-N-OLCs	**H-N-OLCs**
Langmuir	q_{max} (mg/g)	19,607	28,901
	K_L (L/mg)	1,680	5,303
	R^2	0,9777	0,8963
	χ^2	0,578282	4,986161
Freundlinch	n	0,58378	0,74526
	K_f	23,152	7,189
	R^2	0,8042	0,9104
	χ^2	2,06357	13,10784

Table 5.3: Langmuir equilibrium parameter or separation factor values of E-N-OLCs and H-N-OLCs attained for different initial concentrations.

Initial Concentration of the dye solution (mg/L)	**R_L Values E-N-OLCs**	**R_L Values H-N-OLCs**
5	0,1063	0,0363
10	0,0561	0,01855

15	0,0381	0,0124
20	0,0232	0,0093
25	0,0232	0,0074

5.3.4 Comparison of adsorption capacities for different adsorbents

Direct comparison of different adsorption studies in the literature is challenging due to the different optimum adsorption conditions used in the respective studies. Therefore, as a comparison, the pH, adsorbate ion type, Isotherm, Kinetic, and adsorption capacity have been selected for comparison studies. (**Table 5.4**). It can be observed that the optimum adsorption pH for the removal anionic dyes was under acidic conditions (pH < 5). It can also be observed that the most adsorbent equilibrium data were best fit for Langmuir isotherm and PSO kinetic model, indicating single layer coverage adsorption and chemisorption mechanism, However, most studies in which the adsorbent indicated Frundlich isotherm were optimized at lower (pH ≤ *2*) obtained the lowest adsorption capacity while our carbons with the same pH exhibited higher capacity. This proves that our H-N-OLCs are best candidates for adsorption of anionic dyes in acid medium.

Table 5.4: Comparison of different adsorbents.

Adsorbent	**Adsorbate dye ion type**	**Isotherm**	**Kinetic**	**pH**	**Qe ($mg.g^{-1}$)**	**Reference**
E-N-OLC	Anionic	Langmuir	PSO	1	19.6	This work
H-N-OLC	Anionic	Frundlich	PSO	1	28.9	This work
Pine bark	Anionic	Frundlich	PSO, Intra-particle diffusion	2	1.6	[39]
Organic-matter rich	Anionic	Langmuir	PSO	4	24.1	[40]

clay						
Multiwalled carbon nanotubes (MWCNTs)	Anionic	Langmuir	PSO	2	30.3	[41]
Single walled carbon nanotubes (SWCNTs)	Anionic	Langmuir	PSO	3	74.2	[42]
Mesoporous zeolite	Anionic	Freundlich	PSO	1	5.5	[43]
Kaolinite	Anionic	Langmuir	PSO	2.5	1.2	[44]
Banana peel	Anionic	Langmuir	Intra-particle diffusion	6-7	21.0	[45]

5.4. Conclusions

The pristine, Nitrogen doped and oxidized OLC nanoparticles were employed as nano-adsorbents for the removal of tartrazine dye in aqueous solution using a batch adsorption method. The nitrogen doped engine and household waste oil derived OLC nanoparticles had the highest removal percentages of 72% and 83% respectively. These removal percentages were obtained at acid condition (pH < 1.8). The Nitrogen doped OLCs were proven to be suitable adsorbents due to their enhanced particle surface. The incorporation of nitrogen onto the carbon matrix results into surface defects which promotes an increase in surface area. While the oxidation of nanocarbon materials with an oxygen containing groups promotes repulsive force with the anionic tartrazine dye. The PSO R^2 and χ 2 values provided evidence that the kinetics data of both E-N-OLCs and H-N-OLCs best fits the PSO model which suggests that the dye-OLC interaction involves chemical bonding. This is an indication that

this nano-adsorbents are suitable for the removal of the dye of variable concentrations in water. The equilibrium data was also fitted using Langmuir and Freundlich adsorption isotherms. In which the correlation coefficient R^2 and χ 2 showed that the Langmuir isotherm model best fitted the experimental data of E-N-OLCs. This suggest that the dye-E-OLCs interaction is through a monolayer coverage of the carbon surface by the dye. In the case of H-N-OLCs, the experimental data best fitted Freundlich isotherm model indicating a multilayer coverage.

REFERENCES

[1] A. K. Mishra, T. Arockiadoss, and S. Ramaprabhu, "Study of removal of azo dye by functionalized multi walled carbon nanotubes," *Chemical Engineering Journal*, vol. 162, no. 3, pp. 1026–1034, Sep. 2010, doi: 10.1016/J.CEJ.2010.07.014.

[2] A. Mittal, J. Mittal, and L. Kurup, "Adsorption isotherms, kinetics and column operations for the removal of hazardous dye, Tartrazine from aqueous solutions using waste materials—Bottom Ash and De-Oiled Soya, as adsorbents," *J Hazard Mater*, vol. 136, no. 3, pp. 567–578, Aug. 2006, doi: 10.1016/J.JHAZMAT.2005.12.037.

[3] T. Robinson, G. McMullan, R. Marchant, and P. Nigam, "Remediation of dyes in textile effluent: a critical review on current treatment technologies with a proposed alternative," *Bioresour Technol*, vol. 77, no. 3, pp. 247–255, May 2001, doi: 10.1016/S0960-8524(00)00080-8.

[4] S. Song, Y. Ma, H. Shen, M. Zhang, and Z. Zhang, "Removal and recycling of ppm levels of methylene blue from an aqueous solution with graphene oxide," *RSC Adv*, vol. 5, no. 35, pp. 27922–27932, 2015, doi: 10.1039/c4ra16982d.

[5] I. M. Jauris *et al.*, "Adsorption of sodium diclofenac on graphene: A combined experimental and theoretical study," *Physical Chemistry Chemical Physics*, vol. 18, no. 3, pp. 1526–1536, 2016, doi: 10.1039/c5cp05940b.

[6] M. B. Seymour, C. Su, Y. Gao, Y. Lu, and Y. Li, "Characterization of carbon nano-Onions for heavy metal ion remediation," *Journal of Nanoparticle Research*, vol. 14, no. 9, Sep. 2012, doi: 10.1007/s11051-012-1087-y.

[7] C. Sakulthaew, C. Chokejaroenrat, A. Poapolathep, T. Satapanajaru, and S. Poapolathep, "Hexavalent chromium adsorption from aqueous solution using carbon nano-onions (CNOs)," *Chemosphere*, vol. 184, pp. 1168–1174, Oct. 2017, doi: 10.1016/J.CHEMOSPHERE.2017.06.094.

[8] M. Zhou, Q. Li, S. Zhong, J. Chen, H. Lin, and X. L. Wu, "Facile large scale fabrication of magnetic carbon nano-onions for efficient removal of bisphenol A," *Mater Chem Phys*, vol. 198, pp. 186–192, Sep. 2017, doi: 10.1016/J.MATCHEMPHYS.2017.05.020.

[9] M. E. Plonska-Brzezinska, "Carbon Nano-Onions: A Review of Recent Progress in Synthesis and Applications," May 01, 2019, *Wiley-VCH Verlag*. doi: 10.1002/cnma.201800583.

[10] C. G. Renda, L. A. Goulart, C. H. M. Fernandes, L. H. Mascaro, J. M. De Aquino, and R. Bertholdo, "Novel onion-like carbon structures modified with iron oxide as photocatalysts for the degradation of persistent pollutants," *J Environ Chem Eng*, vol. 9, no. 1, p. 104934, Feb. 2021, doi: 10.1016/J.JECE.2020.104934.

[11] P. Kumari, K. M. Tripathi, K. Awasthi, and R. Gupta, "Cost-Effective and Ecologically Sustainable Carbon Nano-Onions for Antibiotic Removal from Wastewater," *Ind Eng Chem*

Res, vol. 62, no. 35, pp. 13837–13847, Sep. 2023, doi: 10.1021/ACS.IECR.3C01700/SUPPL_FILE/IE3C01700_SI_001.PDF.

[12] P. Kumari, K. M. Tripathi, K. Awasthi, and R. Gupta, "Sustainable carbon nano-onions as an adsorbent for the efficient removal of oxo-anions," *Environmental Science and Pollution Research*, vol. 30, no. 6, pp. 15480–15489, Feb. 2023, doi: 10.1007/S11356-022-22883-3/METRICS.

[13] O. Mykhailiv, H. Zubyk, and M. E. Plonska-Brzezinska, "Carbon nano-onions: Unique carbon nanostructures with fascinating properties and their potential applications," *Inorganica Chim Acta*, vol. 468, pp. 49–66, Nov. 2017, doi: 10.1016/J.ICA.2017.07.021.

[14] "Determination of Point of Zero Charge (PZC) of Concrete Particles Adsorbents", doi: 10.1088/1757-899X/1184/1/012004.

[15] H. Qiu, L. Lv, B. C. Pan, Q. J. Zhang, W. M. Zhang, and Q. X. Zhang, "Critical review in adsorption kinetic models," *Journal of Zhejiang University: Science A*, vol. 10, no. 5, pp. 716–724, May 2009, doi: 10.1631/JZUS.A0820524/METRICS.

[16] K. Y. Foo and B. H. Hameed, "Insights into the modeling of adsorption isotherm systems," *Chemical Engineering Journal*, vol. 156, no. 1, pp. 2–10, Jan. 2010, doi: 10.1016/J.CEJ.2009.09.013.

[17] R. Sivaranjanee, P. S. Kumar, and S. Mahalaxmi, "A review on agro-based materials on the separation of environmental pollutants from water system," *Chemical Engineering Research and Design*, vol. 181, pp. 423–457, May 2022, doi: 10.1016/J.CHERD.2022.04.002.

[18] G. B. B. Varadwaj, O. A. Oyetade, S. Rana, B. S. Martincigh, S. B. Jonnalagadda, and V. O. Nyamori, "Facile Synthesis of Three-Dimensional Mg-Al Layered Double Hydroxide/Partially Reduced Graphene Oxide Nanocomposites for the Effective Removal of Pb2+ from Aqueous Solution," *ACS Appl Mater Interfaces*, vol. 9, no. 20, pp. 17290–17305, May 2017, doi: 10.1021/acsami.6b16528.

[19] S. Husien, R. M. El-taweel, A. I. Salim, I. S. Fahim, L. A. Said, and A. G. Radwan, "Review of activated carbon adsorbent material for textile dyes removal: Preparation, and modelling," *Current Research in Green and Sustainable Chemistry*, vol. 5, p. 100325, Jan. 2022, doi: 10.1016/J.CRGSC.2022.100325.

[20] W. Konicki, I. Pełech, E. Mijowska, and I. Jasińska, "Adsorption of anionic dye Direct Red 23 onto magnetic multi-walled carbon nanotubes-Fe 3C nanocomposite: Kinetics, equilibrium and thermodynamics," *Chemical Engineering Journal*, vol. 210, pp. 87–95, Nov. 2012, doi: 10.1016/j.cej.2012.08.025.

[21] Gunture, J. Kaushik, A. K. Garg, D. Saini, P. Khare, and S. K. Sonkar, "Pollutant diesel soot derived onion-like nanocarbons for the adsorption of organic dyes and environmental assessment of treated wastewater," *Ind Eng Chem Res*, vol. 59, no. 26, pp. 12065–12074, Jul. 2020, doi: 10.1021/ACS.IECR.0C01267/SUPPL_FILE/IE0C01267_SI_001.PDF.

[22] Z. Yang, H. Nie, X. Chen, X. Chen, and S. Huang, “Recent progress in doped carbon nanomaterials as effective cathode catalysts for fuel cell oxygen reduction reaction,” 2013, *Elsevier B.V.* doi: 10.1016/j.jpowsour.2013.02.057.

[23] R. Q. Long and R. T. Yang, “Carbon nanotubes as superior sorbent for dioxin removal [1],” Mar. 07, 2001. doi: 10.1021/ja003830l.

[24] Y. H. Li *et al.*, “Adsorption of fluoride from water by amorphous alumina supported on carbon nanotubes,” *Chem Phys Lett*, vol. 350, no. 5–6, pp. 412–416, Dec. 2001, doi: 10.1016/S0009-2614(01)01351-3.

[25] K. Y. Foo and B. H. Hameed, “An overview of dye removal via activated carbon adsorption process,” *Desalination Water Treat*, vol. 19, no. 1–3, pp. 255–274, 2010, doi: 10.5004/dwt.2010.1214.

[26] D. Xue, H. Xia, W. Yan, J. Zhang, and S. Mu, “Defect Engineering on Carbon-Based Catalysts for Electrocatalytic CO2 Reduction,” Jan. 01, 2021, *Springer Science and Business Media B.V.* doi: 10.1007/s40820-020-00538-7.

[27] M. A. Salam, M. R. Abukhadra, and M. Mostafa, “Effective decontamination of As(V), Hg(II), and U(VI) toxic ions from water using novel muscovite/zeolite aluminosilicate composite: adsorption behavior and mechanism,” *Environmental Science and Pollution Research*, vol. 27, no. 12, pp. 13247–13260, Apr. 2020, doi: 10.1007/s11356-020-07945-8.

[28] M. Shaban, M. I. Sayed, M. G. Shahien, M. R. Abukhadra, and Z. M. Ahmed, “Adsorption behavior of inorganic- and organic-modified kaolinite for Congo red dye from water, kinetic modeling, and equilibrium studies,” *J Solgel Sci Technol*, vol. 87, no. 2, pp. 427–441, Aug. 2018, doi: 10.1007/s10971-018-4719-6.

[29] H. I. Adegoke, F. A. Adekola, I. T. Olowookere, and A. L. Yaqub, “Thermodynamic studies on adsorption of lead (II) Ion from aqueous solution using magnetite, activated carbon and composites,” *Journal of Applied Sciences and Environmental Management*, vol. 21, no. 3, p. 440, Jul. 2017, doi: 10.4314/jasem.v21i3.5.

[30] I. A. A. Hamza, B. S. Martincigh, J. C. Ngila, and V. O. Nyamori, “Adsorption studies of aqueous Pb(II) onto a sugarcane bagasse/multi-walled carbon nanotube composite,” *Physics and Chemistry of the Earth, Parts A/B/C*, vol. 66, pp. 157–166, Jan. 2013, doi: 10.1016/J.PCE.2013.08.006.

[31] M. Rahimnejad, K. Pirzadeh, I. Mahdavi, and S. M. Peyghambarzadeh, “Pb (II) removal from aqueous solution by adsorption on activated carbon from kiwi peel,” *Environ Eng Manag J*, vol. 17, no. 6, pp. 1293–1300, 2018, doi: 10.30638/eemj.2018.128.

[32] T. D. Ntuli *et al.*, “Removal of hexavalent chromium via an adsorption coupled reduction mechanism using olive oil derived carbon nano-onions,” *Environ Nanotechnol Monit Manag*, vol. 16, p. 100477, Dec. 2021, doi: 10.1016/J.ENMM.2021.100477.

[33] C. H. Wu, “Adsorption of reactive dye onto carbon nanotubes: Equilibrium, kinetics and thermodynamics,” *J Hazard Mater*, vol. 144, no. 1–2, pp. 93–100, Jun. 2007, doi: 10.1016/J.JHAZMAT.2006.09.083.

[34] R. A. Venkatesan and M. Balachandran, “Novel carbon nano-onions from paraffinum liquidum for rapid and efficient removal of industrial dye from wastewater,” *Environmental Science and Pollution Research*, vol. 27, no. 35, pp. 43845–43864, Dec. 2020, doi: 10.1007/s11356-020-09981-w.

[35] B. Bonelli, F. S. Freyria, I. Rossetti, and R. Sethi, *Nanomaterials for the Detection and Removal of Wastewater Pollutants*. Elsevier, 2020.

[36] Ö. Gerçel and H. F. Gerçel, “Adsorption of lead(II) ions from aqueous solutions by activated carbon prepared from biomass plant material of Euphorbia rigida,” *Chemical Engineering Journal*, vol. 132, no. 1–3, pp. 289–297, Aug. 2007, doi: 10.1016/J.CEJ.2007.01.010.

[37] T. D. Ntuli and V. E. Pakade, “Hexavalent chromium removal by polyacrylic acid-grafted Macadamia nutshell powder through adsorption–reduction mechanism: Adsorption isotherms, kinetics and thermodynamics,” *Chem Eng Commun*, vol. 207, no. 3, pp. 279–294, Mar. 2020, doi: 10.1080/00986445.2019.1581619.

[38] W. Konicki, I. Pełech, E. Mijowska, and I. Jasińska, “Adsorption of anionic dye Direct Red 23 onto magnetic multi-walled carbon nanotubes-Fe 3C nanocomposite: Kinetics, equilibrium and thermodynamics,” *Chemical Engineering Journal*, vol. 210, pp. 87–95, Nov. 2012, doi: 10.1016/j.cej.2012.08.025.

[39] K. Litefti, M. S. Freire, M. Stitou, and J. González-Álvarez, “Adsorption of an anionic dye (Congo red) from aqueous solutions by pine bark,” *Scientific Reports 2019 9:1*, vol. 9, no. 1, pp. 1–11, Nov. 2019, doi: 10.1038/s41598-019-53046-z.

[40] A. M. Zayed, M. S. M. Abdel Wahed, E. A. Mohamed, and M. Sillanpää, “Insights on the role of organic matters of some Egyptian clays in methyl orange adsorption: Isotherm and kinetic studies,” *Appl Clay Sci*, vol. 166, pp. 49–60, Dec. 2018, doi: 10.1016/J.CLAY.2018.09.013.

[41] K. M. Abualnaja, A. E. Alprol, M. A. Abu-Saied, M. Ashour, and A. T. Mansour, “Removing of Anionic Dye from Aqueous Solutions by Adsorption Using of Multiwalled Carbon Nanotubes and Poly (Acrylonitrile-styrene) Impregnated with Activated Carbon,” *Sustainability 2021, Vol. 13, Page 7077*, vol. 13, no. 13, p. 7077, Jun. 2021, doi: 10.3390/SU13137077.

[42] A. ZabihiSahebi, S. Koushkbaghi, M. Pishnamazi, A. Askari, R. Khosravi, and M. Irani, “Synthesis of cellulose acetate/chitosan/SWCNT/Fe3O4/TiO2 composite nanofibers for the removal of Cr(VI), As(V), Methylene blue and Congo red from aqueous solutions,” *Int J Biol Macromol*, vol. 140, pp. 1296–1304, Nov. 2019, doi: 10.1016/J.IJBIOMAC.2019.08.214.

[43] S. Radoor, J. Karayil, A. Jayakumar, J. Parameswaranpillai, and S. Siengchin, “Efficient removal of methyl orange from aqueous solution using mesoporous ZSM-5 zeolite: Synthesis, kinetics and isotherm studies,” *Colloids Surf A Physicochem Eng Asp*, vol. 611, p. 125852, Feb. 2021, doi: 10.1016/J.COLSURFA.2020.125852.

[44] G. Fumba *et al.*, “Equilibrium and Kinetic Adsorption Studies of Methyl Orange from Aqueous Solutions Using Kaolinite, Metakaolinite and Activated Geopolymer as Low Cost Adsorbents,” *Journal of Academia and Industrial Research (JAIR)*, vol. 3, p. 156, 2014.

[45] G. Annadurai, R. S. Juang, and D. J. Lee, “Use of cellulose-based wastes for adsorption of dyes from aqueous solutions,” *J Hazard Mater*, vol. 92, no. 3, pp. 263–274, Jun. 2002, doi: 10.1016/S0304-3894(02)00017-1.

CHAPTER 6

General conclusions and recommendations

6.1 Conclusion

Flame pyrolysis was used to synthesize pOLCs using four different waste oils. The synthesized OLCs were found to be quasi-spherical and agglomerated with a particle size between 29 and 42 nm. HRTEM confirmed the disconnection of the concentric multi-layers. All pOLCs were found to be disordered and amorphous, and presented similar thermal strength, and high surface areas. The pOLCs of engine and household waste oils were modified by N-doping and functionalising of the surface of the N-doped OLCs through an oxidation reaction. The nitrogen content was found to be 4.71% and 3.91% for the H-N-OLCs and E-N-OLCs respectively. Various characterisation techniques revealed that the morphological properties such as shape and structure were unaltered post modifications. However, the particle sizes decreased after the N-doping and oxidation reactions. This was attributed to the defects on the carbon lattice and surface areas which were found to increase with functionalisation as confirmed by Raman, XRD, and BET analysis.

The optimum conditions for the removal of the tartrazine dye were found to be at pH = 1, C_o = 20 mg/L, mass = 0.03 g, and T = 25°C. All the pOLCs were employed as adsorbents and the superior adsorbents amongst the four were E-pOLCs and H-pOLCs in that order respectively. These carbons were then further used for the adsorption as H-N-OLCs, H-ox-OLCs, E-N-OLCs, and E-ox-OLCs. H-N-OLCs exhibited the highest removal percentage of 83% followed by 72% for the E-N-OLCs. It was then deduced that the ox-OLCs were not ideal adsorbents for the removal of tartrazine dye. This was attributed to ionic repulsions that occurred between the adsorbent and adsorbate. The q_e of the E-N-OLCs and H-N-OLCs were found to be within the range of adsorbents that have been employed in literature for the adsorption of anionic dyes. The kinetic data for the E-N-OLCs and H-N-OLCs was better explained by the pseudo-second-order kinetic model indicating the possibility of chemisorption. The experimental data fitted well with the Langmuir adsorption isotherm showing that the removal of tartrazine dye was via a monolayer surface coverage.

Overall, the conversion of waste oil to carbon proved to be an efficient way to produce OLCs that poses ideal properties such as porosity and high surface area for their use in adsorption studies.

6.2 Recommendations and future work

i. Based on the findings from this study, OLCs are promising adsorbent materials that can be improved in order to increase their adsorption capacity. The optimisation of adsorption capacity can be achieved by using higher concentrations of dopants to increase to increase defects which will lead to higher surface area.

ii. The N-doped and oxidised carbon materials can be further characterized using techniques such as XPS, and FTIR to identify the expected elements and functional groups. CHNS analysis is also needed to quantify the nitrogen, carbon, and oxygen content present in the synthesized materials.

iii. To understand the adsorption process better, the characterization of adsorbents after use is crucial. Characterization of H-N-OLCs and E-N-OLCs post-adsorption with gas chromatography–mass spectrometry (GCMS) is required to identify the compounds on the carbon surface.

iv. There is also a need to evaluate the selectivity, stability, regeneration, and thermodynamics of the nano-adsorbents.

v. The effect of temperature will also need to be studied so as to model the thermodynamics and describe the adsorption mechanism.

Appendix A: Supplementary Information

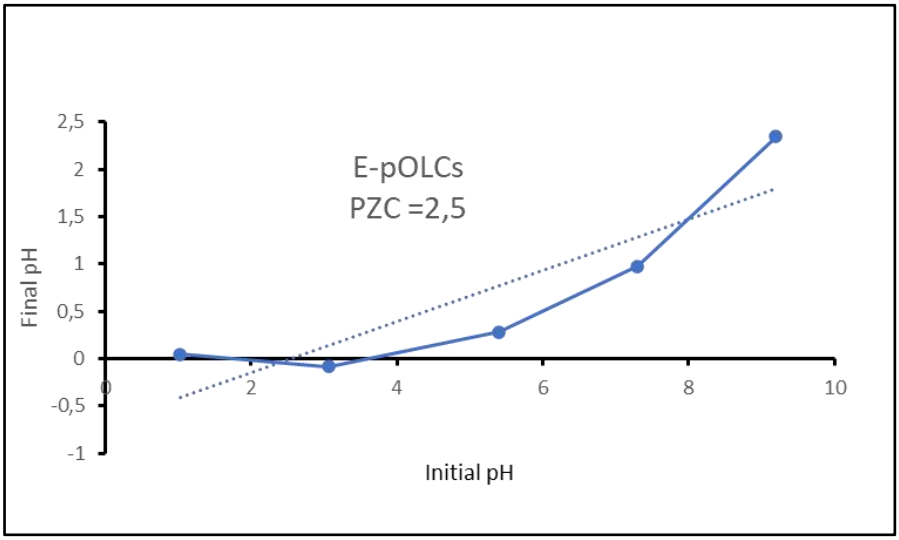

Figure S1: Curve for the point of zero charge of E-pOLCs

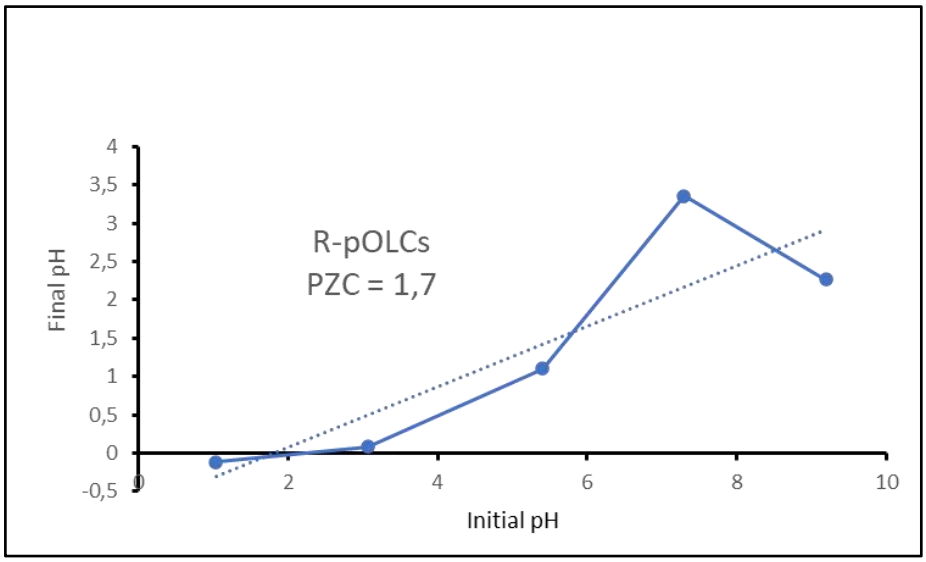

Figure S2: Curve for the point of zero charge of R-pOLCs

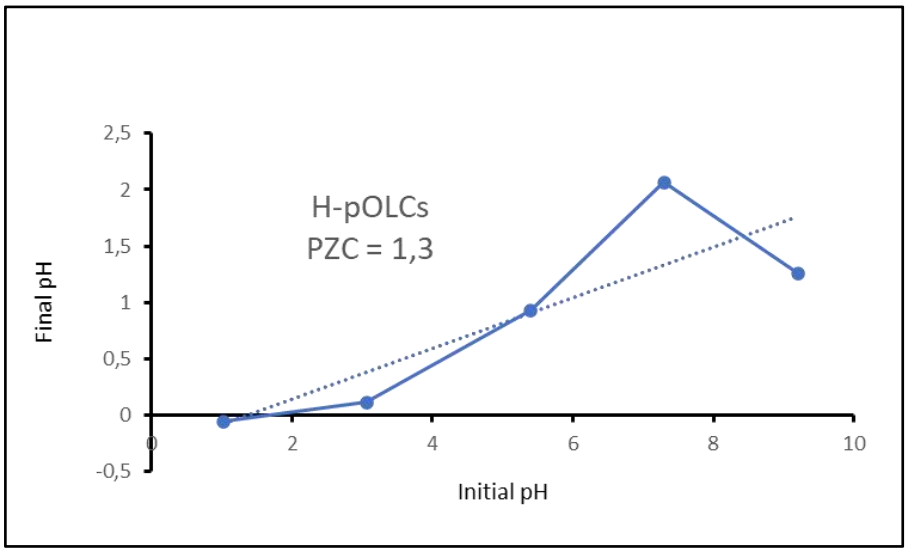

Figure S2: Curve for the point of zero charge of H-pOLCs

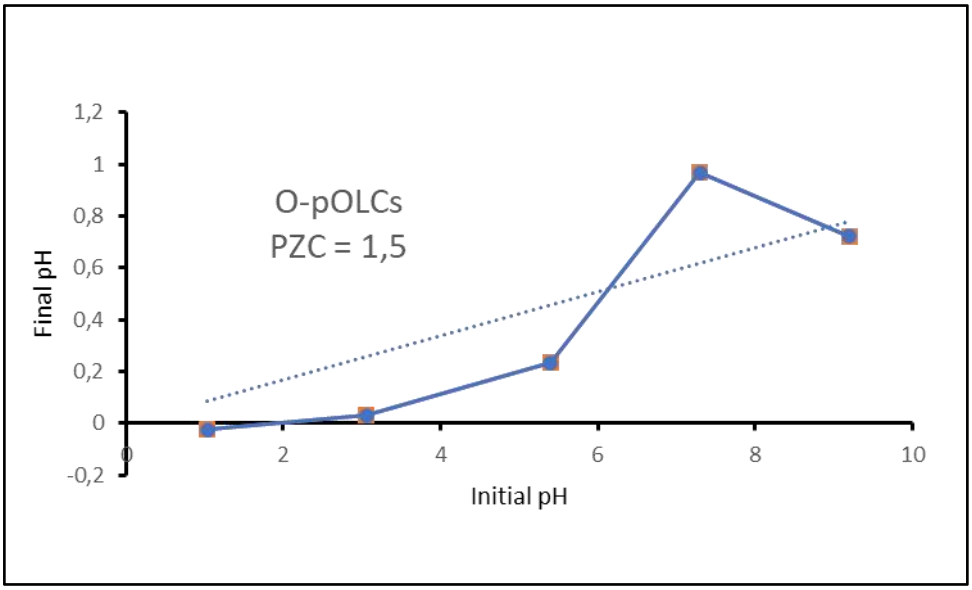

Figure S4: Curve for the point of zero charge of O-pOLCs